LBL-8181 c.2

Lawrence Berkeley Laboratory

UNIVERSITY OF CALIFORNIA, BERKELEY, CA

INDEPENDENT PARTICLE ASPECTS OF NUCLEAR DYNAMICS

Michael Cornelius Robel
(Ph. D. thesis)

May 1979

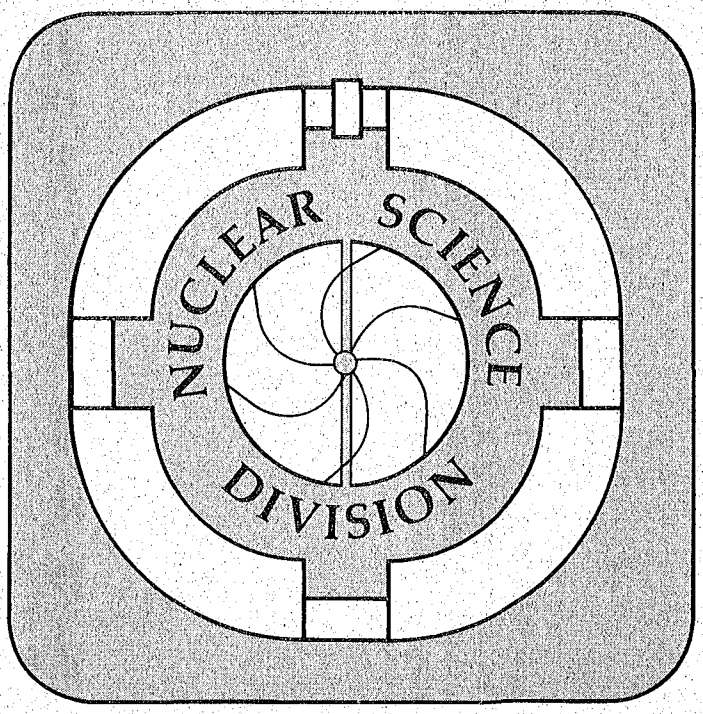

RECEIVED
LAWRENCE
BERKELEY LABORATORY

JUN 14 1979

LIBRARY AND
DOCUMENTS SECTION

LBL-8181 c.2

Prepared for the U. S. Department of Energy
under Contract W-7405-ENG-48

LEGAL NOTICE

This report was prepared as an account of work sponsored by the United States Government. Neither the United States nor the Department of Energy, nor any of their employees, nor any of their contractors, subcontractors, or their employees, makes any warranty, express or implied, or assumes any legal liability or responsibility for the accuracy, completeness or usefulness of any information, apparatus, product or process disclosed, or represents that its use would not infringe privately owned rights.

LBL-8181

INDEPENDENT PARTICLE ASPECTS OF NUCLEAR DYNAMICS

by

Michael Cornelius Robel

Lawrence Berkeley Laboratory
University of California
Berkeley, California 94720

INDEPENDENT PARTICLE ASPECTS OF NUCLEAR DYNAMICS

BY

MICHAEL CORNELIUS ROBEL

ABSTRACT

A generalization of the independent particle model from nuclear statics to nuclear dynamics is sought. Attention is centered on the average behavior of nuclear dynamics, as opposed to detailed behavior, such as that characteristic of shell effects in nuclear statics. In many situations, all that is needed is a model of dissipation in nuclear dynamics.

Completely independent nucleons produce dissipation only when they interact with the surface of a nucleus or when they cross from one nucleus to another. The first possibility manifests itself whenever a nuclear surface deforms. Dissipation is then described by a simple "wall formula." The second mechanism for dissipation is relevant whenever two nuclei are moving relative to one another and are in sufficient contact that nucleons can move between them. Another simple expression, the "window formula," describes dissipation in this case. Neither of the two formulae has any free parameters.

These formulae are expected to be the leading contribution to dissipation if certain conditions are met. One requirement is that the velocities of deformation and of relative nuclear motion must be slow enough, compared to internal, nucleonic speeds, that the nucleons move independently, but fast enough that the dynamics is outside the superfluid regime. In addition, any region connecting two nuclei must be small enough to operate merely as a conduit between them, but large enough that diffraction of nucleons passing through it is insignificant. The one-body formulae are then the major source of nuclear dissipation, but corrections are still necessary and are sometimes of the order of the formula contributions themselves. The most important errors are caused by regularities of nuclear shape and motion and by differences in density between two nuclei in contact. The former are the dynamic generalization of shell effects.

The one-body model is applied to nuclear vibrations. The wall formula supplies the dissipation, which is appended to the standard, hydrodynamical theory of vibrations. Results are consistent with experiment. (So also have been the results of various applications of both formulae performed by others).

Some of the nucleons exchanged between two nuclei in contact may pass through their new host nuclei, penetrate its surface, and be emitted from the nuclear system. The combination of internal,

Fermi motion and relative nuclear motion with refraction at the host's surface is calculated to produce well-focused emission patterns in velocity space, which are called "Fermi jets."

The speed of relative nuclear motion must exceed a threshold value, if nucleons are to overcome their binding to the nuclear system, but it must be less than the Fermi speed, if the independent particle assumption is to hold. Even then, residual two-body interactions with other nucleons in the host nucleus are expected to substantially reduce the strength of jets. Other emission processes are computed to overlap and obliterate much, or sometimes all, of calculated jetting patterns.

Experimental confirmation of the existence of Fermi jets would confirm the assumptions underlying the one-body formulae. Fermi jets might then be a tool with which to study the early stages of nuclear collisions, during which they would be produced.

Gilbert Shapiro

TO MY MOTHER,

DOROTHY BROWN LYMAN

ACKNOWLEDGEMENTS

A considerable pleasure associated with this dissertation is the opportunity it provides the author to thank the many persons who helped him during the course of this work.

W. J. Swiatecki was his research advisor. He originated the basic ideas underlying the "one-body" model of nuclear dissipation and guided its development and much of its subsequent growth, as well as participating closely in many phases of the work himself. In particular, he suggested to the author many of the topics and ideas in Chapter II of this dissertation, plus the problem that Chapter III addresses. In addition to being an original and enthusiastic teacher and colleague, he has also been an unfailing source of kindness, patience, and encouragement.

The author was priviledged to work closely with other people participating in the creation and development of the one-body model: J. Blocki, Y. Boneh, and J. Randrup.

Between pisci-tuberous punning, D. K. Scott found time to draw, first, Dr. Swiatecki's and, thereby, the author's attention to [1]--the starting point of Chapter III. Both he and L. G. Moretto showed alacrity in planning and expedition in performing experiments on the subject. Professor Moretto also provided a great many acute suggestions concerning the work in Chapter III and its presentation. The author regrets that he did not have time while in

Rome to execute Professor Moretto's mouth-watering instructions on seeking out the best food in Trastevere. The author has also had many useful conversations with members of the Moretto group, in particular, G. J Mathews, G. U. Rattazzi, R. P. Schmitt, and J. S. Sventek. In addition, J. S. Sventek's generosity in imparting his considerable knowledge of computers deserves special mention.

The author is happy to acknowledge useful discussions with M. Blann, J. P. Bondorf, H. Flocard, D. L. Hillis, J. I. Kapusta, Y. Karant, S. E. Koonin, D. J. Morrissey, A. M. Poskanzer, A. J. Sierk, M. S. Weiss, and C. Y. Wong.

The comments of G. Shapiro, as head of the dissertation committee, were particularly useful because he was the only person to read the manuscript who was not already thoroughly familiar with the subject matter. He was therefore in a good position to detect gaps and obscurities in the presentation.

The physical translation of this dissertation from a labyrinthine scrawl into its final form owes much to others, too. The figures first began to progress from the author's rough sketchs under the experienced guidance of G. G. Miranda. He also performed the more congenial task of supervising M. Harding, who puffed stogies and did the work. D. J. Craig cheerfully undertook the task of typing many pages of equations. She claimed not to be so cheerful toward its end, but the author was never able to tell the

difference. (The author prepared the verbal part of the text on a computer.)

This work was performed under the auspices of the Nuclear Physics Division of the U.S. Department of Energy under contract W-7405-ENG-48. The author thanks the U.S. citizens, particularly those in the upper income tax brackets, who paid for it all. He acclaims the generosity of those who did so willingly. He tenders his apology to those who paid only from a sense of civil duty or of coercion.

TABLE OF CONTENTS

CHAPTER I: INTRODUCTION..... 1

CHAPTER II: ONE-BODY DISSIPATION..... 8

A. INTRODUCTION..... 8

B. THE WALL FORMULA..... 10

C. THE WINDOW FORMULA..... 27

D. ASSUMPTIONS..... 38

1. The independent-particle model..... 39

2. Semi-classical treatment..... 44

3. The Pauli exclusion principle..... 52

4. The nature of the surface..... 56

5. Randomization and drifts..... 61

a. randomization..... 61

b. drifts..... 65

6. Dissipation and irreversibility..... 86

7. Nuclear density..... 90

8. Net transfers of nucleons and the window definition. 93

9. Summary..... 97

E. APPLICATIONS..... 99

1. Nuclear vibrations..... 99

2. Other developments..... 105

F. CONCLUSIONS..... 112

CHAPTER III: FERMI JETS..... 120

A. INTRODUCTION..... 120

B. ONE DIMENSION..... 125

C. ASSUMPTIONS..... 126

D. THE KINEMATICS OF EMITTED NUCLEONS..... 142

E. INITIAL JETTING..... 147

F. THE NUMBER OF EMITTED NUCLEONS..... 154

G. FERMI JETS AND EVAPORATION: CALCULATED RESULTS..... 160

H. CONCLUSIONS..... 169

APPENDICES

A. SOME GEOMETRICAL LEMMAS..... 177

B. AN EXAMPLE OF A NON-ISOTROPIC DISTRIBUTION..... 180

C. INTEGRAL EVALUATION AND APPROXIMATION..... 183

1. Evaluation..... 183

2. Approximation..... 186

D. TEMPERATURES AND NEUTRON EXCESSES..... 190

1. Fermi gases at positive temperatures..... 190

2. Temperature magnitudes..... 193

3. Neutron excesses..... 194

E. DISSIPATIVE AND COLLECTIVE ENERGY TRANSFERS IN A ONE-DIMENSIONAL EXAMPLE..... 196

REFERENCES..... 199

TABLES..... 203

FIGURE CAPTIONS..... 210

FIGURES..... 223

CHAPTER I

INTRODUCTION

The liquid-drop and shell models have long been two of the main tools for understanding nuclear statics.

Partly, this is because each embodies an important nuclear fact. The liquid drop model expresses the saturation property of nuclei: nuclear binding energies per nucleon and nuclear densities are rather independent of the atomic weight and number. The shell model follows from the operation of the Pauli exclusion principle in nuclei composed of many nucleons to so reduce the effective nucleon-nucleon cross section from its free-space value that the nucleon mean free path in such nuclei becomes comparable to the nuclear dimensions.

The models are popular mainly, however, because they are so useful.

The liquid drop model describes nuclear binding energies. It has also been extended into nuclear dynamics to calculate potentials for fission, alpha-decay, and nuclear vibrations. Attempts have even been made to use it in calculations of inertia in nuclear rotations and vibrations; these results are wrong, but the discrepancies have been revealing. It must be stressed, however, that the liquid drop model describes only average properties. These

average properties vary slowly with atomic number and weight except for a small, rapid fluctuation. The model reproduces the average behavior with considerable accuracy--the error is only a fraction of one percent in the case of binding energies--but it cannot account for the fluctuations.

Perfectly complementing the liquid drop model is the shell model. Its predictions of the average trends of the properties in question are wrong, but those of the fluctuations are right. Its particular domain also includes those nuclear properties in which a distinguished role is played by one or a few nucleons. The shell model (modified, if necessary, to include such effects as collective deformations, residual interactions, and core polarizations) is the tool most commonly used to interpret the properties of low energy nuclear states: spin, parity, isospin, energy, magnetic dipole moment, permanent deformation, and electric quadrupole moment. It also plays a crucial role in the understanding of alpha-, beta-, and gamma-transitions. In dynamics, theoretical analysis of one- and two-nucleon transfers between particular nuclear states (or, in other words, between nuclear peripheries) is founded on shell model ideas.

These lists display the domains of the two models in both their scope and their complementarity, which last is intensified at the conceptual level. The essence of the shell model is the

independent particle assumption: nucleons move as (nearly) independent particles in a common nuclear potential. This seems to contradict the inspiration for the liquid drop model: ordinary liquids, in which mean free paths are short. The resolution of the paradox was clarified in the past few years and is illustrated by the leptodermous theorem [2]. This theorem states that the liquid drop model applies to any average, predominantly local, static property of a thin-skinned system. Shell effects are either detailed, rather than average, properties or non-local corrections to average properties--distinctions very like those manifested in the earlier discussion of the applications of the two models. The truth of the theorem has nothing to do with the classical or quantal nature of a system and is perfectly consistent with an independent-particle model.

The independent particle model that succeeds in nuclear statics should also prosper in nuclear dynamics, in particular, that of slowly deforming systems. The goal here is to discover the analog of the liquid drop model: a description of the broad trend with atomic weight and number of the average properties of nuclear dynamics. Such a description cannot be expected to cover properties other than average and there will be corrections even to the calculations of average properties. Like the static independent-particle model, this "one-body" model will turn out to

apply to a broad range of nuclear phenomena.

The development of the basic one-body model and its application to nuclear dynamics is the subject of Chapter II. It is argued that nuclear dynamics can often be analyzed by adding only a description of dissipation to features already extensively studied in nuclear statics. The one-body model of dissipation is derived here by appealing to the independent particle approximation in order to justify a picture of nuclear systems in which the nucleons behave like a gas of completely non-interacting, classical particles that bounce around inside a perfectly reflecting, perfectly sharp nuclear surface, exchanging energy with it.

The relevant range of nuclear configurations is shown in Fig. 1. The first case is that of a single, deforming nucleus and the dissipation is then described by a simple "wall formula:"

$$\frac{dE_{gas}}{dt} = \rho \langle v \rangle_r \oint_S dS\, \vec{V}\cdot\hat{n}(\vec{V} - \vec{V}_o) \cdot \hat{n} + \cdots . \qquad (1.1)$$

In this equation, dE_{gas}/dt is the power dissipated, ρ is the nuclear mass density, and S is the nuclear surface, each point of which has a normal $\hat{n}(\vec{r})$ and a velocity $\vec{V}(\vec{r})$. The nucleon gas is described in the wall formula by a mean, "drift," velocity field $\vec{V}_o(\vec{r})$ about which the gas has a distribution with a mean speed $\langle v \rangle_r$. Note the absence of free parameters in the wall formula. At the opposite

extreme of nuclear configurations is the third case in Fig. 1 where two nuclei are connected by a <u>small</u> opening, so that the distinction between the two nuclei is clear cut. The corresponding "window formula" says that the one-body force on nucleus 1 is

$$\vec{F}_1^{\text{exchange}}(W) + \vec{F}_1^{\text{wall}}(S;\ \vec{V} \equiv \vec{V}_o) \tag{1.2}$$

$$= -\frac{1}{4}\rho\langle v\rangle_r \int_W dW\ [\vec{V}_{01}(\vec{r},t) - \vec{V}_{02}(\vec{r},t)] \cdot [\overleftrightarrow{I} + \hat{n}_1(\vec{r})\hat{n}_1(\vec{r})] \ .$$

Here, W is the window surface, $\overleftrightarrow{I}$ is the identity dyadic, $\hat{n}_1(\vec{r})$ is the normal at $\vec{r}$ on W pointing away from nucleus 1, and $\vec{V}_{01}$ and $\vec{V}_{02}$ are the drift velocities of the two nuclei. Again, the formula contains no free parameters. There is, at present, no formula to describe the intermediate case in which there exists a constriction between parts of the system, but that constriction cannot be treated as small.

Such simple formulae reflect a simple picture of nuclei. Detailed examination of the assumptions behind this picture suggests that the formulae are indeed a first approximation to reality when deformations, relative speeds, and window sizes are all small, but that even then significant corrections would be needed for an accurate treatment. Some errors, such as those proceding from the diffuseness of nuclear surfaces, can be eliminated by refining the one-body model; others, such as shell effects, necessarily escape

the model. These errors may sometimes be of the same order of magnitude as the one-body results themselves.

Once the basic model is expounded and its underlying principles examined, it is developed in two directions. First, there are descriptions of the application of the model directly to a number of important situations: nuclear vibrations, fission, collisions, the diffusion of properties between nuclei, and giant dipole resonances. To obtain results rapidly and simply, these preliminary calculations are allowed to be crude in varying degrees. The results themselves diverge from experiment no more than could be attributed to the respective crudities, but, since there is no certainty to such attributions, the most that can be said with assurance is that the one-body model is not contradicted by the experiments considered here. In particular, one-body processes seem capable of accounting for the large losses of translational and rotational kinetic energy characteristic of deep-inelastic nuclear collisions. A further, purely theoretical point emerges: dissipation is often more important than inertial or kinetic terms in discussing deformational degrees of freedom.

Next, suppose that a nucleon that has crossed through a window from one nucleus to another passes through the nucleus it has entered without suffering any two-body collisions. It will then eventually reach a nuclear surface. If the relative nuclear motion

is large enough, the nucleon may go "over" the wall and be emitted from the nuclear system. This development is treated in a separate chapter, III, because it concentrates on the motion of nucleons instead of nuclei. It nonetheless concerns an average property of nuclei, because the nucleons initially crossing the window are described statistically, not in terms, say, of shell-model states. (This statistical approach is pressed quite far, quite successfully in calculations of the diffusion of properties between nuclei [3]-[4].) The final laboratory distributions expected in these "Fermi jets" of nucleons are notably focused in phase space and often contain a component moving much more rapidly in the laboratory than the projectile ever did, a result of internal Fermi motion in combination with relative nuclear motion. Experimental detection of Fermi jets would not only be intrinsically interesting, it would also add support to the wall and window pictures, the core of the one-body model, and, if sufficiently profuse, provide information on details of nuclear collisions. It must be pointed out, however, that the activity of other emission mechanisms may render detection difficult and that two-body effects are likely to weaken jetting, perhaps fatally.

CHAPTER II

ONE-BODY DISSIPATION

A. INTRODUCTION

A dynamical problem can generally be analyzed into the interplay of potential energy, dissipative, and kinetic energy(i.e., inertial) terms. If all degrees of freedom are followed explicitly, the problem can always be expressed solely through potential and kinetic terms. Convenience or necessity often require that a few, distinguished coordinates be followed explicitly as they evolve in time under the properly averaged influence of the rest, whose evolution is treated statistically, if at all. The more readily a coordinate may be observed experimentally, the more likely it is to be distinguished as a collective, or macroscopic, coordinate from the remaining internal, or microscopic, coordinates. The average influence of the undistinguished coordinates on the distinguished ones can be expressed by a function of the distinguished coordinates that is called dissipative because statistical or thermal treatment of the undistinguished variables generally requires that flows of energy from distinguished to undistinguished coordinates be at least partly irreversible.

Average nuclear dynamics--that part of nuclear dynamics

which varies slowly with atomic weight and number--is sought, so average potential, dissipation, and kinetic terms are required. The average potentials are already known to be given by the liquid drop model, for isolated nuclei, and by the proximity force [2], for (nuclear) interactions between nuclei. The kinetic terms corresponding to translations and rotations are also understood; nuclear masses are known and there is much information about nuclear moments of inertia. Little is known about the inertias corresponding to nuclear deformations, but we shall see that dissipation often turns out to dominate kinetic energy in deformation dynamics. Average nuclear dynamics thus demands just one new thing: the average dissipation.

To find it, the discussion in Chapter I suggests that the independent particle model be enlisted. In this model, nucleons do not interact (directly) with each other, but only with the common nuclear potential. Dissipation can occur, therefore, only when nucleons interact with the nuclear surface, if there exists a frame in which <u>changes</u> in the nuclear and Coulomb potentials in the nuclear interior can be neglected. Experience of nuclear statics leads one to expect that such "<u>one-body dissipation</u>," involving only one nucleon, will dominate two-body dissipation, involving the residual interaction of two nucleons.

Chapter II is arranged as follows. The wall formula is

derived in Section B and the window formula, in Section C. The assumptions introduced in Sections B and C are examined in detail in Section D. Application of the wall and window formulae to nuclear vibrations, fission, collisions, the diffusion of properties between nuclei, and giant dipole resonances is then discussed in Section E. Summary and discussion of these results plus their future extension and exploitation are the themes of the final section, F [5]-[6].

B. THE WALL FORMULA

Section A's preview of the one-body model proposed to neglect changes in the potential inside nuclei. Also, nucleons interact conservatively with static non-uniformities in the potential, so such non-uniformities can be ignored in dissipation calculations. The interior potential is therefore taken to be uniform. The actual surface is thin; it can be made infinitely thin as an approximation. These observations about the interior and the surface mean that the nuclear potential can be approximated as a square well. A nucleus is then similar to a non-interacting gas in a box where the gas represents the nucleons and the box, the nuclear surface. This model is well defined, but it allows the box and the gas to be quite independent, whereas the nuclear surface is just a manifestation of the nucleons. This self-consistency question will be deferred until Section D. Furthermore, calculations can be

performed in the model no matter how fast the box is moving with respect to the gas, but Section D will also show that the model itself diverges from reality as the relative speeds increase. This section and the next one present, because they are of some theoretical interest and for the sake of completeness, formulae valid in the model to all orders in the box motion, but only the terms of lowest order are physically significant.

To find the power transmitted <u>from</u> the box <u>to</u> the gas, recall first that power is just force times velocity. The force exerted on the gas by a surface element, $d\vec{S}$, is

$$d\vec{F} = -\overleftrightarrow{P} \cdot d\vec{S} \quad , \tag{2.1}$$

where $\overleftrightarrow{P}$ is the pressure tensor of the gas. Let $\vec{V}$ be the velocity of the surface element as shown in Fig. 2. Then, the total power absorbed by the gas is

$$\frac{dE_{gas}}{dt} = \oint_S d\vec{F} \cdot \vec{V} = -\oint_S dS\ \vec{V}(\vec{r}) \cdot \overleftrightarrow{P}(\vec{r}) \cdot \hat{n}(\vec{r}) \quad , \tag{2.2}$$

where $\vec{r}$ is a point on the surface, S, with a normal, $\hat{n}(\vec{r})$. ($d\vec{S} = dS\ \hat{n}$.) Note that equation (2.2) implicitly assumes that $\overleftrightarrow{P}$ is a local function of the surface, which is true only if the gas particles can be localized, in other words, are classical. In the spirit of the calculation, which seeks average effects, not shell structure, the nuclear system need only be "large," which many are, and the surface not too contorted for this assumption to be

approximately correct.

The calculation of the pressure is very like the derivation of the ideal gas law. Only the motion of the box introduces anything new. Indeed, in the limit of zero motion, the pressure reduces to the ideal gas result and, to the next order in the wall velocity, the pressure increases slightly as the wall is slowly pressed in and decreases as it moves out, just as one might have expected.

To actually find the pressure, observe first that $d\vec{F}$ in equation (2.1) is just the momentum transfer from $d\vec{S}$ to the gas, per unit time. This transfer rate is the product of the rate with which gas particles collide with the wall and of the momentum changes they suffer thereby.

Let $F(\vec{v},\vec{r})$ describe the distribution of gas particles so that

$$F(\vec{v},\vec{r})\ d\vec{v}\ d\vec{r} \tag{2.3}$$

is the number of particles with velocities $\vec{v}'$ and positions $\vec{r}'$ in the region $(\vec{r},\ \vec{r}+d\vec{r})\ \times\ (\vec{v},\ \vec{v}+d\vec{v})$. The collision flux per unit volume of velocity space, $\Phi(\vec{v},\vec{r})$ between particles with velocity $\vec{v}$ and the wall can be related to F with the aid of Fig. 3. In the rest frame of $d\vec{S}$, the only particles with velocity

$$\vec{u} = \vec{v} - \vec{V} \tag{2.4}$$

that can collide with $d\vec{S}$ during the time interval t, t+dt are those

value of Φ, but the fluctuations would be large.

At each point in space-time, the number of particles in a particular velocity interval in the wall frame is equal to the number in the corresponding lab interval:

$$F(\vec{v})d\vec{v} = \bar{F}(\vec{u})\, d\vec{u} \quad , \tag{2.6}$$

whenever $\vec{v}$, $\vec{u}$, $d\vec{v}$, and $d\vec{u}$ are related by equation (2.4). Equations (2.5), (2.6), and (2.2) then imply

$$\Phi(\vec{v},\vec{r},t) = \theta[(\vec{v}-\vec{V})\cdot\hat{n}]\ (\vec{v}-\vec{V})\cdot\hat{n}\ \ F(\vec{v},\vec{r},t) \quad . \tag{2.7}$$

The next step is to find the momentum change of a colliding particle. Having already assumed that the particles are classical and that the surface is sharp, it must further be assumed that the particles make elastic collisions with a wall compared to which they have relative masses that are wholly negligible. As Fig. 4 illustrates, the particle velocities in the wall frame before and after collision are related by

$$u_n' = -u_n \quad , \qquad \vec{u}_t' = \vec{u}_t \quad . \tag{2.8}$$

(The velocities after collision are superscripted `prime' and the normal and tangential components of velocities are subscripted `n' and `t.') Therefore, the change in momentum is

in the volume indicated in Fig. 3 at t and every such particle will so collide. The number of such particles with lab velocities in the range $\vec{v}$, $\vec{v}+d\vec{v}$ is then the product of the number density of particles and the volume:

$$\Phi(\vec{v},\vec{r},t)d\vec{v}\ dS\ dt = [\bar{F}(\vec{u},\vec{r},t)d\vec{u}][(dS)(\vec{u}\cdot\hat{n}dt)\theta(\vec{u}\cdot\hat{n})] \quad . \qquad (2.5)$$

$\bar{F}$ is the distribution function in the wall frame and $\theta(\vec{u}\cdot\hat{n})$ is inserted to exclude particles with $\vec{u}\cdot\hat{n}<0$, which will leave the wall, not collide with it.

The zero limits of the ranges $d\vec{v}$, dS, and dt will be taken, so variations of Φ and $\bar{F}$ with their arguments are negligible. For the same reason, $d\vec{S}$ remains planar and, in this frame, motionless. In general, its size, shape, orientation, and velocity field would change. Two-body collisions would also scatter some particles in the volume at t so that they would not strike $d\vec{S}$ during t, $t+dt$ with velocity in $\vec{u}$, $\vec{u}+d\vec{u}$ and would scatter some particles that were outside the volume at t or that had the wrong initial velocities into $d\vec{S}$ during t, $t+dt$ with velocity in $\vec{u}$, $\vec{u}+d\vec{u}$. This effect also disappears when the limit is taken, so that the independent particle approximation need not be invoked. Of course, it might turn out that all finite values of $d\vec{v}$, dS, and dt that meet these conditions would be so small that the value of expression (2.5) would be much less than 1. In that case, (2.5) would still yield the correct mean

$$\Delta\vec{p} = m(\vec{v}' - \vec{v}) = m(\vec{u}' - \vec{u}) = m(u_n' - u_n)\hat{n}$$
$$= -2m\, u_n \hat{n} = -2m\, \vec{u}\cdot\hat{n}\, \hat{n} = -2m(\vec{v} - \vec{V})\cdot\hat{n}\, \hat{n} \quad . \tag{2.9}$$

The pieces of $d\vec{F}$ are now in hand:

$$d\vec{F} = \int_{(\infty)} d\vec{v}\, [\Phi(\vec{v},\vec{r},t)dS]\, \Delta\vec{p}(\vec{v},\vec{r},t)$$
$$= -2m \int_{(\infty)} d\vec{v}\, F(\vec{v},\vec{r},t)\, \theta[(\vec{v} - \vec{V})\cdot\hat{n}][(\vec{v} - \vec{V})\cdot\hat{n}]^2\, d\vec{S} \quad , \tag{2.10}$$

where the indicated region of velocity integration is all velocity space. In view of equation (2.1), the pressure is evidently scalar--

$$\overleftrightarrow{P} = P\, \overleftrightarrow{I} \quad , \tag{2.11}$$

where $\overleftrightarrow{I}$ is the identity tensor--and

$$P(\vec{r},t) = 2m \int_{(\infty)} d\vec{v}\, F(\vec{v},\vec{r},t)\, \theta\{[\vec{v} - \vec{V}(\vec{r},t)]\cdot\hat{n}(\vec{r},t)\}$$
$$\times \{[\vec{v} - \vec{V}(\vec{r},t)]\cdot\hat{n}(\vec{r},t)\}^2 \quad . \tag{2.12}$$

Hence, equation (2.2) becomes

$$\frac{dE_{gas}}{dt} = -\oint_S dS\ \vec{V}\cdot\hat{n}P$$

$$= -2m \oint_S dS\ \vec{V}\cdot\hat{n} \int_{(\infty)} d\vec{v}\ F(\vec{v},\vec{r},t)\ \theta[(\vec{v}-\vec{V})\cdot\hat{n}][(\vec{v}-\vec{V})\cdot\hat{n}]^2 \quad . \tag{2.13}$$

The expression for P with $\vec{V}$ set to zero arises in standard derivations of the ideal gas law.

The power absorbed and the pressure exerted by a gas in a box can now be calculated at any instant at which the distribution is known. The distribution function of an isolated, static nucleus can be taken to be a zero-temperature Fermi-Dirac distribution, which is equivalent to averaging over the detailed single-particle states. What happens to the distribution if the nucleus is deforming and interacting with another nucleus? In principle, the time evolution of the distribution could be followed, but to do so would be difficult and, in any case, would involve just that detailed solution of single-particle orbits which experience of nuclear statics suggests should be unnecessary at the level of approximation sought here. Instead, picture a deforming box filled with swarming gas particles. They collide only with the walls, bouncing rapidly to and fro. As long as the wall and its deformations are not too symmetric, the particle distribution bombarding the wall will tend to be randomized in the following

sense. The distribution at each point should not favor any velocity direction, nor should it depend on position. In other words,

$$F(\vec{v},\vec{r},t) = F(|\vec{v}|,t) \quad . \tag{2.14}$$

In physics, randomization often procedes subject to constraints. In this case, note that equation (2.14) leads to a zero mean velocity, which is nonsense if the nucleus is moving with a constant velocity. Instead,

$$F(\vec{v},\vec{r},t) = F_r[\vec{v} - \vec{V}_o(\vec{r},t),t] \tag{2.15a}$$

$$F_r(\vec{v},t) = F_r(|\vec{v}|,t) = F_r(v,t) \tag{2.15b}$$

must be allowed. The drift velocity, $\vec{V}_o$, will be independent of $\vec{r}$ for translations, but not for rotations; it will change with time if the overall nuclear velocity or angular velocity changes. The drift velocity will be specified more quantitatively in Section D. Since, for example, a Fermi gas originally at zero temperature might be heated by dissipation, an explicit time dependence in the right hand side of equations (2.14) and (2.15) has been included. In this example, F_r would depend on time only through an increasing temperature.

Equation (2.15) changes (2.12) and (2.13) into

$$P(\vec{r},t) = 2m \int_{(\infty)} d\vec{v}\ F_r(v,t)\ \theta\Big[\{\vec{v} - [\vec{V}(\vec{r},t) - \vec{V}_o(\vec{r},t)]\} \cdot \hat{n}(\vec{r},t)\Big]$$
$$\times \Big[\{\vec{v} - [\vec{V}(\vec{r},t) - \vec{V}_o(\vec{r},t)]\} \cdot \hat{n}(\vec{r},t)\Big]^2 \qquad (2.16)$$

and

$$\frac{dE_{gas}}{dt}(t) = -\oint_S dS\ \vec{V}\cdot\hat{n}\ P \qquad (2.17a)$$

$$= -2m \oint_S dS\ \vec{V}\cdot\hat{n} \int_{(\infty)} d\vec{v}\ F_r(v,t)\ \theta\{[\vec{v}-(\vec{V}-\vec{V}_o)]\cdot\hat{n}\} \qquad (2.17b)$$
$$\times\ \{[\vec{v} - (\vec{V}-\vec{V}_o)]\cdot\hat{n}\}^2 \quad .$$

These equations are the general wall formulae. They will soon be expanded and specialized, but it is instructive to examine some of their general properties first.

To begin with, P is properly non-negative. Next, suppose that $\vec{V} = \vec{V}_o \equiv 0$--the traditional static case. Then,

$$P(\vec{r},t) = 2m \int_0^\infty dv\ F_r(v)\ v^4 \int d\hat{v}\ \theta(v\ \hat{v}\cdot n)(\hat{v}\cdot\hat{n})^2$$
$$= \frac{4\pi}{3}\ m \int_0^\infty dv\ F_r(v)\ v^4 = \frac{1}{3}\ m \int_{(\infty)} d\vec{v}\ F_r(v)v^2 \quad . \qquad (2.18)$$

F is normalized so that the total number of gas particles is

$$N = \int_S d\vec{r} \int_{(\infty)} d\vec{v}\ F(\vec{v},\vec{r},t) = \int_S d\vec{r} \int_{(\infty)} d\vec{v}\ F_r[\vec{v} - \vec{V}_o(\vec{r},t),t]$$

$$= \int_S d\vec{r} \int_{(\infty)} d\vec{v}\ F_r(\vec{v},t) = \Omega(t) \int_{(\infty)} d\vec{v}\ F_r(\vec{v},t) \quad , \tag{2.19}$$

where Ω is the volume of the box. Consequently, the mean of a function of velocity, $h(\vec{v})$, with respect to F_r is

$$\langle h(\vec{v}) \rangle_r = \int_{(\infty)} d\vec{v}\ F_r(\vec{v},t)\ h(\vec{v}) \Big/ \int_{(\infty)} d\vec{v}\ F_r(\vec{v},t)$$

$$= [\Omega(t)/N] \int_{(\infty)} d\vec{v}\ F_r(\vec{v},t)\ h(\vec{v}) \quad . \tag{2.20}$$

P becomes

$$P(\vec{r},t) = \frac{2}{3}\ \frac{N}{\Omega(t)}\ \langle \frac{1}{2}\ m\vec{v}^2 \rangle_r\ (t) \quad . \tag{2.21}$$

For a Maxwell-Boltzmann distribution,

$$\langle \frac{1}{2}\ m\vec{v}^2 \rangle_r = \frac{3}{2}\ \kappa T \tag{2.22}$$

and

$$P(\vec{r},t)\ \Omega(t) = N\ \kappa\ T(t) \tag{2.23}$$

--the ideal gas law. The same conclusion may be reached more generally by noting that

$$P_{\text{ideal gas}}(\vec{r},t) = \frac{2}{3} U(\vec{r},t)/\Omega \quad , \tag{2.24}$$

where

$$U(t) = N \langle \frac{1}{2} m\vec{v}^2 \rangle_r (t) \tag{2.25}$$

is the total internal energy of the gas. At the same time,

$$\frac{dE_{gas}}{dt}(t) = 0 \quad , \tag{2.26}$$

since $\vec{V} \equiv 0$. Everything is as it should be in this limiting case.

Now suppose that the wall is moving very rapidly. The integrand in equation (2.16) can never be negative, but, as

$$U(\vec{r},t) \equiv [\vec{V}(\vec{r},t) - \vec{V}_o(\vec{r},t)] \cdot \hat{n}(\vec{r},t) \tag{2.27}$$

grows, the region where the integrand is non-zero shrinks and, for each fixed point within the region, decreases in value. In consequence,

$$\lim_{U \to +\infty} P = 0 \quad . \tag{2.28}$$

This positive limit corresponds to infinitely rapid expansion: the gas particles can never catch up with the wall in order to collide with it. The negative limit corresponds to compression, for which the pressure should become infinite, as inspection of equation (2.16) readily confirms.

One of the first questions raised by the wall formulae is,

Do they behave properly under Galilean transformations? Suppose equations (2.12) and (2.13) refer to the original frame with respect to which a primed frame is moving with velocity $\vec{B}$. In the second frame,

$$S' = S \quad , \quad \vec{V}'(\vec{r},t) = \vec{V}(\vec{r},t) - \vec{B} \quad , \quad F'(\vec{v},\vec{r},t) = F(\vec{v}+\vec{B},\vec{r},t) \quad . \tag{2.29}$$

Equation (2.12) immediately becomes

$$P'(\vec{r},t) = P(\vec{r},t) \quad , \tag{2.30}$$

but

$$\begin{aligned} \left(\frac{dE_{gas}}{dt}\right)'(t) &= -\oint_S dS\ \vec{V}'\cdot\hat{n}\ P' = -\oint_S dS\ (\vec{V}-\vec{B})\cdot\hat{n}\ P \\ &= \frac{dE_{gas}}{dt}(t) + \vec{B}\cdot\oint_S dS\ P\hat{n} \quad . \end{aligned} \tag{2.31}$$

This should be no surprise. Both force (in the absence of mass changes) and length are Galilean invariants, so pressure is, too. Time is also invariant, but energy is not, so power will not be, either. For an object with mass M and velocity $\vec{Q}$,

$$E' = \frac{1}{2} M(\vec{Q} - \vec{B})^2 = E - M\vec{Q} \cdot \vec{B} + \frac{1}{2} M\vec{B}^2 \tag{2.32a}$$

$$\left(\frac{dE}{dt}\right)' = \frac{dE'}{dt} - \frac{d(M\vec{Q})}{dt} \cdot \vec{B} = \frac{dE}{dt} - \vec{B} \cdot \vec{F} \quad , \tag{2.32b}$$

where $\vec{F}$ is the force on the object. In equation (2.31),

$$\vec{F}_{gas} = - \oint_S dS \; P \; \hat{n} \quad . \tag{2.33}$$

The existence of such a force means that the gas and box tend to separate. If the gas represents nucleons and the box represents the nuclear surface, that is absurd. Self-consistency requires that $\vec{F}_{gas}$ vanish, with consequences to be discussed in detail later. With this requirement, the dissipative power can be determined without referring to a particular inertial frame. If there are no drift velocities and if the distribution function is isotropic, then the pressure in equation (2.18) is independent of position. Equation (2.33) then becomes

$$\vec{F}_{gas} = -P \oint_S dS \; \hat{n} = 0 \quad , \tag{2.34}$$

which is zero because the integral vanishes identically for any box S (see Appendix A). This is obviously true also for any uniform drift. Either a non-uniform drift or a non-isotropic F_r can produce a non-zero $\vec{F}_{gas}$. The first possibility will be examined later. The second is ruled out by our randomization hypothesis. Appendix B

presents an example in which the distribution function is non-isotropic, but is homogeneous and satisfies $\langle\vec{v}\rangle = 0$. The box too is static, yet $\vec{F}_{gas} \neq 0$.

The $\vec{v}$-integrals in equation (2.16), like some in the next section can be performed in part and simplified as explained in Appendix C.1. When equations (2.16) and (C11) are compared with the aid of (C1)-(C3), one discovers that

$$P(r,t) = \rho \left\langle \frac{1}{3} \frac{(v-U)^3}{v} + \varepsilon(U)\, \theta(|U|-v)\, \frac{1}{3} \frac{(|U|-v)^3}{v} \right\rangle_r , \tag{2.35}$$

where ρ is the mass density of the gas.

For sufficiently slow deformations,

$$|U| \ll \langle v\rangle_r . \tag{2.36}$$

Appendix C.2 shows how equation (2.35) can be approximated in this regime. To do so, several more very credible assumptions are needed. First, F_r is assumed not to be radically skewed in any respect, so that

$$\langle v^s\rangle_r = O[(\langle v\rangle_r)^s] . \tag{2.37}$$

Secondly, F_r is assumed to be roughly uniform over the interval from 0 to $\langle v\rangle_r$ or to be peaked around $\langle v\rangle_r$, as the first two drawings in Fig. 5 illustrate, but it is assumed <u>not</u> to be concentrated near zero, in the interval from 0 to $|U|$, as in the third drawing. Both

of these assumptions are true of Fermi-Dirac distributions of any temperature and of Maxwell-Boltzmann distributions. Using equation (C27) and the definitions (C12) and (C15),

$$P(\vec{r},t) = \frac{1}{3}\rho\langle v^2\rangle_r - \rho\langle v\rangle_r\,[\vec{V}(\vec{r},t) - \vec{V}_o(\vec{r},t)]\cdot\hat{n}(\vec{r},t) + O[(U/\langle v\rangle_r)^2\langle v^2\rangle_r] \quad . \tag{2.38}$$

The ideal gas law is again recovered in the first term. The next term is the lowest order correction. If the wall is pushed in (relative to the drift motion), the pressure rises; if it is pulled out, the pressure drops.

Likewise, equation (2.17) for the power becomes

$$\begin{aligned}\frac{dE_{gas}}{dt} &= -\frac{1}{3}\rho\langle v^2\rangle \oint_S dS\,\vec{V}\cdot\hat{n} + \ldots \\ &= P_{\text{ideal gas}}\frac{d\Omega}{dt} + \rho\langle v\rangle_r \oint_S dS\,\vec{V}\cdot\hat{n}\,(\vec{V}-\vec{V}_o)\cdot\hat{n} + \ldots \quad .\end{aligned} \tag{2.39}$$

The equality of the two expressions for the first term in the expansion follows from another geometrical result, equation (A7). Since nuclear matter is but slightly compressible, this term can be neglected. The first term is reversible, for it describes adiabatic expansion and compression. The second term--

$$\frac{dE_{gas}}{dt} = \rho \langle v \rangle_r \oint_S dS\, \vec{V}\cdot\hat{n}(\vec{V} - \vec{V}_o) \cdot \hat{n} + \ldots \tag{2.40}$$

--admits irreversibilty and will be wholly irreversible, provided $\vec{V}_o$ transforms like a velocity under time reversal [7].

Equations (2.35) and (2.38) for the pressure and (2.39) and (2.40) for the power are the specialized wall formulae corresponding to the more general expressions in (2.16) and (2.17). Equation (2.40) provides a simple expression, in which there are no adjustable parameters, for the one-body dissipation of the energy of wall motion into gas motion. This presumes, of course, that deformation is slow, the gas compressibility is negligible, and the drift velocity is prescribed somehow.

F_r must be known if the wall formula is to be used. A zero-temperature Fermi-Dirac gas is the natural choice inspired by experience of average nuclear statics. Let v_F be the Fermi speed,

$$v_F = \frac{2\pi\hbar}{m}\left(\frac{3}{16\pi}\ \frac{A}{\Omega}\right)^{1/3} = \frac{\pi}{2}\left(\frac{3}{\pi}\right)^{2/3} \frac{\hbar}{mr_o} \quad , \tag{2.41}$$

where A is the atomic weight and r_o is the nuclear radius parameter (so that the nuclear radius is

$$R = r_o A^{1/3} \quad). \tag{2.42}$$

Then,

$$F_r(v) = \frac{N}{\Omega} \frac{1}{\frac{4}{3}\pi v_F^{\,3}} \theta(v_F - v) \quad , \tag{2.43}$$

$$\langle v^n \rangle_r = \frac{3}{n+3} v_F^{\,n} \quad , \tag{2.44}$$

and

$$\langle \theta(|U| - v)\, v^n \rangle_r = \theta(|U| - v_F) \langle v^n \rangle_r + \theta(v_F - |U|) \frac{3}{n+3} \frac{|U|^{n+3}}{v_F^{\,3}} \quad , \tag{2.45}$$

wherefore

$$\begin{aligned} P = \rho\Big[& \theta(v_F - |U|) \left(\frac{1}{5} v_F^{\,2} - \frac{3}{4} v_F U + U^2 - \frac{1}{2} v_F^{\,-1} U^3 + \frac{1}{20} v_F^{\,-3} U^5 \right) \\ & + \theta(|U| - v_F)\, \theta(-U) \left(2U^2 + \frac{2}{5} v_F^{\,2} \right) \Big] \quad . \end{aligned} \tag{2.46}$$

Expression (2.41) presupposes that the nucleus is composed of A identical nucleons, each of which can have four possible orientations in spin-isospin space (e.g., up/proton or down/neutron) or, equivalently, of equal numbers of protons and neutrons. Appendix D analyzes the effects of neutron excesses and temperatures on one-body formulae and finds that both are small. This may seem surprising, since 100 or 200 MeV can sometimes be dissipated in collisions, but, even then, the excitation energy <u>per nucleon</u> and the temperature remain small compared to the Fermi energy.

C. THE WINDOW FORMULA

Consider now two nuclei, 1 and 2, connected by the small window, W, shown in Fig. 6. Each nucleus is idealized as a gas of semiclassical, independent particles inside a classical box. Before contact, the two gases have the same, normal nuclear density. They may have been heated by dissipation of collective, deforming motion, but, as shown in Appendix D, this effect can be neglected. Their drift velocities, however, are quite unequal. Once the two nuclei make contact, nucleon motion will prevent the formation of significant density inhomogeneities, provided that the relative nuclear motion is sufficiently slow. As the relative nuclear motion becomes more rapid, this refinement of the gas/box model becomes inconsistent both with the model and with reality. Here, the mathematical consequences of the refinement will sometimes be worked out to all orders in the relative nuclear velocity, but again only the lowest order terms can be significant. With this refinement, the two nuclei form one nuclear system to the extent that there is one, sharp surface, within which the potential is flat. In particular, the connecting region is a wide open window for nucleons. Since the window grows in size from zero, the elimination of the finite difference between the two drift velocities need <u>not</u> be rapid on the collision time scale. The two nuclei and their connection are distinguished only by differences among their

respective velocity distributions. The connection is, in reality, a three-dimensional region. It may nonetheless be approximated as a two-dimensional, possibly non-planar, surface, if it is small enough. The location and movement of this surface will be discussed later; for now, let them be arbitrary.

Two nuclei in contact exert forces on each other due to the passage of nucleons back and forth through the window, carrying momentum as they go. There are also Coulomb and nuclear potential forces, but such forces are familiar. In this picture, the window acts merely as an immaterial classifier: as soon as a nucleon crosses it, its momentum is to be subtracted from that of the nucleus it has left and added to that of the nucleus it has entered. Some such nucleons may actually escape the two-nucleus system altogether. This possibility is the subject of Chapter III and it is shown there that the effect can have only a small influence on the window formula.

The detailed calculation begins with the notation introduced by Fig. 6. The normal pointing outward from nucleus 1 at point $\vec{r}$ on W is $\hat{n}_1$; the corresponding normal for 2 is

$$\hat{n}_2 = -\hat{n}_1 \quad . \tag{2.47}$$

The window itself can move and deform; let $\vec{V}$ be its velocity at $\vec{r}$. The force on 1 due to particle exchange is just the difference between the rates of momentum transfer into and out of 1:

$$\vec{F}_1^{\text{exchange}}(W) = \int dW \int_{(\infty)} d\vec{v} \left\{ \theta[(\vec{v}-\vec{V})\cdot\hat{n}_2]\ (\vec{v}-\vec{V})\cdot\hat{n}_2\ F_2(\vec{v},\vec{r},t) \right.$$

$$\left. -\theta[(\vec{v}-\vec{V})\cdot\hat{n}_2]\ (\vec{v}-\vec{V})\cdot\hat{n}_1\ F_1(\vec{v},\vec{r},t) \right\} m\vec{v} \quad , \tag{2.48}$$

to obtain which use has been made of equation (2.7) for the flux. The symbols F_1 and F_2 denote the distribution functions in 1 and 2. Nuclear matter is all rather alike, so it is at least a good first approximation to say that

$$F_i(\vec{v},\vec{r},t) = F_r[\vec{v} - \vec{V}_{oi}(\vec{r},t),t] \quad , \tag{2.49}$$

where i runs from 1 to 2 and F_r is isotropic. The force can then be re-written as

$$\vec{F}_i^{\text{exchange}}(W) = m \int_W dW \int_{(\infty)} F_r(v,t) \left[-\theta(+\vec{v}\cdot\hat{n}_1 - U_1)(+\vec{v}\cdot\hat{n}_1 - U_1) \right.$$

$$\times\ (\vec{v}+\vec{V}_{01}) + \theta(-\vec{v}\cdot\hat{n}_1 - U_2)(-\vec{v}\cdot\hat{n}_1 - U_2)(\vec{v}+\vec{V}_{02}) \Big] \ , \tag{2.50}$$

where

$$U_i(\vec{r},t) \equiv [\vec{V} - \vec{V}_{oi}(\vec{r},t)]\cdot\hat{n}_i \quad , \tag{2.51}$$

in analogy to definition (2.27). Note well that $\hat{n}_i$, not $\hat{n}_1$, is used in (2.51). The components of $\vec{v}$ that are perpendicular to $\hat{n}_1$ integrate to zero by symmetry. Equation (2.50) is the general window formula.

In the static case, when $\vec{V}$ and both drift velocities are zero, one might expect the force to vanish. Instead,

$$\vec{F}_1^{\text{exchange}}(W) = -P_{\text{ideal gas}} \int dW\, \hat{n}_1 \quad . \tag{2.52}$$

A pressure exists everywhere in the interior of any gas. If the gas is composed of independent particles, the pressure will be uniform and isotropic. The pressure manifests itself as a force on any surface--material or immaterial--inside the gas. Nucleus 1 will not begin to move, however. The <u>total</u> force on nucleus 1 caused by interactions of the gases and boxes is the exchange force <u>plus</u> the wall force exerted by the surface of 1, S_1:

$$\vec{F}_1^{\text{one-body}} = \vec{F}_1^{\text{exchange}}(W) + \vec{F}_1^{\text{wall}}(S_1) \quad . \tag{2.53}$$

In calculating the force on a nucleus, the nucleus has been identified with its gas. Therefore, equation (2.33) may be invoked and, in this static case only, reduced to

$$\vec{F}_1^{\text{wall}} = -\int_{S_1} dS\, P(\vec{r},t)\, \hat{n} \tag{2.54a}$$

$$= -P_{\text{ideal gas}} \int_{S_1} dS\, \hat{n} \quad . \tag{2.54b}$$

The union of S_1 and W forms a closed surface, over which Appendix A says that the integral of the outward-pointing normal vanishes.

Substitution of equations (2.52) and (2.54) in (2.53) then leads to

$$\vec{F}_1^{\text{one-body}} = 0 \quad . \tag{2.55}$$

In the general case, equation (2.53) still holds. The exchange contribution must be calculated from (2.50) and from the reductions to be made from it presently, while the wall contribution is given by (2.54a) and the pressure wall formulae in Section B. The interesting parts of the force are those that are really new and not just aspects of the wall formula. Examination of the static case showed that some old features are embedded in the exchange force, but it also suggested that these terms can be spotlighted and even canceled out by looking at the total one-body force. To do so, first assume that

$$\vec{V}(\vec{r},t) = \vec{V}_o(\vec{r},t) \quad . \tag{2.56}$$

The wall formula, (2.16), then indicates that

$$P(\vec{r},t) = P_{\text{ideal gas}} \quad , \tag{2.57}$$

just as in the static case. Equation (2.54) can still be used in (2.53). To be sure, in more general situations

$$\vec{F}_1^{\text{one-body}} = \left[\vec{F}_1^{\text{exchange}}(W) + \vec{F}_1^{\text{wall}}(S;\ \vec{V} \equiv \vec{V}_o)\right] + \left[\vec{F}_1^{\text{wall}}(S) - \vec{F}_1^{\text{wall}}(S;\ \vec{V} \equiv \vec{V}_o)\right] \quad , \tag{2.58}$$

but the second, additional term will have nothing directly to do with the window. The upshot is that, in calculating the total one-body force, the uninteresting, lowest order terms in both the exchange- and the wall-contributions can be ignored because they cancel.

The machinery of Appendix C can be applied to the general window formula just as it was to the general wall formula. First, let

$$\vec{U}_i = \vec{V} - \vec{V}_{oi} \quad , \qquad \vec{U}_{it} = \vec{U}_i - U_i\hat{n}_i \tag{2.59}$$

(the subscript `t' is an abbreviation for `transverse'). Then

$$\vec{F}_1^{\text{exchange}}(W) =$$

$$\rho \int_W dW \Big[-\frac{1}{6} \left\langle \frac{(v-U_1)^3}{v} \right\rangle_r \hat{n}_1 + \frac{1}{4} \left\langle \frac{(v-U_1)^2}{v} \right\rangle_r (\vec{U}_{1t} - \vec{V})$$

$$- \frac{1}{6} \left\langle \frac{(v-U_2)^3}{v} \right\rangle_r \hat{n}_1 - \frac{1}{4} \left\langle \frac{(v-U_2)^2}{v} \right\rangle_r (\vec{U}_{2t} - \vec{V})$$

$$- \varepsilon(U_1) \frac{1}{6} \left\langle \theta(|U_1| - v) \frac{(|U_1| - v)^3}{v} \right\rangle_r \hat{n}_1$$

$$- \frac{1}{4} \left\langle \theta(|U_1| - v) \frac{(|U_1| - v)^2}{v} \right\rangle_r (\vec{U}_{1t} - \vec{V})$$

$$- \varepsilon(U_2) \frac{1}{6} \left\langle \theta(|U_2| - v) \frac{(|U_2| - v)^3}{v} \right\rangle_r \hat{n}_1 \tag{2.60}$$

$$+ \frac{1}{4} \left\langle \theta(|U_2| - v) \frac{(|U_2| - v)^2}{v} \right\rangle_r (\vec{U}_{2t} - \vec{V}) \Big] .$$

[Like equation (2.48), this expression is the difference between two terms that are identical except for an interchange of 1 and 2]. Furthermore,

$$\vec{F}_1^{\text{exchange}}(W) + \vec{F}_1^{\text{wall}}(S;\ \vec{V} \equiv \vec{V}_o)$$

$$= \frac{1}{4}\rho\langle v\rangle_r \int_W dW\ (\vec{U}_1-\vec{U}_2)\cdot(\overleftrightarrow{I}+\hat{n}_1\hat{n}_1) + O\left[\langle v\rangle_r |U|\left(\frac{|U|}{\langle v\rangle_r}\right)\right]$$

$$= -\frac{1}{4}\rho\langle v\rangle_r \int_W dW\ [\vec{V}_{01}(\vec{r},t) - \vec{V}_{02}(\vec{r},t)]\cdot[\overleftrightarrow{I} + \hat{n}_1(\vec{r})\hat{n}_1(\vec{r})] + \ldots$$

$$\cong -\frac{1}{4}\rho\langle v\rangle_r\ A(W)\ (\vec{V}_{01} - \vec{V}_{02})\cdot(\overleftrightarrow{I} + \hat{n}_1\hat{n}_1) \quad , \qquad (2.61)$$

where $|U|$ stands for any of $|\vec{V}|$, the $|\vec{V}_{oi}|$, or the $|\vec{U}_i|$, and $A(W)$ is the window area [8]. The second and third expressions in equation (2.61) constitute versions of the specialized window formula. Equation (2.60) can easily be further specialized to a zero-temperature Fermi-Dirac gas with the aid of (2.44)-(2.45), but the result is more notable for length than for interest or utility.

Like the specialized wall formula, the specialized window formula is simple and free of adjustable parameters. The dyadic sum is a striking, new feature. It gives the normal component of the drift velocity difference twice the weight of the tangential component. To understand its origin, consider first the situation in the absence of any drift velocities. Apart from the leading order term that has already been identified as a wall effect, there is no force. Gas particles pass back and forth through the window

carrying momentum, but the fluxes cancel. The introduction of drift velocities has two effects. First, the average momentum of particles in nucleus i changes, from 0 to $m\vec{V}_{oi}$. Secondly, the number flux of particles changes, as given by equation (2.7). The first effect is independent of the direction of $\vec{V}_{oi}$, but the second singles out the normal component.

The exchange force is not Galilean invariant. In the nomenclature of Section B and equation (2.27), it is easy to see that

$$\vec{V}'_{oi}(\vec{r},t) = \vec{V}_{oi}(\vec{r},t) - \vec{B} \quad . \tag{2.62}$$

Let $\dot{N}_1$ be the net rate of particle transfer into 1. It is the difference between the individual rates from 2 to 1 and from 1 to 2, $\dot{N}_{2\to 1}$ and $\dot{N}_{1\to 2}$, which are simply the fluxes of equation (2.7) integrated over velocity and window element. Therefore,

$$\begin{aligned}
\dot{N}_1 &= \dot{N}_{2\to 1} - \dot{N}_{1\to 2} \\
&= \int_W dW \int_{(\infty)} d\vec{v} \left\{\theta[(\vec{v}-\vec{V})\cdot n_2]\ (\vec{v}-\vec{V})\cdot\hat{n}_2\ F_2(\vec{v},\vec{r},t) - (2\to 1)\right\} \qquad (2.63) \\
&= \int_W dW \int_{(\infty)} d\vec{v}\ F_r(v)\left[\theta(-\vec{v}\cdot\hat{n}_1-U_2)(-\vec{v}\cdot\hat{n}_1-U_2) - \theta(\vec{v}\cdot\hat{n}_1-U_1)(\vec{v}\cdot\hat{n}_1-U_1)\right] .
\end{aligned}$$

Comparison of equation (2.63) with the change in $\vec{F}_1^{exchange}$, as expressed in (2.50), under the Galilean transformation labeled by $\vec{B}$ leads to

$$\left[\vec{F}_1^{exchange}(W)\right]' = \vec{F}_1^{exchange}(W) - m\dot{N}_1 \vec{B} \quad , \qquad (2.64)$$

The full, one-body force transforms in the same way as does the exchange part, since invariance of the wall pressure implies invariance of the wall contribution, as well.

It is important to stress that the specialized window formula, (2.61), <u>is</u> Galilean invariant. Non-invariance appears only in the next-order term:

$$\vec{F}_1^{exchange}(W) = \ldots - \frac{1}{2}\rho\left[(U_1\vec{U}_1 - U_2\vec{U}_2) - (U_1-U_2)\vec{V}\right]\ldots \qquad (2.65)$$

It is therefore negligible for slow deformations. However interesting the following discussion of invariance may be, it is not vital.

A simple example is shown in Fig. 7. In both frames a single gas with a uniform drift is divided by an imaginary plane into two parts, 1 and 2. The drift in Frame A is 0, but the window is moving with a normal velocity $\vec{B}$. Frame B is moving at velocity $\vec{B}$ with respect to A; in this frame, the window is motionless, but the drift is $-\vec{B}$. In both frames, the particle flow is the same. Indeed, all three rates in equation (2.63) are obviously Galilean

invariants. There is no force on 1 in Frame A because the new particles being acquired by 1 are at rest, on the average. There <u>is</u> a force in Frame B because the particles being acquired by 1 have there an average velocity of $-\vec{B}$.

Figure 8 displays as a second example a collection of non-interacting points of mass m and velocity $\vec{v}$. If another such particle joins the collection, the collection momentum increases, but the velocity of the collection remains the same.

Forces, in general, are <u>not</u> Galilean invariants. Newton's Second Law is often regarded as <u>defining</u> forces. Under a Galilean transformation

$$\vec{F}' = \left(\frac{d}{dt}\vec{P}\right)' = \left[\frac{d}{dt}(m\vec{v})\right]' = \left(\frac{dm}{dt}\right)'\vec{v}' + m'\left(\frac{d\vec{v}}{dt}\right)' , \qquad (2.66)$$

where

$$m' = m , \quad \left(\frac{dm}{dt}\right)' = \frac{dm}{dt} , \quad \vec{v}' = \vec{v} - \vec{B} , \quad \left(\frac{d\vec{v}}{dt}\right)' = \frac{d\vec{v}}{dt} , \qquad (2.67)$$

since time is a Galilean invariant. Therefore,

$$\vec{F}' = \vec{F} - \frac{dm}{dt}\vec{B} , \qquad (2.68)$$

in concord with equation (2.64).

Calculations for an object with variable mass can be slightly paradoxical, but experience, such as that with simple rocket problems, indicates that nothing more than care is needed for their success. Also, collision formalisms routinely treat the two-nucleus system as a whole; no matter escapes explicit

accounting by such formalisms.

The exchange force can be split into invariant and non-invariant parts. It is tempting to identify the latter with that part of the force in equation (2.60) in which $\vec{V}$ appears:

(2.69)

since (2.63) can be developed further into

$$\dot{N}_1 = \frac{1}{4} n \int_W dW \left[- \left\langle \frac{(v-U_1)^2}{v} \right\rangle_r + \left\langle \frac{(v-U_2)^2}{v} \right\rangle_r \right. \tag{2.70}$$

$$\left. + \left\langle \theta(|U_1|-V) \frac{(|U_1|-V)^2}{v} \right\rangle_r - \left\langle \theta(|U_2|-V) \frac{(|U_2|-V)^2}{v} \right\rangle_r \right]$$

and since the non-invariance is due to the number flow $\dot{N}_1$. This decomposition, however, is not unique.

$$[\vec{F}_1^{\text{exchange}}(W)]_{\text{non-invariant}} = m \dot{N}_1 \vec{V} \quad , \tag{2.71}$$

would do as well. In general, given one decomposition, another can be created by adding to the non-invariant part and subtracting from the invariant part <u>any</u> invariant vector.

D. ASSUMPTIONS

Several assumptions were introduced as need arose during the

derivations of the wall and window formulae. They were discussed but briefly in order to maintain the momentum of the narrative. Now is the time for further consideration of these assumptions and of some others only implicit in the one-body model. Are they valid? When? If they are approximate, how large are the errors involved in their acceptance? Can they be relaxed?

Some of the answers to these questions are to be found in the work of others. This work is summarized and discussed here for several reasons. First, it provides the context for some of the author's results. Secondly, some of the answers are only implicit in other investigations and must be pointed out. Thirdly, coverage of their work leads to a more complete, coherent, and unified account of the subject at hand. The absence of such an account has led both to uncritical acceptance of doubtful aspects of the one-body model and to skepticism concerning aspects whose past explications have been more conclusive than well known. While attempting to meet these needs here, care has been taken to distinguish the author's contributions from those of others.

1. The independent particle model

The assumption that nucleons move nearly independently inside nuclei is fundamental and necessary to the one-body model. Without it, two-body nucleon-nucleon interactions would be more important as a source of dissipation than would one-body

interactions between nucleons and the nuclear potential. Independence is the main reason dissipation due to deformation is largely restricted to the nuclear surface and it causes the window formula to depend only on the distribution functions of the two nuclei, not on a third, distinct function associated with the window region.

Residual two-body interactions certainly exist in nuclei, so independence is at best approximate. The most straightforward theoretical way to test the assumption would be to apply the one-body formulae and residual two-body calculations to the same situation and compare the results.

The concept of a mean free path leads to a different approach that is simple and general, though less exact than detailed comparison calculations. In each application of the one-body model, there is a characteristic nucleon path length associated with one-body interactions. For deforming nuclei, this length is the typical distance a nucleon travels between collisions with the surface, which is of the order of the nuclear diameter or radius. In the window case, the interaction is the transfer of a nucleon from one nucleus to the other. The characteristic length is the distance a nucleon travels through the window region and is therefore much smaller, unless the window is very large. The derivation of the window formula assumed, however, that the nucleons

leaving each nucleus were randomized about that nucleus' drift velocity. Section D.5.b develops a prescription of the drift velocity that depends on applying the independent particle assumption to each nucleus, so the characteristic length expands again to nuclear dimensions. Whenever the mean free path exceeds this characteristic length, one-body dissipation should dominate two-body dissipation, supposing individual one- and two-body interactions to be about equally effective in producing dissipation. The larger the ratio of the mean free path to the characteristic length, the better the independent particle assumption is. Figure 9 shows, among other things, the mean free path, λ, as a function of nucleon (neutron) energy (calculated on the basis of [9]). Zero on the energy scale corresponds to an unbound nucleon at rest with respect to the nucleus. More immediately relevant is the Fermi sea, ranging in energy from about -50 MeV, at the bottom, to around -8 MeV, at the top. Extrapolation of the graph suggests that λ is then always at least as large as the nuclear diameter, even that of uranium. This is confirmed by the observation of shell structure in large nuclei. A more detailed study by others [10] suggests that the mean free path is always large enough to produce one-body dominance in single, deforming nuclei.

So far, the discussion has ignored nuclear velocities of

deformation in single nuclei and of relative motion in nuclear collisions. If these velocities are sufficiently high, the independent particle assumption breaks down. This occurs because excitation energy injected by collective motion into the nucleon gas is always localized at first near the wall or in the window region, respectively. Only if

$$v \ll v_F \quad , \tag{2.72}$$

where v is the relevant speed of collective motion, will nucleon motion effectively spread this excitation throughout the nucleus. Otherwise, local heating will eventually shorten the mean free path and invalidate the independence assumption. Indeed, the process involves positive feedback, since a shortened mean free path hinders homogenization.

Even at slower speeds, before heating becomes a problem, the interior density will develop inhomogeneities. So then will the potential. This violates the assumption of a single nuclear potential that is uniform, except in the surface region.

Inhomogeneities need not automatically affect dissipation. If there exists an inertial frame in which the potential, though non-uniform, changes sufficiently slowly in time, then the one-body interactions in the interior are mainly conservative, not dissipative. The Coulomb potential in a static nucleus provides just such non-uniformities. The general relation between changes in

shape and changes in interior density is, however, unknown. Even if a given deformation causes more dissipation per unit volume in the surface region than in the interior, the larger volume of the interior might still generate substantial dissipation. The ratio of interior to surface dissipation may speculatively be presumed to vanish as the speed of deformation goes to zero, but there is no guarantee. Further investigation is needed to determine whether interior dissipation is negligible, at least when deformation is slow.

To conclude, the assumption that nucleons move in common potentials that are uniform in the nuclear interior may be valid so long as the relevant nuclear collective speeds are small enough compared to the Fermi speed. The quantitative meaning of "enough" has not been investigated. Even when this assumption is valid, two-body dissipation may not be negligible. Neither the independent-particle nor the uniform-potential assumption can readily be relaxed in the derivation of the wall and window formulae. The time-dependent Hartree-Fock method (TDHF) has been developed by others [11]-[14]. It is designed to handle a variable, inhomogeneous mean field and, as such, generalizes the one-body model so far described. The exact solution of a multiparticle system interacting through two-body interactions can be represented by a series of contributions of which TDHF is the first, followed by

a contribution from residual two-body interactions. This was proved by the authors of [15].

In its most general form, "one-body" simply means that nucleons interact solely through some type of mean field. The assumptions that are examined in the following sections are necessary to the derivation of the wall and window formulae, at least, to that in Sections B and C, but have nothing to do with the most general one-body model conceivable.

2. Semi-classical treatment

Description of the nucleons inside a nucleus by a distribution function $F(\vec{v},\vec{r})$ is completely classical, for it specifies position and momentum simultaneously, in defiance of the uncertainty principle. In all the calculations so far, quantum effects were introduced only when $F_r(\vec{v})$ was taken to be a Fermi-Dirac distribution.

Two dichotomies are easily confused. The first is between classical and quantal effects; the second, between average, local effects and effects produced by features of the entire nucleus, such as its symmetries. As stressed in Chapter I, the differences between the liquid drop model and the shell model derive more from the second dichotomy, than from the first. The object here is to separate quantal effects from non-average effects and to determine their importance.

Phase space localization is possible in large systems. The uncertainty principle states that

$$\Delta p \, \Delta x \gtrsim \hbar \quad . \tag{2.73}$$

For a nucleon,

$$\Delta^3 p \leqslant \frac{4}{3} \pi \, (m \, v_F)^3 \quad , \tag{2.74}$$

and it may therefore be confined in a volume $\Delta\Omega$ given by

$$\frac{\Delta\Omega}{\Omega} \gtrsim \frac{1}{2\pi^3} \frac{1}{A} \quad , \tag{2.75}$$

using equation (2.41). Even for A = 1, this is only 0.02. The numerical constant deserves little confidence, but at least

$$\frac{\Delta\Omega}{\Omega} = O\left(\frac{1}{A}\right) \quad . \tag{2.76}$$

In other words, each nucleon can be localized within its proportionate share of the nuclear volume. Quantum effects would become important for contortions of the nuclear surface whose wavelengths are small compared to the dimensions of $\Delta\Omega$. The nuclear surface is, however, a collective manifestation of the nucleons, so the uncertainty in nucleon position is likely to be a lower limit for contortion wavelengths.

Several studies by other investigators bear on this matter. The first, chronologically, were a series of computer calculations that traced the evolution of independent particles inside an

Temperatures high enough to eliminate superfluidity are readily attained, however. Once this is done, nuclear levels are so close that motion correspondingly slow is unlikely. For practical purposes, temperature and nuclear excitation, not the speed of nuclear motion, determine whether the wall and window formulae apply or whether superfluidity is dominant.

Standard linear-response theory combines a first order perturbation approach with ensembles, so that thermal averaging is introduced; it can be either quantal or classical. Since first order perturbation theory should be adequate to deal with small deformations, this model has been offered by other scientists as a generalization of the original one-body model [16]. The wall formula, however, applies to slow deformations, which need not be small, a difference that will be discussed further in Section D.5.

The quantal and classical linear-response theories were both applied to the interaction of a Fermi gas with a semi-infinite plane surface on which was impressed an arbitrary velocity field [17], [18]. The classical result was identical to the specialized wall formula, equation (2.40), in the absence of drifts, but the quantum result replaced the integral in that formula with

$$\int_S dS \int_S dS' \; K(\vec{r},\vec{r}\,') \; (\vec{V}_o \cdot \hat{n})(\vec{r}) \; (\vec{V}_o \cdot \hat{n})(\vec{r}\,') \quad . \qquad (2.77)$$

In the limit that the velocity field had an infinitely long wavelength, i.e., was uniform,

$$K(\vec{r},\vec{r}\,') = \delta(\vec{r} - \vec{r}\,') \tag{2.78}$$

and the wall formula was recovered; as the wavelength became shorter, the kernel, K, became increasingly non-local. The integrated response,

$$\int_S d\vec{r}\,' \; K(\vec{r},\vec{r}\,') \tag{2.79}$$

shrank until at $\lambda = \lambda_F$, K vanished identically. As the wavelength decreased, the fixed wavelength particles found it increasingly difficult, and, finally, impossible, to see the velocity field. The effect of this non-locality was always to reduce dissipation, often significantly, from its one-body value.

A recent advance is the extension by its discoverers of the leptodermous theorem to one-body dissipation [19]. It then assumes particle independence, randomization, and rather uniform matter and energy densities in the nuclear interior to confine dissipation to the surface, but it does apply to both quantal and classial calculations. As it was in the leptodermous formula for the potential energy, the expansion parameter of the leptodermous formula for the dissipation is the ratio of the diffuseness to the nuclear radius. The leading volume-conserving term in the new

leptodermous expansion is structurally identical to the driftless specialized wall formula. The constant of proportionality is undetermined, but certain requirements are prescribed that govern any model calculation of it. For instance, the constant, in the quantal linear response model, has just the one-body value.

For a sharp surface, the quantal linear-response results appear to contradict the leptodermous dissipation theorem. The authors of the latter attribute this to an incorrect specification of the surface in the linear response treatment. The linear response calculations describe the surface in terms of the potential. The derivation of the leptodermous theorem never introduces a potential and its authors argue that the linear response approach should likewise use the matter density, or a mean of the potential and the density, to describe the surface. The two viewpoints are identical at long wavelengths, but at wavelengths shorter than the Fermi wavelength the density distribution ignores the potential. Since a sharp potential produces a diffuse quantal density, the linear response results correspond to the leptodermous formula for some non-zero diffuseness.

The accuracy of the semi-classical assumption has received much, if contradictory, attention in the case of deformations, but not in the case of windows between nuclei. Diffraction ought to be important when nucleon wavelengths are comparable to or larger than

window dimensions. It alters the number of particles passing through an opening and it introduces interference effects into their angular distribution, but it does not change their velocity. The window force should not be affected much by the introduction of wiggles into the angular distribution, if the average distribution is not changed, but the force will be strongly influenced by any reduction in the number of particles crossing the window. The reduced wavelength, $\lambda\!\!\!^{-}$, ranges from 5 Fm. for 1 MeV nucleons to 0.8 Fm. for 30 MeV nucleons. Window diameters routinely reach 5 Fm. during calculations of heavy ion collisions. Since the mean energy in the Fermi sea is 3/5 the Fermi energy and since the window formula is weighted toward high velocity nucleons, the window force should not be significantly affected by diffraction, except when the window is small. The window is always small during nearly grazing collisions and is small during the first and last stages of more penetrating collisions, when the nuclear surfaces are just touching. In both situations, the window force is automatically small and cannot significantly influence the final collision state.

Semi-classical treatment of nuclear center-of-mass dynamics has been extensively investigated [20]. The size of the quantal effects is indicated by the separation of diffraction peaks in elastic scattering, which is typically of the order of 5° for two nuclei with $A > 10$.

The simplicity of the one-body model depends on the semi-classical assumption. Every consideration of the role played by the assumption in deformations suggests that it is the leading approximation to reality, but estimates of the errors involved in its adoption range from zero to 50% of the one-body results themselves. Something more conclusive is needed. There is a simple justification for the application of the assumption to windows, but more rigor would be desirable.

3. The Pauli exclusion principle

Has the Pauli exclusion principle been abused? Basis for the crucial independent particle assumption, it has otherwise been ignored.

Use of the semi-classical approximation means that the Pauli principle prevents two identical particles from having the same velocity (and spin) only if they are also in approximately the same place. In this sense, the exclusion principle is already included in the derivation of the wall and window formulae.

To see this, note first that when particles collide with the wall, their normal velocites flip inward. Particles initially having inward normal velocities have, in the meantime, begun to leave the neighborhood of the wall, leaving room for the newly scattered particles. Quantitative verification is easiest in the wall frame; there are no difficulties with Galilean relativity

because only numbers and volumes are involved. Every particle in the indicated volume in Fig. 3 at time t that has a velocity in the range $\vec{u},\vec{u}+d\vec{u}$ $(\vec{u}\cdot\hat{n}>0)$ will reflect off the wall, as described by equation (2.8) and Fig. 4, and will wind up in the indicated volume of Fig. 10 at t+dt with a velocity in the range $\vec{u}'$, $\vec{u}'+d\vec{u}'$. The number of particles in the first volume is given by the right hand side of equation (2.5) and by equation (2.6):

$$N_{in} = F(\vec{v},\vec{r},t)\ \vec{u}\cdot\hat{n}\ d\vec{v}\ dS\ dt \quad . \tag{2.80}$$

All these will squeeze into the second volume at t+dt. The number originally there at t is

$$F(\vec{v}',\vec{r},t)\ |\vec{u}'\cdot\hat{n}|\ d\vec{v}'\ dS\ dt \quad , \tag{2.81}$$

(which may be zero), but all these will be gone at t+dt. Of greater interest is the <u>capacity</u> of the second volume at t+dt:

$$N_{cap} = \rho(\vec{v}',\vec{r},\ t+dt)\ |u'\cdot\hat{n}|\ d\vec{v}'\ dS\ dt \quad , \tag{2.82}$$

where ρ is the phase space density. Equations (2.43) and (D1) imply that

$$\rho(\vec{v},\vec{r},t) = \rho = \frac{N}{\Omega}\ \frac{1}{\frac{4}{3}\pi\ v_F^3} \tag{2.83}$$

and

$$F(\vec{v},\vec{r},t) \leqslant \rho \quad . \tag{2.84}$$

Equation (2.8) says that $|\vec{u}'\cdot\hat{n}|$ in (2.82) equals $\vec{u}\cdot\hat{n}$ in (2.81) and, together with (2.4) and the nature of Jacobians, that

$$d\vec{v}' = d\vec{v} \quad . \tag{2.85}$$

Therefore,

$$N_{in} \leqslant N_{cap} \quad , \tag{2.86}$$

which is the quantitative verification sought. Proof in the window case is similar.

A different way of reaching the same result has been developed by another investigator [21]. Any state of a system consisting of N classical particles can be represented by one point in 6N-dimensional phase space. The evolution of the system is then represented by an orbit in phase space. If the particles are identical and do not interact, a single, N-particle system can be regarded as an ensemble of N identical one-particle systems having different initial conditions. When particle motion is governed only by a (time-dependent) potential that constitutes a deforming box, the ensemble is constrained to lie entirely inside the box at each instant of time. For example, a Fermi gas is started inside a deforming cube at t and the phase space is projected onto 2 dimensions each in configuration and velocity space in Fig. 11. Applied to an ensemble of one-particle systems, Liouville's theorem

states that the density in 6-dimensional phase space is constant in time along single-particle orbits. The initial density is given by the Fermi-Dirac distribution, equation (2.83), which is really an average expression of the Pauli principle. Maintenance of this density by Liouville's theorem amounts to maintenance of the Pauli principle, in an average sense.

One sees that average treatment of the Pauli principle suffices for observables that express only average particle behavior. When fluctuations in particle behavior are involved, the Pauli principle must be explicitly included. This is because both justifications for ignoring the Pauli principle rely on the distribution function, which specifies the mean number of particles in each region of phase space. Fluctuations involve the probability that a specified number--often quite different from the mean--of particles finish in each region. Work by others on diffusion of particles through a window [3], [4], to be discussed in Section E.5, illustrates this point very nicely. In finding the mean number transferred, the Pauli principle can be neglected; in finding the variance in the number, it must be treated explicity.

The discussion in this sub-section actually resembles the quantal handling of the Pauli principle in the context of independent particles. Each multiparticle state is either an antisymmetrized direct product of single-particle states or a linear

combination of such products. Each single-particle state evolves under the influence of a single-particle Hamiltonian. Once antisymmetry is imposed, it is preserved automatically.

Neglecting the Pauli principle should introduce no error in addition to that caused by making the localization approximation. The similarity of the quantal and classical approaches also implies an absence of new errors. All the quantal models considered in this dissertation are independent particle models and accordingly need not concern themselves with the Pauli principle.

4. The nature of the surface

Two important idealizations of the surface have been made. First, perfect sharpness has been imposed in place of the considerable diffuseness found in nuclei. The corresponding result should again be the most important contribution to the actual dissipation, with non-zero diffuseness leading to corrections. The importance of these corrections first appeared in the computer cranking results [6]. The quantal results agreed with those of the classical Monte-Carlo calculations and of the wall formula only when the diffuseness was set to a value much smaller than the physical one. When the physical value was used, the quantal answer was only half the classical one.

A localized particle colliding with a sharp wall interacts instantaneously with but one point on the wall, to which corresponds

just one normal wall velocity. When that same particle collides with a diffuse wall, represented by a smooth potential, it interacts with a subset of the surface over a period of time. In doing so, it samples a tangential range of surface positions and of corresponding surface normals and velocities. Moreover, these ranges are evaluated over a time interval. Figure 12 shows the collision process and the potential profile in the two cases, except that motion of the wall during the collision process has been excluded in the interest of clarity. Consideration of a range of positions means that the tangential derivatives of the the position, normal, and velocity are important, while the range in time is associated with the corresponding set of time derivatives. Only first order derivatives are needed for the first order diffuseness corrections. Not all of these derivatives are distinct or even new. Note first that a range of positions is associated with a single normal if there is no curvature. No change in pressure or power results from the presence of such a range. On the other hand, the curvature specifies the tangential gradients of both the position and the normal. The two gradient corrections are together equivalent to one curvature correction. The tangential gradient of the velocity is both distinct and new. Turning to the time derivatives, that of the position is just the original velocity. If the velocity were spatially uniform, the surface normal would be constant in time.

Therefore, the time derivative of that normal is synonymous with the tangential gradient of the velocity. The time derivative of the velocity does introduce a new feature: the acceleration. The acceleration correction has been shown by others to be reversible [19], but the other two corrections, the curvature and velocity-gradient corrections, do affect dissipation.

The corrections can probably be calculated, to first order in the ratio of the diffuseness to the nuclear radius, by a method very similar to that used in the derivation of the wall formula. Exhaustive calculations of the corrections have already been made in one of the first papers to apply the linear response model [17]. These support the cranking calculations in concluding that the corrections can be substantial. The leptodermous theorem for dissipation specifies the functional form of the corrections, but not their numerical coefficients, which can be determined only with the aid of more detailed models. Symmetry arguments in the derivation of that theorem lead to the conclusion that the velocity gradient contributes only to second order in the diffuseness [19], leaving curvature as the only source of first order correction to the dissipation.

Diffuseness is also important when two nuclei are connected by a window. With diffuseness present, the potential experienced by a nucleon will vary with its distance along the axis joining the two

nuclei and with its distance from this axis. When the window is fully open, that is, when the potential everywhere inside the connecting region is the same as that in the nuclear interiors, nucleons whose velocities are merely pointed in the right direction will cross the window unimpeded. If the potential is more positive, only the most energetic nucleons can cross the window, and, if the potential varies in space, so will the (classical) penetrability. Another investigator has created a theory of "proximity friction" [22] that generalizes the window formula by means of the "proximity trick" used to find the proximity potential [2]. It calculates an effective window area that can be substituted in the specialized window formula to obtain the correct force. For a given nuclear surface shape and potential profile, the theory computes the effective window area as a function of nuclear separation. Proximity friction is itself approximate because its derivation freezes the total potential for each nuclear separation. It may be observed here that this approximation probably leads to the dominant contribution to the force between two nuclei, but the magnitude of the error is really unknown.

The second idealization of the surface has been that it collides with nucleons elastically and as if it were infinitely massive (i.e., the nucleons suffer specular reflection). These notions can look dubious when one recalls that the nuclear surface

is created by the nucleons near it. This matter is one aspect of the problem of maintaining self-consistency between the nucleons and the nuclear surface. Since the leptodermous dissipation theorem locates the surface solely through the density profile and never introduces a potential, this aspect of self-consistency never arises. Thus, the agreement between two respective leading terms of the specialized wall formula and of the leptodermous result justifies the second idealization. This agreement, however, extends only to the functional form of these terms; the coefficients multiplying each term have always been calculated in models that assume specular reflection of nucleons from the surface.

Diffuseness thus contributes large corrections to the one-body formulae. These probably can be included in the wall formula, and have already been incorporated in proximity friction. The leptodermous approach gives the form of the corrections as functionals of the surface, but not the constant coefficients multiplying each functional. On the other hand, the assumption of specular reflection does not introduce any changes into the <u>form</u> of the leptodermous-dissipation expansion, but the possibility that some coefficients in the expansion are changed, to an unknown extent, remains. TDHF requires neither assumption about the surface and gives unambiguous results.

5. Randomization and drifts

It is time now to expand upon the introduction to randomization and drifts given during the wall formula derivation in Section B.

a. randomization

Ignore, for the moment, translations and rotations and focus attention on particles about to strike a particular point on the wall at some instant. Thanks to the independent particle assumption, the origins of their inertial motion include every section of the nucleus, except the point being struck. This assumes the wall to be convex; even if it is not, many different sections of the wall contribute to the bombardment of the point. The starting time of each particle on its trajectory varies with the particle speed and the distance traveled. The velocity spectrum of the arriving particles thus embodies a picture of the shape and movement of the entire wall smeared over time, and therefore randomizes, unless the shape and movement are too regular. If the spectrum, for any fixed speed, favored a particular direction, it would point back to a favored originating point elsewhere on the surface. Randomization forbids such distinction and therefore forces the arriving spectrum to be isotropic at each point on the surface. Furthermore, if the spectrum differed from point to point on the surface, the favored points would again point back to favored

points of origin. Randomization prevents this distinction, also. Equation (2.14) then results.

Of course, nuclei--whether in their ground states, deforming, or interacting through a window--usually are symmetric. Reliance on randomization therefore leads to errors that must be corrected by the generalization of shell corrections from statics to dynamics.

The size of these errors was investigated in the cranking calculations [6]. The less the regularity, the better the agreement with the wall formula. For standard, second order, multipole deformations of a sphere, the difference between the wall formula and the classical cranking results was as much as a factor of two; for fourth order deformations, the comparison was slightly more favorable; and, for sixth order deformations, agreement was good, within 10% or less.

The authors fix responsibility for differences between classical, Monte-Carlo calculations and wall formula results on the failure of randomization by observing that the differences disappeared when randomization was forced by giving each particle a new, random position and velocity whenever its path length since it was last randomized exceeded a certain value. They associate symmetry and randomization because symmetry can introduce additional constants of motion that break phase space up into cells that do not

communicate. Volume conservation no longer suffices to cause the leading conservative term in the power to vanish; instead, it can make a large, but reversible contribution. The next, dissipative term should also be affected. In particular, the authors observe that second order multipole deformations are very similar to spheroidal deformations, which produce a separable problem. Randomization should be strongly retarded, although not prevented, for second order deformations. As the order increases, the resemblance to a spheroid fades. Let it be noted here that the sixth order deformation is still highly regular, in the sense of nearly possessing an exact symmetry. The role of the leading conservative term was verified by the authors' analysis of a deforming rectangular box, while the conservative nature of a large fraction of each discrepancy between the cranking calculations and the wall formula is made obvious by frequent decreases in the differences.

Quantal cranking calculations led to similar results. The only new feature was the sensitivity to nuclear size mentioned in Section D.2. The potential sources of non-randomization must therefore be expanded to include any property of the entire nuclear shape.

Quantal linear response calculations have not dealt with these matters, but classical calculations have been performed for

multipole deformations of a sphere. The results should be directly comparable to the corresponding classical cranking results. In particular, the cranking excitation at the end of a full period *ipso facto* should be purely dissipative. This reasoning is supported by linear response calculations indicating that, in the case considered in [6], the dissipation should nearly have attained its asymptotic value by the end of a period. Surprisingly, the two dissipation calculations strongly disagree.

The authors of [19] claim that the linear response calculation erred in always regarding the surface as spherical when it took account of particle reflections. It should be observed here that this explanation is all the more credible when it is recalled that even the regularity of a sixth order multipole deformation is incapable of disrupting randomization. Only the last, highest degree of regularity can do so. The difference between a slightly deformed sphere and a perfect one can therefore be very important.

Nonetheless, the failure of randomization through the existence of regularities can be substantial. In [19], the ratio of the classical cranking dissipation at the end of a cycle, in the case mentioned above, to that predicted by the wall formula was shown to be 0.51, 1.35, 1.04 for multipole deformations of order two, four, six. Shell corrections are therefore likely to be important in nuclear dynamics. The only available model capable of

correctly incorporating such shell effects is TDHF.

In light of this section, the distinction between quantal effects and effects produced by the entire nucleus can be alternatively formulated in terms of locality. When the semi-classical and randomization approximations are made, each point on the surface makes its own, independent contribution to dissipation. This effect is sharply local. Diffuseness causes neighboring points to cooperate in producing dissipation, a fuzzy locality over distances of the order of the diffuseness. Purely quantal effects, if they exist, will be similarly local, over distances of the order of the Fermi wavelength, which is about the same as the diffuseness. On the other hand, the independent particle assumption combines with failures of randomization to allow points even on opposite sides of the nucleus to cooperate, which is utterly non-local.

b. drifts

Admitting translations and rotations leads to the introduction of a drift velocity, $\vec{V}_o(\vec{r},t)$. In one frame, both wall and gas may be at rest, in the sense that the distribution function is isotropic in velocity and uniform over the wall, as in equation (2.14). In any other inertial frame, the gas distribution function is isotropic and uniform only about a drift velocity, as in (2.15). In this case, the drift velocity is just the velocity difference

between the two frames:

$$\vec{V}_o(\vec{r},t) = \vec{V}_o(t) \quad . \tag{2.87}$$

The case of rotation is more complicated because two frames that are mutually rotating are not mutually inertial, although the familiar example of rigid rotation certainly implies a corresponding spatial dependence of the drift velocity.

Note also that the mean velocity of a randomized distribution having a drift is easily calculated from equation (2.15):

$$\langle \vec{v} \rangle_F (\vec{r},t) \equiv \int_{(\infty)} d\vec{v} \; F(\vec{v},\vec{r},t)\vec{v} \Big/ \int_{(\infty)} d\vec{v} \; F(\vec{v},\vec{r},t) = \vec{V}_o(\vec{r},t) \; . \tag{2.88}$$

The wall and window formulae rely on global randomization about a single drift velocity for each nucleus. Their polar opposite, (isothermal) hydrodynamics, relies on local randomization, at each point in space, about the local fluid-velocity field, but hydrodynamics also leads straight to equation (2.15), where $\vec{V}_o$ is identified as the fluid-velocity field,

$$\vec{v}(\vec{r},t) \equiv \langle \vec{v} \rangle_F (\vec{r},t) \quad . \tag{2.89}$$

This convergence suggests that (2.15) is certainly general enough to describe a broad range of physical phenomena, but it can also

mislead. The boundary condition for hydrodynamics is

$$\vec{v}(\vec{r}_s,t)\cdot\hat{n}(\vec{r}_s,t) = \vec{V}(\vec{r}_s,t)\cdot\hat{n}(\vec{r}_s,t) \quad . \tag{2.90}$$

The subscript `S' emphasizes that this equation applies only to points on the surface S. This boundary condition simply prevents matter from leaving the surface. If the analogous expression with $\vec{V}_o$ in place of $\vec{v}$ is substituted in equations (2.16) and (2.17), both the pressure and dissipation always vanish identically.

The avoidance of this futility is subtle. Until now, F usually has been limited unobtrusively to describing those particles which are both near the wall and closing it. Particles near the wall and leaving it have just collided with it and therefore are strongly affected by its particular velocity. They are highly non-random and are not described by F in equation (2.15). Indeed, (2.15) is incomplete. It should be

$$\begin{aligned} F(\vec{v},\vec{r}_s,t) &= \theta\left\{[\vec{v}-\vec{V}(\vec{r}_s,t)]\cdot\hat{n}(\vec{r}_s,t)\right\} F_r[\vec{v}-\vec{V}_o(\vec{r}_s,t),t] \\ &+ \theta\left\{-[\vec{v}-\vec{V}(\vec{r}_s,t)]\cdot\hat{n}(\vec{r}_s,t)\right\} F_r[\vec{v}'(\vec{r}_s,t)-\vec{V}_o(\vec{r}_s,t),t] \ , \end{aligned} \tag{2.91}$$

instead.

The particular function multiplying the second theta function is determined by Liouville's theorem, which says, for

independent particles, that F is constant along orbits in single-particle phase space. Equation (2.91) applies only to points on the wall. Consider then a particle orbit just before and just after collision. Labeling the two segments unprimed and primed, respectively,

$$\vec{r}_s' = \vec{r}_s \quad , \qquad t' = t \tag{2.92}$$

and $\vec{v}'$ is determined by equation (2.8). Therefore,

$$F(\vec{v}',\vec{r}_s,t) = F(\vec{v},\vec{r}_s,t) \tag{2.93}$$

and (2.91) follows. Note also that the function multiplying the second theta function depends on the wall motion, since $\vec{v}'$ is a function of $\vec{V}$.

Now the mean velocity is no longer equal to $\vec{V}_o$, but it does satisfy the boundary condition:

$$[\vec{v}(\vec{r}_s,t) - \vec{V}(\vec{r}_s,t)] \cdot \hat{n}(\vec{r}_s,t) = \langle (\vec{v} - \vec{V}) \cdot \hat{n} \rangle_F \quad . \tag{2.94}$$

Ordinarily, the density

$$\rho(\vec{r},t) = m \int_{(\infty)} d\vec{v} \;\; F(\vec{v},\vec{r},t) \tag{2.95}$$

should equal $N/\Omega(t)$, as in equation (2.19). Here,

$$\rho(\vec{r}_s,t) = 2\int_{(\infty)} d\vec{v} \quad F_r(v) \quad \theta(\vec{v}\cdot\hat{n} - U) \quad . \tag{2.96}$$

Once more, the techniques of Appendix C apply. They produce

$$\rho(r_s,t) = \rho_o(t)\left[1 - \langle v^{-1}\rangle_r U - \varepsilon(U)\langle\theta(|U| - v)\rangle_r + \langle\theta(|U| - v)v^{-1}\rangle_r U\right]$$

$$\cong \rho_o(t)\left(1 - \langle v^{-1}\rangle_r U\right) \quad , \tag{2.97}$$

where

$$\rho_o(t) = \frac{N}{\Omega(t)} \tag{2.98}$$

is the mean density of the nucleus. Expansion lowers the gas density at the surface and compression raises it. Although equation (2.97) thus has the right qualitative behavior, it probably exaggerates quantitatively, for it is known that nuclear compressibility is a fraction of the Fermi-gas compressibility.

The revision of F in (2.91) does not change the general wall formula because F appears there only in the form

$$\theta[(\vec{v} - \vec{V})\cdot\hat{n}] \quad F(\vec{v},\vec{r}_s,t) \quad , \tag{2.99}$$

which is obviously the same for both (2.15a) and (2.91).

This resolution of the boundary condition paradox simultaneously allows the pressure and dissipation to be non-zero, maintains both boundary condition and wall formula unchanged, and causes the surface density to behave in a natural way.

Equation (2.91) applies to deforming nuclei. At a window between two nuclei, the first term is the same, but the second will depend not only on the window motion, but also on the characteristics of the gas on the other side of the window. Obviously,

$$F(\vec{v},\vec{r}_W,t) = \theta\left\{[\vec{v}-\vec{V}(\vec{r}_W,t)]\cdot\hat{n}_1(\vec{r}_W,t)\right\} F_r[\vec{v}-\vec{V}_{01}(\vec{r},t),t]$$
$$+ \theta\left\{-[\vec{v}-\vec{V}(\vec{r}_W,t)]\cdot\hat{n}_1(\vec{r}_W,t)\right\} F_r[\vec{v}-\vec{V}_{02}(\vec{r},t),t] \quad . \tag{2.100}$$

The window formula will remain the same, just as does the wall formula. The boundary condition can now be violated because there is no reason for it to hold: there <u>can</u> be a net flow of matter through the window. The density can also change; that corresponding to equation (2.100) is

$$\rho(\vec{r}_s,t) = \rho_o(t)\Big[1 - \langle v^{-1}\rangle_r \ \tfrac{1}{2}(U_1 + U_2) - \tfrac{1}{2}\,\varepsilon(U_1)\,\langle\theta(|U_1| - v)\rangle_r$$

$$- \tfrac{1}{2}\,\varepsilon(U_2)\,\langle\theta(|U_2|-v)\rangle_r + \tfrac{1}{2}\langle\theta(|U_1|-v)v^{-1}\rangle_r\ U_1$$

$$+ \tfrac{1}{2}\langle\theta(|U_2|-v)v^{-1}\rangle_r\ U_2\Big] \qquad (2.101)$$

$$\cong \rho_o(t)\ [1 + \langle v^{-1}\rangle_r\ \tfrac{1}{2}(\vec{V}_{01} - \vec{V}_{02})\cdot\hat{n}_1 + \ldots\ ] \quad .$$

As one might expect, if the nuclei are approaching each other, the density rises and if they are receding from each other, it falls.

The drift has yet to be specified. Equation (2.87) already provides the answer for translations. Analogy with rigid rotation suggests

$$\vec{V}_o(\vec{r}) = \vec{\tau} + \vec{\omega}\times(\vec{r} - \vec{r}_o) \quad . \qquad (2.102)$$

In equation (2.102), the drift prescription explicitly diverges from that of hydrodynamics, whose boundary condition requires the normal components of the surface velocity and of the drift velocity at the surface to be identical. A given drift field uniquely determines $\vec{\omega}$, but not $\vec{\tau}$ and $\vec{r}_o$. Any $\vec{r}_o{}'$ can be used, if

$$\vec{\tau}' = \vec{\tau} + \vec{\omega}\times(\vec{r}_o{}' - \vec{r}_o) \quad . \qquad (2.103)$$

is used also.

Is this form of $\vec{V}_o$ correct? The translational part seems obviously so. There are several arguments concerned with rotation. All, however, seek to answer a somewhat different question: will the distribution function of a gas in a box rotating at a constant frequency eventually become isotropic about a rigid body drift? This second question is too narrow in ignoring deformation and too broad in scrutinizing all the gas particles rather than just those about to strike the wall or cross the window. Still, in the limit of zero deformation, general rotation becomes rigid-box rotation. When gas and box are at rest, on the average, the distinction between incoming and outgoing particles apparently disappears in the absence of deformations. The same may be true when the box, and perhaps the gas, are rotating steadily. If so, then the failure of a gas in a rigidly rotating box to sustain throughout itself a rigidly rotating drift would invalidate equation (2.102).

The first argument is that analytic, quantal studies of Fermi gases in rigidly rotating potentials of arbitrary shape and profile have long been known to confirm the viability of a rigidly rotating drift [23]. Secondly, an analogous classical treatment of a gas possessing an isothermal velocity distribution and contained in a sharp-walled box leads to the same conclusion, except that centrifugal effects must be included in order to obtain an exact

result. More specifically, let f be any differentiable function. Define the distribution function by

$$F(\vec{v},\vec{r},t) = 4\left(\frac{m}{h}\right)^3 f\left[\mu + \frac{1}{2} m(\vec{\omega}\times\vec{r})^2 - \frac{1}{2} m(\vec{v} - \vec{\omega}\times\vec{r})^2\right] \tag{2.104}$$

and the chemical potential analog, μ, by

$$N = \int_S dr \int_{(\infty)} d\vec{v} \; F(\vec{v},\vec{r},t) \quad . \tag{2.105}$$

For a zero-temperature Fermi-Dirac gas at rest,

$$f(\vec{v},\vec{r},t) = \theta(v_F - v) = \theta(E_F - \frac{1}{2} m\vec{v}^2) \quad . \tag{2.106}$$

In equation (2.104), $\vec{v}-\vec{\omega}x\vec{r}$ represents the Coriolis effect of going to a rotating frame and $(\vec{\omega}x\vec{r})^2$, the centrifugal effect. Once established, this distribution function will persist indefinitely. The proof is based on Liouville's theorem, which imposes equation (2.93) at the surface. In the interior, constancy of F along particle orbits leads to the familiar

$$\frac{\partial F}{\partial t} + \vec{v}\cdot\frac{\partial F}{\partial \vec{r}} + \vec{a}\cdot\frac{\partial F}{\partial \vec{v}} = 0 \quad , \tag{2.107}$$

where the acceleration, $\vec{a}$, is zero. It is trivial to verify that the distribution function in equation (2.104) satisfies both (2.93) and (2.107).

Both these arguments concern only possible final states, not the likelihood of their establishment. A third approach, therefore is to change the classical Monte-Carlo code in order to study rigid rotations [24]. An ellipsoid having axes in the ratio 1:1:3 and a volume corresponding to a nucleus with A = 184 was rotated about one of the short axes at a given rate. One specifies an initial particle distribution at will, and then lets the system evolve in time. It would be desirable, but too costly, to study directly the evolution of the distribution function. Instead, one follows the progress of the average particle excitation, where the excitation of a particle is defined as the difference, in the non-rotating, laboratory frame, between the present and initial kinetic energies of the particle. This procedure should indicate if any box-frame stationarity develops asymptotically in time, for one would then expect the power fed into the gas to be constant (positive or zero) and the excitation as a function of time to develope a constant slope. In fact, the power always seems to go to zero. If the initial distribution is stationary, the excitation should always be zero. The nature of the final state may be investigated through the excitation needed to reach it. For example, the enrgy needed to boost a gas of mass M from rest to an angular frequency ω should be roughly

$$\frac{1}{2} I \omega^2 \quad , \tag{2.108}$$

where I is the moment of inertia of a suitably shaped, homogeneous, rigid body of mass M, bounded by a surface S. Comparison is complicated by centrifugal effects and by the heating of the gas. Even so, equation (2.108) should be correct in order of magnitude.

To see what actually happens, look at Fig. 13. It shows the average excitation as a function of time for $\omega = 0.5 \times 10^{22}$ sec^{-1}. The initial distribution was a zero-temperature Fermi gas of uniform density. In the first case, $\vec{V}_o = 0$; in the second, $\vec{V}_o$ was given by equation (2.102). In each instance, the excitation at positive times was least-squares fitted to a straight line. Table 1 shows that the fitted excitation appears to level off with zero slope (i.e.--less than the standard deviation of the slope), which generally means that the asymptotic state is stationary. Taking the nucleon mass to be 939 MeV/c^2 and the nucleus radius constant to be $r_o = 1.15$ Fm., the rotation energy of equation (2.108) is 5.4 MeV. It will be shown in Section D.6 that, when a one-dimensional, single-speed gas with no drift is placed in a one-dimensional box constrained to move at a fixed velocity, exactly half of the work done on the gas is used to bring the gas up to box speed, while the other half goes into heating the gas. Doubling the rigid rotation

energy, 5.4 MeV, may therefore crudely account for heating. The substantial asymptotic excitation, 2.(4) MeV, that appears in the co-rotating case is presumably due to centrifugal effects, which increase the peripheral density and increase the moment of inertia from its rigid body value. Adding these contributions together, one obtains an estimate of the asymptotic energy developing in an initially non-rotating distribution, 13.(2) MeV, which is close to the computer result. This agreement merits no more than limited faith, however, because of the guesswork that produced it.

A fourth argument, the last to be considered here, points the opposite way. Rigid body drifts in the nuclear interior imply rigid body moments of inertia, but experimental moments of inertia are considerably smaller. One qualitative interpretation of the data, which is often made, posits a non-rotating, spherical core, inscribed in the nucleus, so that only nucleons outside the core contribute to the moment of inertia and might perhaps have a rigid body drift. This need not contradict the drift prescription, since only surface drifts count in the one-body model. Even when the nucleus is spherical, making core and nucleus one, the two pictures still agree. On the one hand, there are no drifts at all in the core and it carries no angular momentum; on the other, a rigidly rotating sphere could have a drift, but it would be purely tangential and without effect in the one-body model.

Having settled on the rigid body form embodied in equation (2.102), it remains to determine $\vec{\tau}$ and $\vec{\omega}$. This has been done for a single, deforming nucleus, even in the presence of Coulomb and nuclear proximity forces, but not for a pair of nuclei joined by a window. The discussion of $\vec{\tau}$ and $\vec{\omega}$ will henceforth consider mainly the first situation.

Determination of $\vec{\tau}$ and $\vec{\omega}$ squarely confronts the problem of consistency between gas and box, nucleons and nuclear surface. In the most general model, gas and box could move rather independently. Nuclear self-consistency requires that gas and box move together in the same way as a nucleus shaped like the box would be predicted to move under the influence of any external forces. Conservation of linear momentum states that the total force on, say, the gas, which is the sum of the external force and of the total force exerted by the box on the gas, must equal the external force alone, so that the total force of the box on the gas is zero. More generally, both the total force and total torque exerted by each representative of the nucleus on the other must vanish.

Recalling equation (2.1), the force on the gas, for example, is

$$\vec{F} = \int_S \overrightarrow{dF} \tag{2.109}$$

and the torque about an axis passing through $\vec{r}_o$ is

$$\vec{\tau} = \int_S (\vec{r} - \vec{r}_o) \times \overrightarrow{dF} \quad . \tag{2.110}$$

Following the wall formula derivation, one demands first

$$0 = \vec{F} = -\oint_S dS \;\; P(\vec{r},t;\vec{\tau},\vec{\omega}) \;\; \hat{n}(\vec{r},t) \tag{2.111a}$$

$$0 = \vec{\tau} = -\oint_S dS \;\; P(\vec{r},t;\vec{\tau},\vec{\omega}) \;\; (\vec{r} - \vec{r}_o) \times \hat{n}(\vec{r},t) \quad . \tag{2.111b}$$

Equation (2.111) has been written in a form designed to emphasize the dependence of the pressure on $\vec{\tau}$ and $\vec{\omega}$ via F, and then $\vec{V}_o$. Writing this out, with the aid of (2.16) and (2.102), leads to

$$0 = \vec{F} = -2m \oint_S dS \; \hat{n} \int_{(\infty)} d\vec{v} \; F_r(v) \;\; \theta\Big[\{v-[\vec{V}-\vec{\tau}-\vec{\omega}\times(\vec{r}-\vec{r}_o)]\}\cdot\hat{n}\Big]$$
$$\cdot \Big[\{v-[\vec{V}-\vec{\tau}-\vec{\omega}\times(\vec{r}-\vec{r}_o)]\}\cdot\hat{n}\Big]^2 \tag{2.112a}$$

$$0 = \vec{\tau} = -2m \oint_S dS \; (\vec{r}-\vec{r}_o) \times \hat{n}(\vec{r},t) \int_{(\infty)} d\vec{v} \; F_r(v) \tag{2.112b}$$
$$\cdot \;\; \theta\Big[\{v-[\vec{V} - \vec{\tau} - \vec{\omega} \times (\vec{r} - \vec{r}_o)]\} \cdot \hat{n}\Big] \cdot \Big[\{v-[\vec{V}-\vec{\tau}-\vec{\omega}\times(\vec{r}-\vec{r}_o)]\}\cdot\hat{n}\Big]^2 .$$

These constitute an implicit system of two simultaneous vector

equations in two vector unknowns. They are insoluble analytically, but they can be solved numerically. If one uses only the two leading terms in the specialized wall formula, equation (2.38), one obtains a simpler, analytically soluble system. The contributions of the first, ideal-gas term of the pressure to the force and the torque in (2.111) are proportional respectively to

$$\oint_S dS\ \hat{n} \tag{2.113a}$$

and

$$\oint_S dS\ (\vec{r}-\vec{r}_o)\times\hat{n} = \oint_S dS\ \vec{r}\times\hat{n} - \vec{r}_o \times \oint_S dS\ \hat{n} \quad . \tag{2.113b}$$

The first integral is known to vanish from equations (2.34) and (A6); the second is also zero, as Section A.4 establishes. The contribution of the next term leads to

$$0 = \vec{F} = +\rho\langle v\rangle_r \oint_S dS\ (\vec{V}-\vec{V}_o)\cdot\hat{n}\,\hat{n} + \ldots \tag{2.114a}$$

$$0 = \vec{\tau} = +\rho\langle v\rangle_r \oint_S dS\ (\vec{V}-\vec{V}_o)\cdot\hat{n}\ (\vec{r}-\vec{r}_o)\times\hat{n} + \ldots \quad . \tag{2.114b}$$

Substitution of the rigid body drift of equation (2.102) into these expressions produces successively

$$\oint_S dS\ [\vec{V} - \vec{\tau} - \vec{\omega} \times (\vec{r} - \vec{r}_o)] \cdot \hat{n}\,\hat{n} = 0 \tag{2.115a}$$

$$\oint_S dS\ [\vec{V} - \vec{\tau} - \vec{\omega} \times (\vec{r} - \vec{r}_o)] \cdot \hat{n}(\vec{r} - \vec{r}_o)\times\hat{n} = 0 \tag{2.115b}$$

and

$$\overleftrightarrow{A}\cdot\vec{\tau} + \overleftrightarrow{B}\cdot\vec{\omega} = \vec{a} \tag{2.116a}$$

$$\overleftrightarrow{C}\cdot\vec{\tau} + \overleftrightarrow{B}\cdot\vec{\omega} = \vec{b} \quad , \tag{2.116b}$$

where

$$\overleftrightarrow{A} = \oint_S dS\ \hat{n}\,\hat{n} \quad , \quad \overleftrightarrow{B} = \oint_S dS\ \hat{n}\ (\vec{r} - \vec{r}_o) \times \hat{n} \tag{2.117a}$$

$$\overleftrightarrow{C} = \oint_S dS\ (\vec{r} - \vec{r}_o) \times \hat{n}\,\hat{n} \quad , \quad \overleftrightarrow{D} = \oint_S dS\ (\vec{r} - \vec{r}_o)\times\hat{n}\ (\vec{r} - \vec{r}_o)\times\hat{n} \tag{2.117b}$$

$$\vec{a} = \oint_S dS\ \vec{V}\cdot\hat{n}\,\hat{n} \quad , \quad \vec{b} = \oint_S dS\ \vec{V}\cdot\hat{n}\ (\vec{r} - \vec{r}_o)\cdot\hat{n} \quad . \tag{2.118}$$

Note that $\overleftrightarrow{C}$ is the transpose of $\overleftrightarrow{B}$. The simultaneous vector equations can be solved in the same way as are simultaneous scalar equations. The answer is

$$\vec{\tau} = (\overleftrightarrow{B}^{-1}\,\overleftrightarrow{A} - \overleftrightarrow{D}^{-1}\,\overleftrightarrow{C})^{-1}\;(\overleftrightarrow{B}^{-1}\,\vec{a} - \overleftrightarrow{D}^{-1}\,\vec{b}) \tag{2.119a}$$

$$\vec{\omega} = (\overleftrightarrow{C}^{-1}\,\overleftrightarrow{D} - \overleftrightarrow{A}^{-1}\,\overleftrightarrow{B})^{-1}\;(-\overleftrightarrow{A}^{-1}\,\vec{a} + \overleftrightarrow{C}^{-1}\,\vec{b}) \quad . \tag{2.119b}$$

These expressions presume that all indicated matrix inversions can be performed. If some of the elementary matrices in equations (2.117) are zero, the solution can be simpler than (2.119). For example, suppose S has a center of symmetry at $\vec{r}_o$, so that if

$$\vec{r} = (\vec{r} - \vec{r}_o) + \vec{r}_o \tag{2.120}$$

belongs to S, so does

$$-(\vec{r} - \vec{r}_o) + \vec{r}_o \quad , \tag{2.121}$$

where the normal must then be $-\hat{n}(\vec{r})$. Performing the associated change of variables leaves $\overleftrightarrow{A}$ and $\overleftrightarrow{D}$ unchanged, but reverses the signs of $\overleftrightarrow{B}$ and $\overleftrightarrow{C}$, wherefore they must vanish. No one has investigated whether some of the elementary matrices can be non-zero, but singular or whether the "determinant" matrices in equation (2.119) can ever be singular or the consequences of either such singularity. Apart from this, $\vec{\tau}$ and $\vec{\omega}$ are determined exactly (in the context of the one-body model), but implicitly, by (2.111); and approximately, but explicitly, by (2.119).

These equations relate $\vec{\tau}(t)$ and $\vec{\omega}(t)$ simultaneously to the velocity field of the surface, $\vec{V}(\vec{r},t)$. If gas and box were distinct, $\vec{\tau}$ and $\vec{\omega}$ should also reflect the past history of the box. For instance, were a rigid box suddenly to jump from one translational velocity to another, it would be some time before the gas could catch up. This problem does not arise for a self-consistent nucleus. Of course, rapid accelerations can invalidate the expressions for $\vec{\tau}$ and $\vec{\omega}$, but at a more fundamental level, by invalidating the uniform density assumption.

It is tempting to choose $\vec{\tau}$ and $\vec{\omega}$ to be the center-of-mass velocity and angular velocity (as defined in Section F), in order to prevent the nucleons from drifting apart from the nucleus. The flaw in this approach consists in confusing the nucleons about to strike the nuclear surface with all the nucleons in the nucleus. There is no reason to expect the motion of the two groups to be identical, except in the case that the nucleus is undergoing rigid body motion. If $\vec{V}$ in equation (2.112) has the rigid body form, then the solution is, of course,

$$\vec{V}_o(\vec{r},t) = \vec{V}(\vec{r},t) \quad . \tag{2.122}$$

The general relationship between these two prescriptions of the drift velocity is unknown. A third approach, however, is enlightening. Suppose a drift field is determined by insisting that

it match the surface motion in a least-squares sense. In other words, at each instant

$$LS = \oint_S dS \; [(\vec{V} - \vec{V}_o)\cdot\hat{n}]^2 \tag{2.123}$$

should be a minimum with respect to variations in the velocity field, $\{\vec{V}_o(\vec{r},t)\}$, parameterized by equation (2.102). It is easy to show that this condition is equivalent to the leading order field obtained by insisting on zero force and torque, (2.115). The drift field chosen on dynamical grounds, thus, has a geometrical meaning: the nucleons and the nuclear surface stay together(at least to this order).

If two nuclei are in contact, the requirement that gas and box should exert neither force nor torque on each still holds, but is not sufficient to determine the drifts. This is easiest to see in the case of a small window. The surface S is the joint surface of the two nuclei, shown at the bottom of Fig. 1, and is the union of S_1 and S_2. The integrals in equation (2.111) split into two, one each over S_1 and S_2. If the window is sufficiently small, the nucleons bombarding each surface, S_i, will still be characterized by a single drift velocity, $\vec{V}_{oi}$, and the integrand over each S_i involves the pressure evaluated at the appropriate $(\vec{\tau}_i,\vec{\omega}_i)$. There are still two vector equations, but now there are four vector

unknowns. At present, there is no firmly established way to further specify the drifts.

Investigators making one-body collision calculations such as those in [6] have often neglected deformation by constraining the nuclei to have spherical shapes (truncated by the window), while recognizing that the accuracy of their results can then be at most semi-quantitative. The drift velocities have been identified concurrently with the center-of-mass velocity of each nucleus, that is, with the velocity of each sphere. This prescription is obviously correct in the limit of a vanishingly small window. Otherwise, it is an approximation the quality of which has not been studied. At least, it insures that the total one-body force on the di-nuclear system is zero. This prescription can be generalized. If deformation is admitted, but the window is still made vanishingly small, then each nucleus, i, is effectively isolated for the purpose of determining its drift velocity, which is given by equation (2.111) or (2.119) and where the integrals are now over S_i. The error involved in applying this prescription to finite windows is unknown. So, too, is the method of application itself, namely, whether the integrals should extend over the window. For small windows, diffraction is significant. Is there a useful range of window sizes large enough for diffraction to be neglected and small enough for the preceding window prescription to be

approximately correct?

It would be surprising if the rigid body drift prescription were to add further errors to those associated with the randomization assumption, apart from the centrifugal effect introduced by rotation. Table 1 suggests that the centrifugal effect is substantial. Taking the assymptotic excitation as a crude, linear measure of the difference between the initial and asymptotic states, the centrifugal effect might amount to 18% of the total rotational effect. This ratio varies little with frequency over several orders of magnitude. Another investigator has suggested how to explain this [21]. Suppose that the asymptotic excitation, E_n^* and E_c^*, for initially non- and co-rotating distributions can be expanded in a power series in ω. The excitation cannot depend on the sense of the rotation, so both excitation functions must be even in ω. Both excitations vanish in the limit that ω goes to zero. Symbolically,

$$E_c^* = a_c\omega^2 + b_c\omega^4 + \ldots \tag{2.124a}$$

$$E_n^* = a_n\omega^2 + b_n\omega^4 + \ldots \quad , \tag{2.124b}$$

causing

$$\frac{E_c^*}{E_n^*} = \frac{a_c}{a_n} + O(\omega^2) \quad . \tag{2.125}$$

The 18% error estimate is probably excessive. Centrifugal effects are important only to the extent that a system is compressible. The same factor by which the compressibility of a Fermi gas exceeds that of nuclei probably exaggerates the relative importance of centrifugal effects in this estimate.

It would be useful to modify the cranking-model potentials so that they describe two joined nuclei. The window formula could then be tested in the same way as was the wall formula. Since the window formula incorporates drift velocities, their prescription would also be tested.

The linear response and leptodermous treatments of the wall formula are both restricted to situations in which there are no drifts and do not address more general situations. TDHF calculations follow each nucleon separately and can therefore dispense altogether with drift velocities.

6. Dissipation and irreversibility

Forces and powers have been calculated with little attention paid to the extent to which they are actually dissipative.

The simple example of a one-dimensional gas in a

one-dimensional box, alluded to earlier, illustrates the problem. If the box, originally at rest, is suddenly given a constant speed, half the energy it eventually imparts to the gas is used to bring the gas up to speed; only the remaining half is dissipated into internal motion of the gas. This conclusion is common knowledge in the circle working on the one-body model. Since the example is one of the few that can be handled analytically and since no proof has been exhibited in public or in print, the author's proof is provided in Appendix E.

Generally, the one-body forces and powers are partly dissipative and partly not. The second term of the specialized wall formula for the power, equation (2.38), is even under time reversal in the absence of drifts and is therefore purely irreversible and dissipative. ("Dissipative" and "irreversible" are equivalent). For arbitrary drifts, this conclusion breaks down. The self-consistent choice of drift velocities for single nuclei is embodied in equation (2.112). If a drift field, $\vec{V}_o(\vec{r},t)$ solves (2.112) for a given velocity field, $\vec{V}(\vec{r},t)$, then $-\vec{V}_o(\vec{r},t)$ obviously solves the system for the time-reversed velocity field, $-\vec{V}(\vec{r},t)$. Consequently, $\vec{V}_o(\vec{r},t)$ is odd under time reversal. Those terms in the expansion of the power wall formula, equation (2.39), that are <u>even</u> in $\vec{V}$ and $\vec{V}-\vec{V}_o$ are purely dissipative, while those that are <u>odd</u> are purely conservative. The most conspicuous example of the latter

is the lowest order term, proprtional to the rate of change of the nuclear volume. The corresponding rule for the pressure is that terms <u>odd</u> in $\vec{V}$ and $\vec{V}-\vec{V}_o$ are dissipative and <u>even</u> terms are conservative. The specialized wall formula for the power, equation (2.40), is purely dissipative.

A choice of drift velocity designed to conserve linear and angular momentum and to preserve self-consistency thus turns out to neatly classify the wall formula contributions as dissipative or conservative, but this is not the last loose end it ties off. By insisting that the force exerted on the gas by the wall be zero, this drift prescription also insures the Galilean invariance of the power in equation (2.31). Although power need not be a Galilean invariant in general, the <u>dissipative</u> power ought to be invariant. This is because that power increases internal excitation and temperature, which last is known to be invariant. The feature of the one-dimensional example that caused part of the energy increase to flow into collective motion was that the box and gas were able to exert net forces on each other.

The window force could be decomposed into dissipative and conservative components, as was the wall pressure, if the two drift velocities were so specified as to change sign under time reversal. Such a specification does not exist now. If one is found in the future, it is not unlikely that it will so change sign. In the

meantime, the spherical-nucleus approximation sets the drift velocity equal to the displacement velocity of the spheres, causing it to change sign under time reversal. In this approximation, those terms in the window force, such as the specialized window formula, that are odd in the drift and window velocities are dissipative and the rest are conservative. The same classification applies when the tentative drift prescription for deforming nuclei connected by a vanishingly small window is employed.

Other models also shed some light on the distinction between dissipation and conservation. The classical and quantal cranking calculations spectacularly reveal the existence of reversible components in the power, when the latter turns negative [6]. In some quantal calculations, the originators of the cranking calculations tried to separate the conservative and dissipative processes by excluding from the excitation energy that part of it caused by evolution of the energy levels, in contrast to that caused by changes in their population. The former is reversible. This exclusion improved agreement between the wall formula and the computer calculations, thereby supporting the dissipative nature of the specialized wall formula for the power.

The linear response treatments explicitly separate the dissipative and conservative contributions [16]. It has already been pointed out that the circumstances most favorable to the

validity of the wall formula occur when the nuclear surface and its deformations are assymetric and their deviations from planarity have wavelengths long compared to those of the nucleons. In this limit, the linear response results were shown in [17] and [18] to reduce to those of the specialized wall formula in the absence of drifts. This conclusion is now seen here to support further the dissipative quality of the formula.

The leptodermous approach is equivalent to a driftless one-body approach in its handling of dissipation and irreversibility.

TDHF calculations need not concern themselves with dissipation since all degrees of freedom are treated in the same way. It is possible to compare, for example, initial and final collective and kinetic energy in a collision once the two nuclei separate, but, since some probability spreads throughout the normalization volume, the decision about which nucleus each piece of wave function should be said to belong to is somewhat arbitrary and introduces corresponding errors.

7. Nuclear density

The derivation of the wall and window formulae assumed that nuclear density was constant in time, uniform in space, and identical in different nuclei. All these assumptions are but first approximations. Nuclear matter <u>is</u> compressible, so the density can

change in time and become inhomogeneous even in nuclear interiors. In Section D.1, the point was made that the development of density inhomogeneities implies the breakdown of the wall and window formulae, but that it may occur only when the velocity of deformation is no longer negligible compared to the Fermi speed. There is the additional possibility that the average nuclear density might change as well. Since it cannot very well do so in the absence of nuclear deformation or interpenetration, this effect, too, may never become significant unless the nuclear speeds become comparable to the nucleon speeds.

Nuclear density varies slightly, but systematically, with atomic weight and number. The effective sharp radius

$$R = 1.28\ A^{1/3} - 0.76 + 0.8\ A^{-1/3} \tag{2.126}$$

is taken from [2] and the corresponding number density per cubic Fermi ranges from 0.162 for A = 60 to 0.146 for A = 138, a difference of 11% of the latter. Although such a final, relative error in a dynamical result might be acceptable, such a density difference can induce much larger relative changes in the window force.

To see this, one can trace the identities of the two gases through the derivation of the window formula. One finds

$$\vec{F}_1^{\text{exchange}}(W) = \int_W dW \Big[-\frac{1}{3}\rho_1 \langle v^2 \rangle_1 \hat{n}_1 + \frac{1}{6}\left(\rho_1 \langle v^2 \rangle_1 - \rho_2 \langle v^2 \rangle_2\right)\hat{n}_1$$

$$- \frac{1}{4} \frac{\rho_1 \langle v \rangle_1 + \rho_2 \langle v \rangle_2}{2} (\vec{V}_{01} - \vec{V}_{02}) \cdot (\overleftrightarrow{I} + \hat{n}_1 \hat{n}_1)$$

$$- \frac{1}{4} (\rho_1 \langle v \rangle_1 - \rho_2 \langle v \rangle_2) \Big\{ \frac{1}{2} (\vec{V}_{01} + \vec{V}_{02}) \tag{2.127}$$

$$- \left[\vec{V} - \frac{1}{2} (\vec{V}_{01} + \vec{V}_{02}) \right] \cdot \hat{n}_1 \hat{n}_1 \Big\} + \ldots \Big] \quad ,$$

where the subscripts on the densities and velocity moments denote the gas in question. Note that a different density leads to a different Fermi speed and thence to a different velocity moment. The first term in equation (2.127) is just the familiar, lowest order term that is canceled by the lowest order wall term. The second term is not so canceled. In magnitude, it differs from the specialized window formula by a factor

$$O\left[\frac{\rho_1 - \rho_2}{(\rho_1 + \rho_2)/2} \right] O\left[\frac{V_F}{|\vec{V}_{01} - \vec{V}_{02}|} \right] \quad , \tag{2.128}$$

which could easily be of order 1. It is conservative in nature. The third term is the analog of the ordinary specialized window formula. Finally, the fourth term can also be of the same order as

the specialized window formula, because it involves a different combination of nuclear velocities. Based on its apparent behavior under time reversal, it is as likely to be purely dissipative as is the specialized window formula; however, it is not Galilean invariant. For collisions of fairly symmetric nuclear combinations, this term is negligible, but it might be important for asymmetric combinations.

The computer cranking, linear response, and leptodermous models all posit constant densities and none apply to nuclear collisions in which nucleons are transferred. TDHF calculations never rely on a density except when setting the size of the initial states.

8. Net transfers of nucleons and the window definition

It is surprising that the window velocity does not appear in the specialized window formula, but only in the next term of the general window formula, equation (2.65), and in the fourth term of (2.127). It has therefore not been urgent to define the window.

Someone else has suggested a definition [21] that begins by observing that there should be no net transfer of mass between identical nuclei. The window must then be so defined that $\dot{N}_1 = 0$ in equation (2.63). This can be accomplished by requiring that

$$\left\{\vec{V}(\vec{r},t) - \tfrac{1}{2}\left[\vec{V}_{01}(\vec{r},t) + \vec{V}_{02}(\vec{r},t)\right]\right\}\cdot\hat{n}_1(\vec{r},t) \qquad (2.129)$$

vanish everywhere on the window at all times. The proof has been supplied by the present author and follows. $\dot{N}_1$ in equation (2.63) is a function only of U_1 and U_2, or of

$$U_{\pm} = U_1 \pm U_2 \quad . \qquad (2.130)$$

Strictly speaking, the theta functions prevent $\dot{N}_1$ from being analytic, but experience (or direct verification) says that $\dot{N}_1$ is actually a multinomial in U_1 and U_2 (or in $U_{\pm}$), as long as all velocities are less than the Fermi speed. Equation (2.63) is plainly odd under exchange of U_1 and U_2. Therefore, the only terms that can appear in the multinomial must be odd in U_-, so $\dot{N}_1$ is a product of U_- and of another multinomial in U_1 and U_2. $\dot{N}_1$ is zero if U_- is zero and U_- is just twice expression (2.129). Note that this result is exact, given the general window formula. Expression (2.129) actually defines only the normal component of $\vec{V}$, but that is sufficient to define a surface.

What happens when the two nuclei are different? Mass transfers are then almost inevitable, so $\dot{N}_1 = 0$ will not serve to define the window. Equation (2.129) should still be retained, in order to exclude from $\dot{N}_1$ a fictitious component that would persist

even in the case of identical nuclei. The exchange force would no longer be a Galilean invariant.

For a two-dimensional window to approximate well the three-dimensional region connecting two nuclei, the window must be small. In the limit of zero size, the shape and the position of the window will always be obvious, but the velocity will still have to be specified. Even in this limit, the accuracy of the suggested window definition, equation (2.129), is unknown and diffraction may have to be included in exchange force calculations. There are no quantitative estimates of the errors involved in supposing the window to be two-dimensional when it is no longer small. The failure of the specialized window formula to depend on $\vec{V}$ means that the definition of the window <u>velocity field</u> can be, at most, a small source of error. Any definition of the window is certain to be somewhat arbitrary, since the boundary between two nuclei is not self-evident. Perhaps the only real requirement is that two nuclei theoretically separate, or form a compound nucleus, in a sensible manner (e.g., the window should not finish inside one of two separated nuclei).

Nuclear motion injects matter, and, indirectly, thermal excitation, into the connecting region. From there, nucleonic motion carries the matter into the nuclear interiors. As long as the window is small, nucleonic motion homogenizes conditions <u>within</u>

the nuclei much more rapidly than between nuclei. That is why the model that leads to the window formula can follow explicitly the evolution of the drift velocities (at the window) or densities toward a single value common to both nuclei, while assuming the homogenization of each nucleus to be instantaneous. The accuracy of this separation can be assessed by recalling that the nucleon distribution function at each place and time in a nucleus is determined by the activity of the surface at (various) earlier times. This is a consequence of the independent particle assumption. When a nucleus is connected by a window to some other nucleus, its surface, though pierced by the window, may be closed mathematically by incorporating the window in it. Each part of this mathematical surface contributes to the distribution function. The window contribution may be very different qualitatively from that of the rest of the surface, but the quantitative difference should be small. The flux of particles entering through the window is the product of their number density and speed. The speed is of the order of the Fermi speed, because that speed is assumed to be much larger than that of relative nuclear motion. Number density and Fermi speed are roughly the same in all nuclei. The approximate relative importance of the window contribution thus should be just the ratio of the window area to the nuclear surface area:

$$\frac{A(W)}{A(S)} = \frac{1}{4}\left(\frac{a}{R}\right)^2 , \qquad (2.131)$$

where a is the window radius (presuming the window to be circular). Obviously, the window radius need not be tiny. For a window with a diameter of 5 Fm., in a uranium nucleus, the ratio is only 0.03.

Once more, the computer cranking and linear response models have not dealt with these window matters and TDHF need not.

9. Summary

The preceding discussion of the assumptions underlying the one-body model showed that the general model is an approximation that can be good only when nuclear speeds of deformation and of relative motion are small enough compared to nucleon speeds that the independent particle assumption holds, and when internal excitation is large enough that nuclear dynamics is not that of a superfluid. One-body effects then dominate two-body effects, although two-body effects may still be significant. For the wall and window formulae to be correct, the speeds must also be small enough that the uniform potential assumption is satisfied. Even then, symmetry effects may be of the same order as the formulae themselves.

Regarding the wall as perfectly reflective seems to be a good approximation, but the diffuseness of nuclear surfaces means

that significant curvature corrections must be made to the wall formula and that the proximity trick must be applied to the window formula.

If the drifts are properly specified, randomization, assisted by two-body collisions, should be sufficient to determine that part of the nucleon distribution relevant to the wall and window formulae and to insure that the leading volume-conserving terms of these formulae are purely dissipative. Symmetry makes itself felt by hindering randomization. A single set of constraints on the drift velocities insures conservation of momentum, both linear and angular, and self-consistency between nucleons and the nuclear surface. The drift velocity prescription for isolated nuclei is known, but not that for two overlapping nuclei, except perhaps in the limit of a vanishingly small window. Insisting on a small window may be no more drastic than requiring deformations to be slow, but it may also force inclusion of diffractive effects.

The idealization of a three-dimensional connecting region between two nuclei as a two-dimensional window is also valid only for small windows. For two nuclei of similar density, the velocity of the window is irrelevant to the specialized window formula. If the densities are significantly different, then the window velocity must be specified, which has tentatively been done.

As should be obvious by now, TDHF has the great advantage of

requiring the validity only of the independent particle assumption. To extract any information from the model, however, requires long and costly numerical calculations. The results do include shell effects, but are ipso facto specific to the nuclear species considered. Other comments on TDHF may be found in [19].

E. APPLICATIONS

1. Nuclear vibrations

Nuclear vibrations are an important topic of nuclear spectroscopy [25]. It is convenient to begin with a standard model of nuclear vibrations described, for example, in [26]. This Lagrangian model includes a liquid drop potential energy and a hydrodynamical kinetic energy. It has already been argued in Section D.5.a that randomization, not hydrodynamics, is relevant to systems with long mean free paths; comparison of the effects of one-body dissipation with those of hydrodynamics will support this view.

In the notation of [26], the model may be summarized as follows. The surface is described by its radius as a function of solid angle and is expanded perturbatively in spherical harmonics about a sphere of radius R_0:

$$R(\theta,\phi) = R_0\left[1 + \sum_{\lambda\mu} \alpha_{\lambda\mu}\, Y^*_{\lambda\mu}(\theta,\phi)\right] \quad . \tag{2.132}$$

Keeping R real forces

$$\alpha^*_{\lambda\mu} = (-1)^{\mu}\, \alpha_{\lambda-\mu} \tag{2.133}$$

and maintaining the volume equal to that of the original sphere leads to

$$\alpha_{00} = -(4\pi)^{-\frac{1}{2}} \sum_{\lambda\mu} |\alpha_{\lambda\mu}|^2 \quad , \tag{2.134}$$

where terms of higher order in the α's are neglected because the α's are presumed small. Harmonics having non-zero μ's carry angular momentum. Excluding them prevents rotation, in the sense that the expectation values of all components of the angular momentum then vanish, and will simplify the prescription of the drift velocity.

The liquid drop potential energy is the sum of the surface energy and the Coulomb energy. The surface energy is just the product of the surface tension parameter, $\mathcal{S}$, and the surface area. Its expansion is

$$V_{surf} = 4\pi R_0^2 \mathcal{S} + \tfrac{1}{2} R_0^2 \mathcal{S} \sum_{\lambda>0} (\lambda-1)(\lambda+2)(\alpha_{\lambda 0})^2 + \ldots \quad . \tag{2.135}$$

The Coulomb energy is the self-energy of a uniform charge

distribution inside the nuclear surface. Expanding it, one finds

$$V_{Coul} = \frac{3}{5}\frac{Z^2e^2}{R_0} - \frac{3}{4\pi}\frac{Z^2e^2}{R_0}\sum_{\lambda>0}\frac{\lambda-1}{2\lambda+1}(\alpha_{\lambda 0})^2 + \ldots \quad , \qquad (2.136)$$

where Ze is the nuclear charge. For incompressible, irrotational hydrodynamics, the total kinetic energy is

$$T = \tfrac{1}{2} M\rho_0 R_0^5 \sum_{\lambda>0}\frac{1}{\lambda}(\dot{\alpha}_{\lambda 0})^2 + \ldots \quad . \qquad (2.137)$$

Dissipation can be introduced into this formalism via the Rayleigh dissipation function, which is described, for instance, in [27]. This function equals half the dissipated power, as given by the specialized wall formula, equation (2.40).

To apply that formula, note first that neither V_{surf} nor V_{Coul} provide any restoring force for $\lambda = 1$. This is because the $\lambda = 1$ mode corresponds to simple displacement. Restricting attention to $\lambda > 1$, combined with the previous decision to exclude $\mu \neq 0$, thus allows the drift velocity to be set equal to zero. The next step is to find the normal component of the surface velocity. The surface normal is

$$\hat{n}(\theta,\phi) = \left[R^2 + \left(\frac{\partial R}{\partial\theta}\right)^2 + \frac{1}{\sin^2\theta}\left(\frac{\partial R}{\partial\phi}\right)^2\right]^{-\frac{1}{2}} \times \left(R\hat{r} - \frac{\partial R}{\partial\theta}\hat{\theta} - \frac{1}{\sin\theta}\frac{\partial R}{\partial\phi}\hat{\phi}\right), \tag{2.138}$$

where $\hat{r}$, $\hat{\theta}$, $\hat{\phi}$ are the unit vectors generated by changes in r, θ, ϕ. The velocity is

$$\vec{V}[R(\Omega)\ \hat{r}(\Omega)] = \dot{R}(\Omega)\ \hat{r}(\Omega) \tag{2.139}$$

(which was already used in the kinetic term). Therefore, the Rayleigh function becomes

$$\mathcal{F} = \tfrac{1}{2}M\rho_0\langle v\rangle_r\ R_0^{\ 4}\sum_{\lambda>1}(\dot{\alpha}_{\lambda 0})^2 + \ldots \quad . \tag{2.140}$$

The equations of motion are

$$\frac{d}{dt}\left(\frac{\partial L}{\partial\dot{q}_i}\right) - \frac{\partial L}{\partial q_i} + \frac{\partial\mathcal{F}}{\partial\dot{q}_i} = 0 \tag{2.141}$$

for an arbitrary set of generalized coordinates, q_i, i = 1, 2, ... Here, the generalized coordinates are $\alpha_{\lambda 0}$, λ = 2, 3, ... and the equations of motion become a system of uncoupled, second order, linear differential equations with constant coefficients. The solution can be written as

$$\alpha_{\lambda 0} \propto e^{i\hat{\omega}_\lambda t} \quad , \tag{2.142}$$

if

$$\hat{\omega}_\lambda = i\gamma_\lambda \pm \sqrt{\omega_\lambda^{\,2} - \gamma_\lambda^{\,2}} \quad . \tag{2.143}$$

In this expression, ω_λ is the frequency in the absence of dissipation

$$\omega_\lambda = \left\{ \frac{\mathcal{S}}{M\rho_0 \, R_0^{\,3}} \, \frac{\lambda(\lambda-1)}{2\lambda+1} \left[(2\lambda+1)(\lambda+2) - 20x \right] \right\}^{\frac{1}{2}} \quad , \tag{2.144}$$

where x is the fissility,

$$x = \frac{3}{40\pi} \, \frac{Z^2 e^2}{\mathcal{S} \, R_0^{\,3}} \quad , \tag{2.145}$$

and

$$\gamma_\lambda = \frac{\langle v \rangle_r}{2R_0} \, \lambda \quad . \tag{2.146}$$

The presence of a small γ_λ in equation (2.143) causes the general solution to the equations of motion to be a transient oscillation. When γ_λ exceeds ω_λ, however, ω_λ becomes purely imaginary and the solution decays without oscillating.

The ratio $\gamma_\lambda/\omega_\lambda$ is a measure of the degree to which the system is damped. If the ratio equals 1, the system is critically damped and, if it is greater than 1, the system is overdamped.

Table 2 presents numerical values of the ratio in examples spanning both the periodic table and the plausible range of multipole vibrations. Of the parameters in equations (2.144) and (2.146),

$$\langle v \rangle_r = \frac{3}{4} v_F \quad , \tag{2.147}$$

from (2.44) and, in (2.41), $r_o = 1.1$ Fm. Also,

$$R_0 = r_o A^{1/3} \quad , \tag{2.148}$$

and ρ_0 is determined accordingly. The surface energy coefficient is set by

$$4\pi r_o^2 \mathscr{S} = 17 \text{ MeV} \quad . \tag{2.149}$$

The average nucleon mass is taken to be 939 MeV/c^2 [25].

Table 2 indicates that a vibrating nucleus is overdamped in the one-body model, except for high order spherical harmonics in small nuclei. In such nuclei, the author calculates that even one quantum of excitation produces surface distortions much too large to be handled perturbatively. Indeed, the imposition of complicated, high order spherical harmonics on systems composed of so few particles is probably unjustified. On the other hand, for the Sn and U nuclides, both $\alpha_{\lambda 0}$ and the ratio of the normal velocity to the Fermi speed are small throughout the range of spherical harmonics considered.

Overdamping is a signal that dissipation is more important

that kinetic energy in the dynamics of nuclear vibrations. In such instances, complete neglect of any kinetic term offers a first approximation to nuclear dynamics.

Overdamping of nuclear vibrations has the experimental consequence that vibrational level widths should exceed their level energies and, consequently, their spacings, making the levels unobservable. Actual vibrational spectra consist only of low-lying levels that are few compared to the number of levels seen in nuclear rotational spectra. This comparison is consistent with the one-body model.

The existence of any vibrational levels at all reflects a the breakdown of the semi-classical assumption caused by the failure of a small excitation energy to excite more than a few, low-lying, nuclear states. As discussed in Section D, this paucity of accessible states restricts nuclear dynamics to that of a superfluid. Any comparison of the experimental and one-body widths of these levels is therefore likely to be futile.

2. Other developments

The one-body model has been applied by others to numerous problems in nuclear physics. A brief account of their efforts will serve several purposes. First, it will provide the reader with an appreciation of the broad range of nuclear phenomena to which the one-body model is relevant. Secondly, it will survey the current

relationship between the theoretical model and experimental reality. Finally, these developments represent first efforts to apply the one-body model and an understanding of their possible limitations is needed in planning future refinements and generalizations.

The first task was to deduce some general estimates of the size of one-body effects [6]. For deformations, such as vibrations and fission, the damping time, t_{damp}, is of the order of

$$|T/\dot{E}| \quad . \tag{2.150}$$

The kinetic energy of the collective motion is represented by T. The power, $|\dot{E}|$, is predicted by the wall formula to be of order

$$\rho\langle v\rangle_r \, 4\pi R^2 \, \langle (\vec{V}\cdot\hat{n})^2 \rangle \quad , \tag{2.151}$$

where the square of the normal velocity is averaged over the nuclear surface of radius R. Similarly, the total kinetic energy is of order

$$\rho \frac{4}{3} \pi R^3 \langle (\vec{V}\cdot\hat{n})^2 \rangle \quad . \tag{2.152}$$

Therefore,

$$t_{damp} = O\left(\frac{R}{\langle v\rangle_r}\right) \quad , \tag{2.153}$$

in the range of $(0.7\text{-}1.3)\times 10^{-22}$ sec. This is shorter than many

characteristic collective times, so such motions should be dominated by dissipation.

The corresponding estimate for nuclear collisions makes use of the window formula to calculate the stopping time, t_{stop}, in which the kinetic energy of relative motion is dissipated. This analog of t_{damp} is compared to the collision time,

$$t_{coll} = O\left(\frac{R}{V}\right) \quad , \tag{2.154}$$

where R is the radius of either of the two nuclei and V is their relative speed when they first make nuclear contact. The ratio is

$$\frac{t_{stop}}{t_{coll}} = O\left[\left(\frac{R}{\langle a \rangle}\right)^2 \frac{V}{\langle v \rangle_r}\right] \quad , \tag{2.155}$$

in which <a> is the window radius time-averaged over the collision. If the window becomes large enough and the energy over the barrier is small enough, one-body dissipation should stop the nuclei during the collision, a phenomenon observed experimentally in deep-inelastic collisions.

Detailed fission calculations using the wall formula have been carried out [6]. The potential energy was determined by folding a two-body Yukawa potential over the nuclear density in order to obtain a single potential for the entire nucleus. The collective kinetic energy was calculated using incompressible,

nearly irrotational hydrodynamics. For comparison with wall formula results and with experiment, calculations were also performed that used ordinary two-body viscosity as the source of dissipation and fit the viscosity coefficient to experiment. It turned out that neither method's results changed much when the kinetic energy was deleted. This constitutes another case of dissipation dominance.

To exclude shell effects, the experimental data shown in Fig. 14 were restricted to the fission of nuclei with moderately high initial excitation energies. Accordingly, the theoretical calculations started at the fission saddle point with 1 MeV of kinetic energy in the fission direction. Experimentally, the most probable fission-fragment kinetic energies, shown as a function of $Z^2/A^{1/3}$ in the figure, then corresponded to two equal fragments. To match this, the theoretical calculations constrained the configuration always to be axially symmetric about the fission axis and reflection symmetric through a plane perpendicular to it. Figure 14 shows how well the one-body calculations then agreed with experiment.

Two cautions are in order. First, the one-body calculations used zero drifts in the wall formula all the way to scission and set dissipation to zero thereafter. Before scission, however, the neck joining the two lobes of the original nucleus becomes small enough that the window formula should be used, each lobe having its own

drift. What should be done during the transition from the wall to the window formula is an open question. Finally, the wall formula should be applied separately to each lobe, both before and after scission. One-body calculations incorporating these improvements might produce results very different from those in Fig. 14. The second caution is that the experimental results in Fig. 14 can also be fitted by two-body calculations. The fitted viscosity parameter seems, however, too small to produce the dissipation seen in deep-inelastic collisions.

Detailed one-body calculations for nuclear collisions have also been made, again including some drastic approximations [6]. The potential is given by the sum of the proximity potential [2] and the Coulomb potential created by point or spherical nuclei. The kinetic energy is taken to be that of two rigid spheres. Sphericity, however, is a bad approximation toward the end of collisions. Deformation may produce as much dissipation as does particle exchange [28]. Nonetheless, the dissipation in this model is provided solely by proximity friction [22].

This model has been applied to ^{86}Kr + ^{197}Au collisions at 600, 800, and 1000 MeV. Figure 15 displays the final angular momentum as a function of initial angular momentum. Experimentally, deep-inelastic collisions are thought to lead eventually to configurations in which the nuclei stick together (until they

separate), without rolling or sliding on each other. Here, the lower limit of the final angular momentum is 5/7 the original value--characteristic of configurations in which the nuclei roll on each other without sliding [29]. Perhaps this discrepancy can be removed by taking into account the variations in drift velocities over the window surface. Figure 16 shows the relationship between the scattering angle and the final center-of-mass kinetic energy of the two nuclei. The shapes are qualitatively similar to those observed experimentally [30]. In particular, at large scattering angles, nearly all the kinetic energy (above the Coulomb barrier, E_B) is dissipated. Deep-inelastic collisions are defined experimentally as those collisions in which the nuclei do not fuse, but do lose all their energy of relative motion, save that due to Coulomb repulsion when they separate.

Even though nuclei do not fuse in deep-inelastic collisions, their charge and mass change. The window formula relies on particle exchange, but uses only the mean number exchanged, not the fluctuations. The underlying picture has been used to calculate the coefficients of a Fokker-Plank equation for the diffusion of nuclear properties through the window as they are driven by nuclear potentials, such as the symmetry potential [3], [4]. Both the mean changes and fluctuations of these properties have been calculated. As mentioned in Section D.4, fluctuation calculations, unlike the

wall and window formulae, must take explicit account of the Pauli principle. They have turned out to be very sensitive to the occupancy of levels near the Fermi surface and consequently to the temperature, which must be followed throughout the collision. The means and variances in the charges of two colliding nuclei were calculated as functions of the loss of relative nuclear kinetic energy. Even when various, rather crude models of nuclear dynamics were used, the results agreed quite well with experiment.

The widths of giant dipole resonances will serve as a final application [31]. Their estimation was based on a model of giant dipole resonances that mixes two previous models: the Goldhaber-Teller model [32] and the Steinwedel-Jensen model [33]. In the Goldhaber-Teller model, the resonance is produced by oscillation of the proton and neutron density distributions, both spherical and rigid, through each other in opposite directions. The Steinwedel-Jensen model posits opposing density variations of the two distributions, but constrains them both to remain inside a spherical surface. There, the variations oscillate in the lowest acoustic mode of a spherical cavity. The new giant-dipole-resonance model determines the weights of the two modes.

The wall formula was used to calculate the power dissipated and the widths. To do so, the surface was assumed to remain spherical and fixed. The neutrons and protons were treated

separately and each was assigned a uniform velocity equal to its center-of-mass velocity in the solution to the giant-dipole-resonance problem.

With these assumptions, the calculated widths reproduced experiment by decreasing with A. However, they were always too large, the excess decreasing from 100% at A = 50 to 40% at A = 240.

This application was performed early in the development of the one-body model, when it was less understood than it is now. The most obvious difficulty inheres simply in the use of the Steinwedel-Jensen mode, which is hydrodynamical. Therefore, its use contradicts the one-body model directly. Also, for consistency, the mode's contribution to the drift velocity should be its local velocity field evaluated at the boundary, where it is zero. The mode would then contribute nothing to dissipation. Lastly, the assumption that the surface is rigid is made dubious by the introduction of the Goldhaber-Teller mode. The resolution of these contradictions does not promise to be easy, nor is there any certainty as to what effect their resolution would have on the comparison of theory and experiment.

F. CONCLUSIONS

The goal established in the introductory chapter of this dissertation was the discovery of an analog to the liquid drop model

of nuclear statics that could describe the average behavior of nuclear dynamics. The history of nuclear statics also points to the basic tool: the independent particle assumption. This assumption leads directly to the mean field approach and so is synonymous with the general one-body model.

The liquid drop analogy suggests that nuclear dynamics be analyzed in terms of collective, macroscopic variables and internal, microscopic variables. If one considers the possible combinations of potential, kinetic, and dissipative terms with translational, rotational, and deformational degrees of freedom, one concludes that all the combinations are known except for the various dissipative terms and for the kinetic energy of deformation. Among the several applications of the one-body model thus far discussed, two--vibrations and fission--dealt with the kinetic energy produced by deformation. Both found it less important than dissipation, but they disagreed on its insignificance. The attention of this work has been devoted to dissipation, but it is possible that the kinetic energy of deformations may need to be considered, at least in some situations.

Two simple formulae are the progeny of the one-body model. The wall formula helps to describe a single, deforming nucleus, while the window formula applies to two nuclei connected by a small window. Neither formula contains any free parameters.

These formulae depend on certain assumptions which control the degree of their accuracy and the range of their validity. Of these assumptions, only the independent particle assumption is required by all one-body models, not just that embodied in the two formulae. When the assumptions hold, the formulae are the leading order approximation to reality. For them to hold, collective nuclear motion must be slow enough compared to nucleonic motion that the nucleons move independently in a single, uniform nuclear potential, yet fast enough that the dynamics is not dominated by superfluidity. The nucleus must also be large enough that the quantal nature of the nucleons can be ignored without disaster. Finally, any region connecting two nuclei must be small enough to be regarded as a window and to restrict the number of drift velocities in each nucleus to one, but it must be large enough that nucleon diffraction by the window does not dominate the situation. There is, of course, no guarantee that the two pairs of contrary requirements can always or ever be met.

If they are, then one-body effects outweigh two-body effects, dissipation probably (but not certainly) occurs mainly in the surface regions of nuclei, and operation of the Pauli principle can be ignored. Then, too, the Heisenberg uncertainty principle can be neglected in deformations and is of secondary importance at windows.

Even so, the one-body formulae require corrections. Of unknown size are the effects of residual two-body interactions, dissipation produced in nuclear interiors, and window diffracton. The assumption of specular reflection is special in that its failure cannot change the structure of the wall formula integral, but might change the constant multiplying the integral to an unknown extent.

Several corrections can be of the order of the wall or window formula results. Excessive regularity of motion and shape hinders randomization and so introduces shell effects that can amount to half the formula results. Shell effects, of course, are not average effects. Density differences between nuclei seem able to double or eliminate the window force; fortunately, they are easy to include in the window formula.

In a category of medium sources of error is diffuseness, which can reduce the wall formula by as much as 30%. Other investigators have shown how to add diffuseness to the wall and window formulae. Their refinements retain much of the simplicity of the original formulae.

Rotation may introduce two small sources of error. First, centrifugal force should induce density gradients of 5-10% in nuclei. Secondly, the moment of inertia might be very different from the rigid body value. For a given angular momentum, the angular frequency could be quite unexpected. The resulting change

in the drift velocity, however, will usually have only a small effect on nuclear dynamics, since only its component normal to the surface then matters.

The effects of non-zero temperatures and of differences in the number of neutrons and protons are both small, no more than a few percent of the wall and window results. They are also easy to include in the wall and window formulae.

The original idea of nucleon randomization about a drift velocity yields to a distinction between nucleons approaching and leaving a surface. Only the former need be randomized, a relaxation that preserves the continuity condition at the boundary and causes the density to vary with the surface and drift velocities in a sensible way. The drift velocity assumes a rigid body form in order to remain as simple as possible while incorporating translation and rotation. For deformations of a single nucleus, the drift velocity's actual value is fixed by the conservation of linear and angular momentum. The drift prescription then insures consistency between the nuclear surface and the nucleons composing the nucleus. The drift velocities of two nuclei interacting through a window are known only in the limit that the window is vanishingly small. For an arbitrary drift, the wall and window effects are an inextricable mixture of reversible and irreversible effects. When the formulae are expanded in powers of the ratio of the nuclear velocity to the

mean nucleon velocity, the drift prescription makes each term either purely reversible or purely irreversible. The leading volume-conserving term in each formula is then purely dissipative. Thus, the randomization and drift hypotheses solve many problems, which otherwise appear unrelated, in a way that is beautiful and, therefore (one hopes), true [34].

The one-body formulae have been applied to a variety of nuclear phenomena: nuclear vibrations, fission, collisions, the diffusion of nuclear properties between nuclei, and giant dipole resonances. Simple, order-of-magnitude arguments prove that one-body dissipation can be large enough to account for the large amount of dissipation seen in some experiments. In its more detailed applications, the one-body model is not contradicted by experiment. The crudity of the applications, however, precludes any more satisfactory statement.

Theories usually develop through enunciation of their method, probing of their assumptions, and comparison of their predictions with experiment. The restricted one-body model, embodied in the wall and window formulae, has taken the first steps along each of these paths, but much mileage remains. The paths have crossed in the past and will do so in the future, but the need for progress along one particular path is most urgent.

Nuclear collisions currently constitute the subject of

greatest general interest to which the one-body model can be applied. Other reseachers, using a different model [28], conclude that deformations produce substantial dissipation in collisions. Wall effects must, therefore, be added to window effects in one-body collision calculations. Fortunately, efforts in that direction have already begun elsewhere. One impediment is presented by the connecting region between nuclei. If it is very small, diffraction must be accommodated. When it is large, neither the wall nor the window formula apply. This point needs further study.

Resolution of the same difficulty is also the most immediate task in fission applications. To improve the calculation of widths of giant dipole resonances, more consistent treatment of the two modes that contribute to the resonances is called for. Diffusion calculations have proved encouraging, but their comparison with experiment is made difficult by their superimposition on some model of nuclear dynamics. Are discrepancies to be attributed to errors in reckoning the diffusion or the nuclear motion? Perhaps some tests can be devised that are independent of the dynamics approach chosen.

A way of describing substantial connecting regions is not the only expansion of the model that is needed. For small, but non-vanishing, windows, the nuclear drift velocities have yet to be prescribed. Another related development is the construction of a

formal dynamics that exploits the dissipation dominance often found in deformation dynamics and the absence of dissipative forces in the translational and rotational dynamics of a nuclear system treated as a whole. Such a construction is in progress, for the case of a single nucleus. If it succeeds, perhaps it can be extended to the case of two nuclei connected by a window.

The foundations of the restricted one-body model have not been fully explored, either. The magnitude of two-body, interior-dissipation, and window-diffraction effects have still to be assessed. Some of the errors in the restricted one-body model, such as those caused by two-body and shell effects, are outside its domain, but others, such as the effects of rotation on density and angular frequency, might be explicitly included in its formalism.

CHAPTER III

FERMI JETS

A. INTRODUCTION

In the one-body model, dissipation in nuclear collisions is produced partly by passage of nucleons through a window connecting the nuclei (Fig. 17). Since the model relies on the long mean free paths of nucleons in nuclei, it is natural to suppose that some exchanged nucleons will cross their new host nuclei unimpeded and to ask whether they may then penetrate the nuclear surface and be detected [1], [35]-[37]. The nucleons emitted from a single nucleus constitute a "Fermi jet."

Calculation of the number of nucleons emitted as a function of energy and angle divides naturally into three parts:

(1) calculation of nucleus dynamics;

(2) calculation of nucleon jetting as a function of nuclear positions and velocities;

(3) time integration of the jetting to find the total emission.

Part (1) can be performed by any known model of nuclear dynamics, such as the one-body model and part (3) is familiar mathematics; only part (2) is new. (The author has calculated the effect of jetting on nuclear dynamics and found it to be negligibly small).

Unlike the basic one-body model, which was devised to account for carefully measured phenomena, Fermi jet calculations are designed to determine whether jets are likely to exist and, if they are, to guide experimenters seeking to find them. Motivation for studying nucleon emission here arises first from its promise of administering sharp tests to the window picture, as nucleons seek to cross from one nucleus to the other; to the independent particle assumption, as the nucleons cross their new host; and to the wall picture, when they reach the host's surface. Then, too, point (1) of the calculation scheme presented above stresses that nucleon emission in general, and jetting in particular, enciphers information about nuclear dynamics. Finally, actual computations of jetting seem to make it a dramatic phenomenon: nucleons can be emitted with energies much larger than the bombardment energy per nucleon and, in many cases, the nucleons emitted by jetting are focused into small regions of velocity space.

These two results have simple, semi-quantitative explanations, which also help intuitive understanding of the jetting model. First, where does the extra nucleon energy come from? Imagine an isolated nucleus moving through a laboratory. Consider the internal (Fermi) motion of nucleons inside the nucleus and their kinetic energy relative to the laboratory. The maximum energy is possessed by any nucleon whose internal, kinetic energy equals the

Fermi energy, E_F, and whose velocity parallels the nuclear velocity. In the non-relativistic approximation, the two speeds add, making the nucleon energy

$$E_{nucleon} = \left(\sqrt{E_{nucleus}} + \sqrt{E_F}\right)^2 \quad , \qquad (3.1)$$

where $E_{nucleus}$ is the nuclear kinetic energy (per nucleon). For $E_{nucleus}$ = 12 MeV/nucleon and E_F = 37 MeV, $E_{nucleon}$ is 91 MeV. Of course, this kinetic energy is inaccessible as long as the nucleon remains bound in the nucleus, but one can use the mean field of another nucleus to kick the nucleon free. The price of this accomplishment is that the nucleon will lose energy in the field. This loss equals the field's depth, about 45 MeV, if the kicking nucleus is at rest in the laboratory. Nonetheless, the nucleon will be left with 46 MeV, instead of 12 MeV. Focusing and the role played by Fermi motion lead to the name "Fermi jets" (deceptively implying, perhaps, that many particles appear in each jet during each nuclear collision).

Focusing originates in surface refraction of the nucleons, as they escape the host nucleus. To the extent that the surface of the host nucleus is sharp, refraction reduces the normal component of the velocity of a nucleon passing through the surface, and leaves the tangential component untouched. If the window is idealized as a point, then the refracted nucleon is always focused toward (or even

past!) the line joining the window to the center of the host nucleus. It is instructive to draw examples in order to see how focusing works out and how it begins to break down as the window expands.

This model of Fermi jets confronts two major difficulties whose exact, quantitative impact is yet to be determined. First, two-body effects seriously threaten the independent particle basis of the model and, secondly, other processes play a major role in emission.

Simple arguments also exist to explain these points. In the example mentioned earlier, the highest-energy bound nucleons had a kinetic energy of 91 MeV, compared to a maximum energy in the Fermi sea of its new host of about 37 MeV. Not surprisingly, the Pauli principle is not as effective in inhibiting two-body interactions between such a nucleon and the sea as it would be if the nucleon were <u>in</u> the sea.

In a typical deep-inelastic nuclear collision, a substantial number of nucleons can be exchanged between the two nuclei, on the order of 10. Of these, only a small fraction will move in the right direction with enough energy to be emitted in the jetting process. These last may number on the order of 1. On the other hand, deep-inelastic collisions can dissipate hundreds of MeV of collective energy into internal excitation. De-excitation proceeds

by particle emission until the excitations of the nuclear fragments are less than the nucleon separation energy, when further particle emission becomes impossible. Each evaporated nucleon, for instance, decreases excitation energy by its separation energy, about 8 MeV, plus the several MeV of kinetic energy it typically possesses. The total number of nucleons emitted during and after a deep-inelastic collision is therefore likely to be an order of magnitude larger than the number of those emitted in jetting.

At least, the existence of jetting in the limiting case in which the projectile is just one nucleon is demonstrated by the success of the optical model, which incorporates long mean free paths, in accounting for proton elastic scattering from nuclei [38]. The rest of this chapter further explores the possibilities of jetting. Section B considers jetting in one dimension. Section C examines the assumptions on which jetting is based. The equations needed to calculate the kinematic properties of jetting are derived in Secion D and are applied, in Section E, to the moment when the window first opens. The next step is to calculate the <u>amount</u> of jetting as a function of the final nucleon energy and angle. The equations needed to do this are derived in Section F and their application is the subject of Section G, which also illustrates the competition offered by evaporation. Section H is devoted to summarizing and discussing the chapter and to suggesting future

investigations of jetting.

B. ONE DIMENSION

The one-dimensional case exhibits in simple expressions some of the main features in three dimensions. In it, the nuclear centers, nuclear positions, and the velocities of both nuclei and nucleons are constrained to be collinear.

Consider nucleons seeking to escape from nucleus 1 in Fig. 18 (called "1-emission," though these nucleons originated in nucleus 2). Suppose the depth of the (square) nuclear potential well, V, and the Fermi energy, E_F, are the same in both nuclei. (Ignore Coulomb effects or restrict the discussion to neutrons.) The separation energy, S, is then also the same. In the rest frame of nucleus 1, the most rapid nucleons crossing 1 will have a speed that is nucleus 2's speed, τ_2, plus the Fermi speed, v_F.

The condition for escape of a nucleon of mass m is

$$\tfrac{1}{2} m (v_F + \tau_2)^2 \geqslant V \quad , \tag{3.2}$$

that is, the final nucleon kinetic energy must be positive:

$$KE_{final} = \tfrac{1}{2}m(2v_F)\tau_2 + \tfrac{1}{2}m(\tau_2)^2 - (V - E_F = S) \geqslant 0 \quad . \tag{3.3}$$

If the first term were missing from equation (3.3), the bombarding

energy per nucleon (over the barrier), $\frac{1}{2}m(\tau_2)^2$, would have to exceed S. The restriction $\tau_2 << v_F$ is necessary if the independent particle assumption is to be valid. Consequently, the first term in equation (3.3) will actually preponderate and the bombarding energy needed for emission will be much reduced, to

$$\left(\sqrt{V} - \sqrt{E_F}\right)^2 << \left(\sqrt{V} - \sqrt{E_F}\right)\left(\sqrt{V} + \sqrt{E_F}\right)$$
$$= V - E_F = S \quad . \tag{3.4}$$

For example, if

$$V \simeq 45 \text{ MeV}, \; E_F \simeq 37 \text{ MeV}, \text{ and } S \simeq 8 \text{ MeV}, \tag{3.5}$$

0.4 MeV per nucleon of bombarding energy will overcome 8 MeV of separation energy. In this instance, $KE_{final} = 0$. If, instead,

$$\tfrac{1}{2}m(\tau_2)^2 = S = 8 \text{ MeV} \quad , \tag{3.6}$$

then

$$KE_{final} = 34 \text{ MeV} >> \tfrac{1}{2}m(\tau_2)^2 \quad . \tag{3.7}$$

C. ASSUMPTIONS

The assumptions underlying the one-body model and the wall and window formulae have varying significance for the jetting process. In addition, the jetting model introduces assumptions of its own.

Calculations of jetting that incorporate these assumptions predict the velocity-space intensity pattern of emitted nucleons. Obviously, failures of these assumptions can change either the number of particles jetted or their pattern. In the absence of other sources of nucleon emission, jetting could be studied without regard to such changes, but there are a host of competing sources. Jetting is a process in which a nucleon undergoes zero two-body collisions and zero one-body surface reflections before it is emitted. An infinity of possible sequences of collisions and reflections can also produce emission, among which evaporation is a limiting case at the opposite extreme from jetting. It will be shown later that these processes probably contribute more total emission than can jetting. Detection of jetting against this background is possible only if jetting is concentrated in a distinctive pattern that dominates total emission in some regions of velocity space. Fortunately, jetting calculations based on the assumptions discussed in this section do produce such patterns in favorable circumstances. Serious failures of the assumptions, however, could so move or disperse the patterns as always to reduce jetting to a small fraction of the total emission at every energy and angle. Its measurement would then require accurate calculations of all competing processes, followed by their subtraction from accurate experimental measurements of the total emission

distribution. In practical terms, detection of Fermi jets would be impossible.

The independent particle assumption is as critical to jetting as it is to the one-body model. In that model, all nucleons of interest are still in their nucleus of origin, relative to which they have negative energy. In jetting, nucleons transferred to another nucleus can have a much larger energy relative to their new host. For ^{20}Ne + ^{64}Cu (^{nat}Cu, really) at 252 MeV, which L. G. Moretto and his collaborators have been studying, the maximum predicted relative energy of protons emitted from Cu is about 40 MeV. In addition to displaying the nucleon mean free path, Fig. 9 calculates the attenuation of nucleons crossing Ne and Cu on a diameter, using for the attenuation factor

$$e^{-s/\lambda} \quad , \tag{3.8}$$

where s is the path length. Neglecting the difference between protons and neutrons, the attenuation factor in Cu is 0.2-0.3. This attenuation is important, but calculations presented in Section F show that it need not prevent the detection of jetting.

Attenuation can be included theoretically by multiplying the jetting rate from a particular nuclear configuration, calculated assuming an infinite mean free path, by the attenuation factor in expression (3.8). This has not been done because of uncertainty as

to which function of energy to use for the mean free path. Reference [39] halves the mean free path of nucleons having energies of 40 MeV, which squares the attenuation factor, reducing it to 0.04-0.09. Such attenuation might make it impossible to detect jetting against the background of other emission mechanisms.

On the other hand, Fig. 9 also shows that the attenuation factor is dramatically more favorable for a small nucleus, such as Ne, and is somewhat better for lower energy nucleons. Moreover, nucleon scattering and absorption are believed to occur predominantly in the nuclear surface [40]. The implication of equation (3.8), that attenuation occurs at a constant rate along the nucleon's path, is misleading; instead, attenuation occurs mainly in two bursts as the nucleon enters and leaves the nucleus. In jetting, each nucleon enters its new host through a window in which conditions are assumed to be much closer to those of the nuclear interior than to those of the ordinary surface. The attenuation factor of such nucleons should then be only the square root of that predicted by equation (3.8). However speculative this chain of reasoning may be, it is safe to conclude that the possibility of detecting jetting in practice hinges on the actual length of the mean free path and on the true nature of the region that connects two colliding nuclei.

It is also important to realize that the quantitative

condition for the validity of the independent particle assumption, equation (2.72), is strained by the one-dimensional condition for jetting:

$$\frac{v}{v_F} > \sqrt{1 + \frac{S}{E_F}} - 1 = 0.10 \quad . \tag{3.9}$$

[As in (2.72), v is the relevant speed of nuclear motion].

In discussing the independent particle assumption, no reference has been made to disruption of the nuclear media. Of course, Chapter II argued that the only important modification needed was the inclusion of changing drift velocities. The argument, however, carefully directed attention to nucleons approaching the nuclear surface. Jetting probes the nuclear interior and is affected by the entire nucleon distribution there. Moreover, the probing is done, not with one nucleon, as in the experiments from which mean free paths are extracted, but with a stream of nucleons. The significance of these distinctions is unknown.

The semi-classical assumption again raises the problem of window diffraction. Compared to window formula calculations, jetting calculations are more concerned with high-energy, short-wavelength nucleons, but are also more sensitive to diffractive effects on the angular distributions of nucleons passing through the window and stress the early stages of a nuclear

collision, when the window is likely to be small. This last point arises because, for jetting to be possible, the nuclei must be moving toward each other at more than some threshold speed. Let L be the orbital angular momentum of the two nuclei and let it be expressed in units of $\hbar$. (The initial angular momentum is usually meant.) In the case of the L=70 wave of $^{20}Ne + ^{64}Cu$ at 252 MeV, the predicted turning point of the nuclear trajectory occurs 2.00×10^{-22} sec after the nuclear surfaces first touch, but no jetting is calculated to occur after 1.64×10^{-22} sec, when the window diameter is 5 Fm. Moreover, jetting at many angles and energies ceases earlier, as does all jetting in more peripheral collisions. (For a grazing collision, L must exceed 100 in this reaction.) In comparison, the reduced wavelength of a nucleon at the top of the Fermi sea is about 0.7 Fm.

Jetting forces consideration of two new quantal effects. Both concern the interaction of a particle with a barrier. In the classical approach used here, a nucleon definitely is or is not emitted at a point on a nuclear surface according as its energy of motion (normal to the surface) is greater or less than the difference between the interior potential and the maximum value of the potential along the normal at the surface point. Quantally, the barrier affects the nucleon at all energies. Other investigators have pointed out that low energy protons can penetrate the Coulomb

barrier [41] and high energy nucleons can be reflected by the surface barrier [21].

The first effect would show up in the emission of protons with final energies, relative to the emitting nucleus, between zero and the Coulomb barrier energy. This fact makes the effect unimportant because there are so many competing sources of low-energy proton emission that such emission is unlikely to evidence jetting.

At energies large enough to allow classical emission, one or more quantal reflections followed by an ultimate transmission would cause the nucleon to come out at a very different angle than that calculated classically. Should this occur frequently, the classical jetting pattern would be seriously disrupted. The situation may be compared with that of a one-dimensional potential step. The one-dimensional reflection coefficient is

$$R = \left(\frac{\sqrt{E+V} - \sqrt{E}}{\sqrt{E+V} + \sqrt{E}} \right)^2 , \qquad (3.10)$$

where E is the nucleon energy <u>outside</u> the nucleus [42]. The coefficient is 0.08 for $E = 20$ MeV and 0.03 for $E = 40$ MeV. Effects of this magnitude would leave the classical jetting pattern substantially intact. <u>Classical</u> reflection can be neglected, as the discussion in connection with equation (3.22) in Section D will

show. Neither the independent-particle nor the semi-classical assumptions can be relaxed in jetting calculations without vastly complicating them.

It is safe to ignore the Pauli principle because any jetted nucleon must have positive total energy with respect to its emitting nucleus, whereas all the nucleons originally in that nucleus are below the Fermi surface. Of course, this ineffectiveness of the Pauli principle is the fundamental cause of the decrease in nucleon mean free paths as nucleon energy increases.

Like the window and wall formulae, the jetting calculations to be presented in this work presume a sharp nuclear surface. The potential step occurring at the surface causes any nucleon passing through it to be refracted. Surface diffuseness alters the refraction. Quantitatively, the deflection must depend on the following ratios: of the diffuseness to the surface radius, of the potential-well depth to the nucleon kinetic energy, and of the tangential to the normal component of the nucleon velocity. Of these quantities, nuclear diffuseness is around 1 Fm., nuclei radii are several Fermis, potential wells are about 50 MeV deep, nucleons inside the nuclear system that are about to escape have energies of 50-90 MeV, and the components of a velocity range from zero up to its full speed. The deflection, therefore, will often be substantial. Greater exactitude, in the context of the jetting

model presented here, would require complicated nucleon trajectory calculations involving the solution of differential equations in two dimensions. The calculations that follow are intended to establish quickly the nature of jetting and the likelihood of its observation. Therefore, some assumptions, such as making the surface sharp, have been made for immediate convenience and some crude results accepted, both of which can be improved later.

Qualitatively, the effect of diffuseness may be favorable. When jetting is calculated assuming a sharp surface, it is focused into a small region of velocity space. As described in Section A, surface refraction helps to accomplish this by strengthening the tangential component of the nucleon velocity, relative to the normal component. The combination of surface diffuseness and curvature tends to bend the nucleon velocity around the curve of the surface, in the direction of the tangential component of the velocity, so that component is further emphasized.

Account <u>is</u> taken of the effects on the window of diffuseness and of volume and potential inhomogeneities by using the effective window area from proximity friction [22]. That area was designed to be used with the window formula, calculating momentum transfer and averaging over all exchanged nucleons. Here, a number transfer is wanted and only the most energetic nucleons matter. The area should be revised accordingly.

One aspect of the wall and window formulae that made the neglect of shell structure more plausible was their integration over the entire nucleon velocity distribution. Jetting calculations seek instead to trace the paths of individual nucleons, so shell effects may be even more important. No existing model can determine their exact role.

Of the remaining assumptions discussed in Section II.D, specular reflection, universality of density among nuclides, and the two-dimensional idealization of the window all have the same implications for jetting as they do for the wall and window formulae. The distinction between dissipative and conservative effects is irrelevant to jetting.

None of the alternative models discussed in Chapter II can currently be applied to jetting. Perhaps some useful studies might be carried out with cranked potentials representing two joined nuclei. In the classical case, it would be necessary to give the potential well depth a finite value, which would be trivial, and to trace and bin emitted nucleons, which would be straightforward. In the quantal case, it would be necessary to decide conceptually how to treat the single-particle wave functions asymptotically and then to implement the decision numerically. This promises to be more difficult. Designed to calculate power, linear response theory is unsuited to jetting calculations. The reliance of TDHF on mean

Coulomb potential creates a barrier to protons that acts merely as a lower threshold for proton emission energies. If it overcomes this barrier, a proton is then influenced by the nuclear Coulomb potentials until it reaches infinity. The concentrated Coulomb potential reproduces the Coulomb threshold accurately, but, outside the surface, it delivers the Coulomb energy to the proton immediately, rather than gradually. This approximation is good if and only if the proton kinetic energy is much larger than variations in the Coulomb potential. Table 3 shows that the approximation is good inside the nucleus, but poor outside. Placing the nucleons on Kepler trajectories corresponding to a one-center Coulomb potential as soon as they leave the surface would be an easy improvement. The potential would schematize the nuclear charge distribution as the sum of the nuclear charges, located at the "center of charge," instead of the center of mass. Neutrons obviate concern with electromagnetic interactions. Most of the jetting calculations in this dissertation deal with protons because they are easier to detect experimentally, but neutron detection has been and is being carried out and is far more convenient, theoretically.

Closely related to the Coulomb discussion is the assumption that there exists an inertial frame in which nucleons experience a time-independent potential while crossing their new host. This can be invalidated by rapid acceleration of the new host, or, in the

case of the Coulomb component of the potential, by rapid motion of the original host. The latter possibility again hinges on the comparison of nuclear and Fermi speeds, equation (2.72). The former possibility is also susceptible to order-of-magnitude analysis. The time, Δt, in which a nucleon moving at speed v crosses a nucleus of radius R is roughly

$$\Delta t \simeq \frac{2R}{v} \quad . \tag{3.11}$$

If the nucleus is experiencing an acceleration a, then, even in an inertial frame motionless with respect to the nucleus at the beginning of the time interval, the nucleus will have moved

$$\Delta r \simeq \frac{1}{2} a(\Delta t)^2 \tag{3.12}$$

at the end of Δt. During the nuclear collision, the two nuclei penetrate each other to some maximum depth s, while losing center-of-mass kinetic energy in the amount ΔE_{CM}. The typical force a nucleus of mass M must experience while this occurs is

$$Ma \simeq \frac{\Delta E_{CM}}{\Delta s} \quad . \tag{3.13}$$

Equations (3.11)-(3.13) combine to produce

$$\frac{\Delta r}{R} \simeq \frac{1}{A} \frac{R}{\Delta s} \frac{\Delta E_{CM}}{E_{nucleon}} \tag{3.14}$$

in which A is the mass number of the nucleus and $E_{nucleon}$ is the nucleon kinetic energy. In calculations, Δs turns out to be a few Fermis. Experimental values of ΔE_{CM} reach several hundred MeV. Bearing in mind that $E_{nucleon}$ must exceed 50 MeV for emission to occur, the ratio in equation (3.14) can range from a fraction of a percent nearly to one, with typical values in the range 5-10%--quite acceptable for exploratory computations. Alternatively, the effect can be included approximately by displacing the nuclear surface which the nucleon is about to strike.

The final assumption needed for the Fermi jet calculations performed here is that the situation is non-relativistic. This assumption is non-trivial because jetting directs attention toward nucleons having kinetic energies (inside nuclei) around 90 MeV. Compare this energy to the nucleon rest energy and it will be apparent that $(v/c)^2$, which determines the magnitude of relativistic corrections, can easily be 10%. This accuracy is suitable for preliminary work and should be easy to improve.

Figure 20 shows the steps by which a nucleon passes through a host nucleus:

(a) crosses the window;

(b) traverses the host interior;

(c) penetrates the surface;

(d) proceeds to the detector.

Diffraction, refraction, reflection, scattering, and absorption--in short, nucleon optics--must be considered. The many assumptions and approximations that have been made amount to neglecting every optical property, except refraction at the new host's surface. Otherwise, the nucleons simply move inertially from the window to the detector.

The summary of this section will begin by observing that the jetting model relies on all the assumptions involved in the derivations of the wall and window formulae in Chapter II, except that the contrast between dissipation and conservation is irrelevant. To these assumptions, it adds only technical assumptions made to simplify preliminary calculations: spherical nuclear surfaces, a universal square-well nuclear potential, and concentration of the Coulomb potential at the nuclear surface. The wall and window formulae are intended to be compared, ultimately, with a large body of fairly accurate experimental data and with other theories that claim considerable accuracy. In that context, an assumption is good if the error introduced by accepting it is no more than about 10%. At this stage, jetting calculations could be wrong by a factor of two or more and still be useful because the

theories of competing processes, such as evaporation, are often in error by that much. By this standard, most of the assumptions are very good. The outstanding exception is the independent particle assumption, which may be so invalidated by two-body scattering and absorption that it endangers detection of jetting. More hopefully, shell effects are expected to change jetting patterns considerably, but not necessarily to obscure them. Diffuseness should also be significant, yet may even improve jet focusing in velocity space. Coulomb effects are difficult to incorporate accurately in the jetting model, but they apply only to protons. Some of the assumptions can be relaxed in the jetting model without much difficulty. The only available alternatives are the cascade and other pre-equilibrium models, and even these may need some changes in the way they describe nuclear surfaces.

D. THE KINEMATICS OF EMITTED NUCLEONS

Notation: Superscripts on velocities refer to the nucleus in which the nucleon is located. (Whenever the exponential `2′ seems likely to be confused with the superscript `2,′ quantities to be squared are placed in parentheses.) The vectors $\vec{u}$, $\vec{v}$ indicate velocities inside, outside the nuclear system. Cursive letters refer to the rest frame of the nucleus in which the nucleon is (or to which it is nearest); ordinary, printed letters refer to the laboratory.

For a nucleon i to be emitted from nucleus 1, it must begin with some velocity relative to the center of the Fermi sphere in 2:

$$\vec{q}\ ; \qquad |\vec{q}| \leqslant v_{Fi}^2 \quad , \tag{3.15}$$

where v_{Fi} is the Fermi speed of nucleon i (p or n) in nucleus 2. The drift velocity of 2 is

$$\vec{V}_o(\vec{r}) = \vec{\tau}_2 + \vec{\omega}_2 \times (\vec{r} - \vec{r}_2) \quad , \tag{3.16}$$

where $\vec{r}_2$ is the center, $\vec{\tau}_2$ is the velocity, and $\vec{\omega}_2$ is the angular velocity of 2. At the window, $\vec{r}_W$ (a point on the window plane),

$$\vec{u}_2 = \vec{q} + \vec{\tau}_2 + \vec{\omega}_2 \times (\vec{r}_W - \vec{r}_2) \quad . \tag{3.17}$$

The nucleon passes the window freely:

$$\vec{u}_1 = \vec{u}_2 \quad . \tag{3.18}$$

The surface potential of 1 is time-independent only in the rest frame of 1 (and then only if the effect of nucleus 2's motion on the Coulomb potential is neglected), in which the proton velocity is

$$\vec{\mathcal{U}}_1 = \vec{u}_1 - \vec{\tau}_1 = \vec{q} + \vec{\tau}_{21} + \vec{\omega}_2 \times (\vec{r}_W - \vec{r}_2) \tag{3.19}$$

$$(\vec{\tau}_{21} \equiv \vec{\tau}_2 - \vec{\tau}_1) \quad .$$

The point S at which the nucleon strikes the surface is found by

following $\vec{u}_1$ from $\vec{r}_W$ (Fig. 21). Energy is conserved in this frame (Fig. 22):

$$\tfrac{1}{2}m(\vec{u}_1)^2 - V_i + V_{ci}(\vec{r}_s) = \tfrac{1}{2}m(\vec{v}_1)^2 + V_{ci}(\vec{r}_s) \quad , \tag{3.20}$$

where $V_{ci}(\vec{r}_S)$ is the Coulomb potential energy of nucleon i at $\vec{r}_S$,

$$V_{ci}(\vec{r}_s) \simeq \frac{Z_1 e^2}{R_1} + \frac{Z_2 e^2}{|\vec{r}_s - \vec{r}_2|} \quad \text{for protons,}$$
$$= 0 \quad \text{for neutrons.} \tag{3.21}$$

In the nuclear square-well approximation, there can be no tangential force, so

$$\vec{v}_{1t} = \vec{u}_{1t} \quad . \tag{3.22}$$

Equation (3.20) then becomes

$$\tfrac{1}{2}m(u_{1n})^2 - V_i = \tfrac{1}{2}m(v_{1n})^2 \quad , \tag{3.23}$$

where the subscript 'n' denotes the vector component normal to the surface and parallel to the surface normal at $\vec{r}_S$, $\vec{n}_S$. Thus,

$$\tfrac{1}{2}m(u_{1n})^2 - V_i \geqslant 0 \quad , \tag{3.24}$$

or

$$\vec{u}_1 \cdot \hat{n}_s > +\sqrt{2V_i/m} \quad . \tag{3.25}$$

This is the emission condition.

Incidentally, as Fig. 23 shows, reflection cannot change

$|\vec{u}_1 \cdot \hat{n}_S|$ in a spherical nucleus. As a result, if a nucleon does not satisfy the emission condition when it first reaches the surface, then it never will, no matter how often it is reflected. If it does satisfy the condition, it will be either emitted or quantally reflected. As Section C showed, quantal reflection is improbable. In neither case can reflection significantly affect the calculation of jetting.

Giving the Coulomb peak zero width means that

$$\tfrac{1}{2} m (u_{1n})^2 - V_i + V_{ci}(\vec{r}_s) = \tfrac{1}{2} m (v^{\infty}_{1n})^2 \quad , \tag{3.26}$$

so

$$\vec{v}^{\infty}_1 \cdot \hat{n}_s = \sqrt{(\vec{u}_1 \cdot \hat{n}_s)^2 - \frac{2}{m}\left[V_i - V_{ci}(\vec{r}_s)\right]} \quad . \tag{3.27}$$

Thus, equation (3.22) may be extended to $\vec{v}^{\infty}_{1t}$, whereby

$$\vec{v}^{\infty}_1 = \vec{u}_1 + (\vec{v}^{\infty}_1 \cdot \hat{n}_s - \vec{u}_1 \cdot \hat{n}_s)\hat{n}_s \quad , \tag{3.28}$$

and finally,

$$\vec{v}^{\infty}_1 = \vec{v}^{\infty}_1 + \vec{\tau}_1 \quad . \tag{3.29}$$

To use equations (3.15)-(3.29), one must know the Fermi energies, E^j_{Fi}, for each nucleon type i and nucleus j, and the nuclear potentials V_p and V_n. The Fermi energies were taken from [50]:

$$E_{Fi}^{j} = E_{F}^{N=Z}\left(\frac{2N_i^j}{A_j}\right)^{2/3} \tag{3.30a}$$

$$E_{F}^{N=Z} = 37 \text{ MeV} \quad , \tag{3.30b}$$

where N_i^j is the number of nucleons of type i in nucleus j, which has the atomic number A_j. The nuclear potential is presumed the same for all nuclei, differing only with the type of nucleon involved. V_i was fit to V_i^j, the potential of nucleon i in nucleus j, defined as

$$V_i^j \equiv E_{Fi}^j + V_{ci}^j(\vec{r}_s) + S_i^j \ , \tag{3.31}$$

where $V_{ci}^j(\vec{r}_S)$ is evaluated at any point on the surface of j and S_i^j is the measured separation energy of i from j. Using the most abundant nuclides in the range $16 \leqq A \leqq 71$, (chosen to bracket Ne + Cu),

$$V_p = 50.(5) \pm (0.5) \text{ MeV} \tag{3.32a}$$

$$V_n = 48.(7) \pm (0.7) \text{ MeV} \quad , \tag{3.32b}$$

where the probable errors result from the least-squares analysis and are satisfactorily small. There is no sign of systematic variations in the potentials with A and Z. These potentials are accurate

for the only nucleons able to escape the nuclear system: those originating close to the top of the Fermi sea.

E. INITIAL JETTING

Analysis of initial jetting, which occurs when the nuclei first touch, avoids the difficulties of nuclear dynamics because, before and after they touch, nuclei move on Coulomb trajectories. There are further simplifications at first contact. First,

$$\vec{\omega}_1 = \vec{\omega}_2 = 0 \quad , \tag{3.33}$$

because the Coulomb interaction cannot exert torques on nuclei that are assumed to be spherical. The second simplification is deduced from Fig. 24, which shows a typical nucleon moving through the window to the surface of its new host. Since the normal to the window pointing out from 2, $\hat{n}_{W2}$, parallels $\vec{r}_1 - \vec{r}_W$ and since, at first contact,

$$|\vec{r}_1 - \vec{r}_W| = |\vec{r}_S - \vec{r}_1| \quad , \tag{3.34}$$

the angles indicated in Fig. 24 are all equal. Therefore,

$$\vec{u}_1 \cdot \hat{n}_s = \vec{u}_1 \cdot \hat{n}_{w2} \quad . \tag{3.35}$$

To see why initial jetting is of interest, note first that jetting requires two things: relative nuclear motion and an open window. At the instant of nuclear contact, the window begins to

open; after that instant, dissipation slows the nuclei. Thus, jetting must occur at that instant or never and the most energetic nucleons should be emitted then. (Since the emission rate is proportional to window area, the rate will be infinitesimal then.)

Equations (3.25), (3.35), (3.9), (3.33), and (3.15) imply

$$|\dot{r}| = \vec{\tau}_{21} \cdot \hat{n}_{w2} \overset{!}{\geqslant} \sqrt{\frac{2}{m} V_i} - v_{Fi}^2 , \tag{3.36}$$

where

$$\dot{\vec{r}} = -\vec{\tau}_{21} = -(\vec{\tau}_2 - \vec{\tau}_1) \tag{3.37}$$

is the relative velocity of the two nuclei.

This result and knowledge of the Coulomb trajectories [51] lead to some useful analytic expressions. The bombardment energy (E_{lab}) threshold for jetting of nucleons i from nucleus j is calculated to be

$$E_{lab} \geqslant \frac{A_P + A_T}{A_T} \left[\frac{Z_P Z_T}{\bar{R}} + A_\mu \left(\sqrt{V_i} - \sqrt{E_{Fi}^2} \right)^2 \right] ; \tag{3.38}$$

where P,T refer to projectile,target; $\bar{R}$ is the distance between the nuclear centers; and A_μ is the reduced atomic mass number. The calculated L-wave threshold is

$$L \leqslant \left\{ 2A_\mu(mc^2) \left[E_{cm} - \frac{Z_P Z_T e^2}{\bar{R}} - A_\mu \left(\sqrt{V_i} - \sqrt{E_{Fi}^2} \right)^2 \right] \right\}^{\frac{1}{2}} \frac{\bar{R}}{\hbar c} \quad , \tag{3.39}$$

in which E_{cm} is the nuclear center-of-mass bombarding energy. This should be compared with the threshold for nuclear contact,

$$L \leqslant \left[2A_\mu(mc^2) \left(E_{cm} - \frac{Z_P Z_T e^2}{\bar{R}} \right) \right]^{\frac{1}{2}} \frac{\bar{R}}{\hbar c} \quad , \tag{3.40}$$

to obtain a crude estimate of the fraction of the nuclear cross section that can be expected to produce jetting. The maximum nucleon energy in the laboratory presumably arises in target emission when all vectors parallel the beam:

$$L = 0 \qquad\qquad \vec{q} = v_{Fi}^P \, \hat{z} \ . \tag{3.41}$$

Application of equations (3.15)-(3.29) to Coulomb trajectories then yields

$$\max(E_i)_{lab} = \left[\left\{\left[\sqrt{E_{Fi}^{P}} + \sqrt{\left(E_{cm} - \frac{Z_P Z_T e}{\bar{R}}\right)/A_\mu}\right]^2 - V_i + V_{ci}^{T}\right\}^{\frac{1}{2}} + \frac{A_\mu}{A_T}\left[\sqrt{\frac{E_{lab}}{A_P}} - \sqrt{\left(E_{cm} - \frac{Z_P Z_T e}{\bar{R}}\right)/A_\mu}\right]\right]^2 , \tag{3.42}$$

where V_{ci}^{T} is the Coulomb potential of nucleon i evaluated on the target surface opposite the point of nuclear contact.

Tables 4 and 5 and Fig. 25 show the result of applying equations (3.38)-(3.42) to ^{86}Kr and ^{74}Se. Some intermediate quantities and basic results are presented in Table 4. Table 5 displays the predicted threshold L and maximum nucleon emission energy as functions of bombarding energy, and the maximum emission energy also is plotted in Fig. 25. Proton and neutron results are similar, except for the threshold bombarding energies. These differ because protons must overcome $V_{cp}(\vec{r}_S)$ to be emitted. When examining the maximum emission energies, keep in mind that the maximum bombarding energy is 8.5 MeV/nucleon. (Table 5 indicates that a narrow range of bombarding energies exists in which protons are emitted from the projectile, but not from the target; this is caused by the proton Fermi energy being larger in the target than in the projectile.)

A computer can be used to map a selection of nucleon velocities in the Fermi sphere of the originating nucleus into the laboratory via equations (3.15)-(3.29). In view of (3.25), (3.35), (3.9), and (3.33), only points in the Fermi sphere satisfying

$$\vec{q} \cdot \hat{n}_{w2} \geqslant \sqrt{\frac{2}{m} V_i} - \vec{\tau}_{21} \cdot \hat{n}_{w2} \tag{3.43}$$

need be considered. All calculations have been restricted to the reaction plane, as have experiments.

Figure 26 shows typical envelopes and some interior structure for proton emission in $^{16}O + {}^{58}Ni$ at 315 MeV. Figures 27-28 illustrate the definitions involved.

In Fig. 28, the z′-axis parallels $\hat{n}_{W2}$ and the x′-axis parallels the product of the components of the beam direction, $\hat{z}$, parallel and perpendicular to $\hat{n}_{W2}$:

$$\hat{z} \cdot \hat{n}_{W2}[\hat{z} - \hat{z} \cdot \hat{n}_{W2}\hat{n}_{W2}] \quad . \tag{3.44}$$

Points are selected in that part of the Fermi sphere of nucleus 2 allowed by equation (3.43) and are restricted to the reaction plane. Five values of $q_{z'}$, labeled 1,2,...5, are selected, ranging in equal steps from the threshold in (3.43) to just under v_{Fi}^2, the difference between which is exaggerated in the diagram. For each value of $q_{z'}$, $q_{x'}$ is scanned in equal steps from its least to its greatest possible value. In both Fig. 28 and Fig. 26, saw-toothed

lines connect the points for which q nearly equals v_{Fi}^2; wavy lines, those for which $q_{z'}$ is the threshold value in equation (3.43) (the two lines meet in circles); and dashed lines connect points for which $q_{z'}$ is fixed at a value above the threshold. Arrows indicate the scanning direction. As Fig. 27 shows, positive angles in Fig. 26 are defined by the side of the beam the projectile is on initially. The vector $\hat{n}_{W2}$ is indicated in Fig. 27 for the case of target emission. In the Fermi sphere, the envelope of points is defined by the saw-toothed and wavy lines. Surprisingly, this is not entirely true of the calculated laboratory results. Where it is not, the envelope is indicated by a solid line in Fig. 26. A related development is that two distinct points in the Fermi sphere can project into the same point in the laboratory. In Fig. 26, shading denotes the areas where this is calculated to occur.

The protons are predicted to be sharply focused in laboratory phase space. This is the one main characteristic of jetting that cannot appear in one dimension. The jetting patterns differ profoundly in appearance for target and projectile emission and for different L waves within each category. The energy ranges, however, do not vary rapidly with L (Table 6). These conclusions and the results in Fig. 26 and Table 6 depend, of course, on the jetting model assumptions. To begin with, the calculations apply only to that fraction of nucleons that avoid all

two-body interactions. Even then, window diffraction may eliminate focusing or, at least, combine with other phenomena, such as surface diffuseness, to alter emission kinematics.

The details of Fig. 26 can be understood in terms of the interplay between $\vec{q}$, $\hat{n}_{W2}$, $\vec{\tau}_{21}$, and $\vec{\tau}_1$. For instance, consider why projectile emission is less focused in angle and is produced at lower energies than is target emission. Apart from asymmetries induced by different Fermi energies and Coulomb potentials, equations (3.15)-(3.29) imply that emission should be mirror-symmetric about the window plane in a frame moving at the average velocity of the nuclei,

$$\tfrac{1}{2}\,(\vec{\tau}_1 + \vec{\tau}_2) \quad . \tag{3.47}$$

In other words, instantaneous target and projectile emission are roughly the same in this frame, up to a mirror transformation. Target emission is forward and projectile emission is backward, in the sense that nucleon velocities have positive and negative components, respectively, along the beam direction. The velocity boost back to the lab is effected by adding the average nuclear velocity to all the nucleon velocities, which moves the mirror plane away from the velocity space origin. Since the average nuclear velocity has a positive component along the beam, it pushes target emission farther forward, but it partly cancels projectile emission velocities. Target emission ends up at higher energies than does

projectile emission. Although target and projectile emission cover approximately the same volume of velocity space, target emission's greater distance from the origin in laboratory velocity space causes it to subtend a smaller angle with respect to that origin.

F. THE NUMBER OF EMITTED NUCLEONS

The number of nucleons emitted can be found by first calculating the emission rate, and then integrating over time. The number of nucleons of type i emitted from nucleus 1 with final velocities in the region $\vec{v}_1^{\infty}$, $\vec{v}_1^{\infty}+\Delta\vec{v}_1^{\infty}$ that originally crossed the window surface element ΔS_W at $\vec{r}_W$ during the time interval t_o, $t_o+\Delta t_o$ is

$$\frac{dN_i}{dS_W dt_o d\vec{v}_1^{\infty}}(\vec{r}_W, t_o, \vec{v}_1^{\infty})\ \Delta S_W \Delta t_o \Delta\vec{v}_1^{\infty} \quad , \tag{3.46}$$

where $dN/dS_W dt_o d\vec{v}_1^{\infty}$ is the rate being sought. Equations (3.15)-(3.29) relate initial and final velocities implicitly:

$$\vec{u}_2,\ \vec{u}_2+\Delta\vec{u}_2 \ \leftrightarrow\ \vec{v}_1^{\infty},\ \vec{v}_1^{\infty}+\Delta\vec{v}_1^{\infty} \quad . \tag{3.47}$$

Thus, expression (3.23) equals the number of particles crossing the window from 2 to 1 with velocities in $\vec{u}_2$, $\vec{u}_2+\Delta\vec{u}_2$:

$$\Phi_i(\vec{r}_w, t_o, \vec{u}_2)\ \Delta S_w \Delta t_o \Delta \vec{u}_2 \quad , \tag{3.48}$$

where Φ_i is the flux of nucleons crossing the window. Equation (2.7) provides

$$\Phi_i(\vec{r}_w, t_o, \vec{u}_2) \ = \ \theta[(\vec{u}_2 - \vec{w})\cdot\hat{n}_{w2}](\vec{u}_2 - \vec{w})\cdot\hat{n}_{w2} \quad F_i(\vec{r}_w, t_o, \vec{u}_2) \quad , \tag{3.49}$$

in which $\vec{w}$ is the window velocity at $\vec{r}_W$, satisfying

$$\vec{w}\cdot\hat{n}_{w2} \ = \ \tfrac{1}{2}(\vec{\tau}_1 + \vec{\tau}_2)\cdot\hat{n}_{w2} \quad , \tag{3.50}$$

by virtue of (2.129), and in which F_i is the phase-space distribution function of nucleons of type i. F_i is presumed to be a zero-temperature Fermi-Dirac distribution about the drift velocity (3.16):

$$F_i(\vec{r}_w, t_o, \vec{u}_2) \ = \tag{3.51}$$

$$n_i^2 \ \frac{1}{\frac{4}{3}\pi\,(v_{Fi}^2)^3}\ \theta\left[v_{Fi}^2 - \left|\vec{u}_2 - \vec{\tau}_2 - \vec{\omega}_2 \times (\vec{r}_w - \vec{r}_2)\right|\right],$$

where n_i^2 is the number density of nucleons i in 2. Equations (3.15)-(3.29) yield the Jacobian

$$\left| \frac{\partial(\vec{u}_2)}{\partial(\vec{v}_1^{\infty})} \right| = \frac{\vec{\mathcal{V}}_1^{\infty} \cdot \hat{n}_s}{\vec{\mathcal{U}}_1 \cdot \hat{n}_s} \quad . \tag{3.52}$$

Putting the pieces together, i.e. equations (3.46)-(3.52),

$$\frac{d^4N_i^1}{dS_w dt_o dE_1^{\infty} d\Omega_1^{\infty}} (\vec{r}_w, t_o, E_1^{\infty}, \theta_1^{\infty}, \phi_1^{\infty}) = \frac{3}{4\pi} \frac{n_i^2}{m(v_{Fi}^2)^3} \theta\left[(\vec{u}_2 - \vec{w}) \cdot \hat{n}_{w2}\right]$$

$$\times \theta\left[v_{Fi}^2 - |\vec{u}_2 - \vec{\tau}_2 - \vec{\omega}_2 \times (\vec{r}_w - \vec{r}_2)|\right] v_1^{\infty} \frac{\vec{\mathcal{V}}_1 \cdot \hat{n}_s}{\vec{\mathcal{U}}_1 \cdot \hat{n}_s}$$

$$\times (\vec{u}_2 - \vec{w}) \cdot \hat{n}_{w2} \tag{3.53}$$

is the number (per unit area, time, energy, and solid angle) wanted.

For a given nuclear trajectory, the nucleon quantity measured is

$$\frac{d^2N_i}{dE_1^{\infty} d\Omega_1^{\infty}} = \int_{-\infty}^{+\infty} dt_o \int_{\text{window}(t_o)} dS_w \left(\frac{d^4N_i^1}{dS_w dt_o dE_1^{\infty} d\Omega_1^{\infty}} + \frac{d^4N_i^2}{dS_w \ldots} \right) . \tag{3.54}$$

If the projectile and target eventually separate at the end of a reaction, then each trajectory corresponds experimentally to the detection of the final projectile and target fragments at particular energies and angles. The correspondence is nearly one-to-one. The

initial specification of a nuclear reaction at fixed energy can, for example, be represented by the value of L. The final energies and angles then cluster about their mean values with small spreads provided by fluctuations in particle exchange, particle emission, and quantal effects. Conversely, specified final fragment energies and angles correspond to a narrow range of trajectories and initial L's. The spreads involved have been studied. Another investigator has shown that particle exchange fluctuations have little effect on trajectories [52]. As mentioned in Section A, the author has calculated the influence of one kind of emission, jetting, on nuclear dynamics and found it to be small. Finally, quantal effects were shown to be small in Section D.2. In light of these arguments, the experimentally measurable quantity on the left-hand side of equation (3.54) can be adequately calculated by applying the right-hand side to one, appropriate trajectory. This statement must be qualified by noting that the effect of fluctuations in emission generated other than by jetting have not been examined.

Very different is the compound nucleus case. The right-hand side of equation (3.54) must then be averaged over those L waves that lead to fusion, weighting each wave by its geometrical partial cross section, which is proportional to 2L+1.

Equation (3.54) can be approximated by

$$\frac{d^2N_i}{dE_1^\infty d\Omega_1^\infty} \simeq \int_{-\infty}^{+\infty} dt_o \; \Delta S_W(t_o) \left(\frac{d^4N_i^1}{dS_W \cdots} + \frac{d^4N_i^2}{dS_W \cdots} \right) , \qquad (3.55)$$

where $\Delta S_W(t_o)$ is the window area at t_o and, for the rates, $\vec{r}_W$ is taken to be the center of the circle defined by the intersection of the two nuclear (sharp) surfaces. This approximation will be made henceforth, but it has been contradicted on the ground that windows become too large for it to be valid [53]. Were $d^4N_i^1/dS_W \cdots$ to be even roughly constant during nuclear contact,

$$\frac{d^2N_i^1}{dE_1^\infty \, d\Omega_1^\infty} = O\left(\frac{d^4N_i^1}{dS_W \cdots} \langle \Delta S_W \rangle \, \tau \right) , \qquad (3.56)$$

where $\langle \Delta S_W \rangle$ is some time average of $\Delta S_W(t_o)$, τ is the one-body stopping time, and $d^4N_i^1/dS_W \cdots$ is evaluated at some time during nuclear contact. We shall see, however, that $d^4N_i^1/dS_W \cdots$ is nonzero only briefly during contact.

At least

$$\frac{d^2N_i^1}{dS_W dt_o} \qquad (3.57)$$

<u>is</u> roughly constant, so

$$N_i \cong \mathcal{O}\left(\frac{d^2 N_i^1}{dS_w dt_o} \langle \Delta S_w \rangle \tau \right) . \tag{3.58}$$

Calculation of (3.57) proceeds by integrating over $\vec{u}_2$ the flux of nucleons crossing the window, (3.49), subject to condition (3.25). The integration is easy only at first contact, when (3.35) holds. Employing an expression in [6] for $\langle \Delta S_W \rangle \tau$, one finds

$$N_i = \mathcal{O}\left\{ A_\mu \left[\frac{1}{2} \frac{v_{Fi}^2}{\langle v_{Fi} \rangle} + \frac{2}{3} \frac{\vec{\tau}_{21} \cdot \hat{n}_{w2}}{\langle v_{Fi} \rangle} - \frac{\sqrt{\frac{2}{m}} V_i \left(\sqrt{\frac{2}{m}} V_i - \vec{\tau}_{21} \cdot \hat{n}_{w2} \right)}{\langle v_{Fi} \rangle v_{Fi}^2} + \frac{1}{6} \frac{\left(\sqrt{\frac{2}{m}} V_i - \vec{\tau}_{21} \cdot \hat{n}_{w2} \right)^3 \left(3\sqrt{\frac{2}{m}} V_i - \vec{\tau}_{21} \cdot \hat{n}_{w2} \right)}{(v_{Fi}^2)^3 \langle v_{Fi} \rangle} \right] \frac{(\vec{\tau}_{21})^2}{(\vec{\tau}_{21})^2 + (\vec{\tau}_{21} \cdot \hat{n}_{w2})^2} \right\}, \tag{3.59}$$

where

$$\langle v_{Fi} \rangle = \tfrac{1}{2}(v_{Fi}^{1} + v_{Fi}^{2}) \tag{3.60}$$

Table 7 gives the resulting estimate of the total number of protons in the Fermi jets from $^{20}Ne + {}^{64}Cu$ at 252 MeV as a function of L. Equation (3.35) causes most of the decline in (3.59) with increasing L. Equation (3.59) and Table 7 are indifferent to assumptions, such as the sharp surface assumption, that affect only the shape of the distribution, but they are sensitive to those, such as the independent particle assumption, that affect the total quantity of jetting. Scattering and absorption are likely to reduce drastically the actual number of nucleons emitted by jetting.

G. FERMI JETS AND EVAPORATION: CALCULATED RESULTS

In specific computations, nuclear trajectories will be calculated here by using a modified version [52] of the one-body code mentioned in Section II.E [6]. The code assumes that the nuclei remain spherical and change neither Z nor A during the collision process. As discussed in Section C, these approximations may be valid during jetting, but not throughout the entire collision. The nuclei either separate eventually or are trapped, orbiting forever (Fig. 29). The latter fate is interpreted as compound nucleus formation.

Calculated jetting varies greatly with L (Fig. 26 and

Table 6), so it is desirable to distinguish L's experimentally. This can be done by measuring nucleon emission at, say, fixed final projectile (fragment) angle in quasi-elastic or deep-inelastic collisions. Unfortunately, the code mentioned above cannot accurately connect initial L's to final projectile fragment angles. Either the code must be profoundly changed or some other means of making the connection must be found. On the other hand, compound-nucleus formation averages experimentally over a broad range of L's, but at least the theoretical calculation can be performed by using geometrical partial cross sections. The maximum L involved in compound-nucleus formation, L_{max}, can be estimated from

$$\sigma_{CN} \stackrel{!}{=} \int_0^{L_{max}} d\sigma(L) = \int_0^{L_{max}} dL\ \pi\lambda\!\!\!^{-2}(2L+1) \quad , \qquad (3.61)$$

where σ_{CN} is the experimental compound-nucleus cross section and $\lambda\!\!\!^{-}$ is the reduced, relative nuclear wavelength. Jetting in compound-nucleus reactions can be obtained by weighting jetting as a function of L by the geometrical partial cross section, and then averaging it over the range from 0 to L_{max}. This is all for the future, however; the calculations to be presented here refer to situations in which the nuclei eventually separate.

Section D shows how to start with $\vec{q}$ and find $\vec{v}_1^{\infty}$. Reversing

the process requires $\vec{r}_S$. $\vec{v}_1^{\infty}$, $\vec{r}_W$, and $\vec{r}_1$ determine a plane (except when $\vec{v}_1^{\infty}$ parallels $\vec{r}_W - \vec{r}_1$). One can scan by computer the intersection of this plane with the surface of nucleus 1 until $\vec{r}_S$ is found. There turn out to be from 0 to 3 solutions.

The program outlined in the introduction, Section A, can now be implemented to calculate the jetting of nucleons from the entire collision process. The results to be given here refer to proton emission from $^{20}Ne + {}^{64}Cu$ at 252 MeV.

The first result demonstrates why equation (3.56) is false. Table 8 lists the time intervals during which jetting is calculated to occur at various proton energies, but at a fixed proton angle of 45°. For this case, L = 70, and it will be recalled from Section C that the turning point is reached at $t_o = 2.00 \times 10^{-22}$ sec. Obviously, for fixed energy and angle, jetting is <u>not</u> uniform in time. As nuclei turn about each other during a collision, the jetting pattern turns (and changes), as well. Figure 30 consists of two plots, one of target emission and the other of projectile emission, both for L = 82. Dots and crosses denote the existence of jetting at the energy and angle indicated on the axes, but a dot means that jetting starts when the nuclear surfaces touch and a cross, that it starts later. In both plots, the sweeping movement of jetting is apparent. Just as Figs. 17 and 27 suggest, target emission sweeps backward and projectile emission sweeps forward,

like the two beams from a (lop-sided) lighthouse. Observe how the maximum energy changes with angle, decreasing as the nuclei simultaneously dissipate their relative motion and turn.

The amount of calculated jetting is displayed variously in Fig. 31. Figure 31(a) depicts target emission for L = 82 in a polar contour plot in which the radius is proton laboratory energy, the polar angle is the proton angle, and the contours provide the number of protons emitted per unit energy and solid angle. Notice how small a region of velocity space is occupied. Other processes, such as those involving one or more collisions or reflections will tend to obscure such pictures in practice and neglected effects, such as diffraction, will tend to deform them. Both Figs. 31(a) and (b) mark the final projectile angle calculated by the nuclear dynamics code; neither mark should be believed.

A contour plot is ideal for a comprehensive view, but it skimps on detail. It is natural to project out the emission components at constant energy and angle. Figure 31(b) shows the angular distribution of both projectile and target calculated emission at L = 70. As one might expect from Figs. 30(a) and 31(a), the higher energy target emission distributions are quite narrow.

An experimenter is more likely to measure protons at fixed angle in coincidence with a final nuclear fragment at some other angle, the coincidence being required in order to select a definite,

though possibly unknown, L. His proton detector will then produce energy spectra. Figures 31(c)-(f) are calculated energy spectra at various angles, now for L = 70. Once more, the effects of nuclear turning and motion dissipation appear as the peaks shift in energy. The narrowness of the spectra is unlikely to be observed. Competition from other mechanisms is likely to produce something like Fig. 32. Rather different from the other spectra is that calculated for L = 0 at a proton angle of 0°. As shown in Fig. 31(g), it is broader in energy and two orders of magnitude larger in peak emission than is any of the other spectra. The absence of nuclear turning prevents the emission from sweeping around in angle. In effect, the spectra that would occur at a range of different angles, if L were larger, are superposed at one angle, producing both changes in the spectrum.

Even ordinary evaporation--the antithesis of jetting--can overwhelm it in unfavorable circumstances. Simplified evaporation calculations were performed for the purpose of comparison and the method will now be outlined. Evaporation is commonly regarded as a slow process on the time scale of nuclear collisions. If so, it is uniquely determined by the final state of the nuclear reaction. The final state is specified in these calculations by the final projectile angle and by the relaxation, $\mathcal{R}$, which is defined as the fractional loss of the center-of-mass kinetic energy over the

barrier. The nucleus velocities and internal excitations can then be reconstructed. The next step is to follow each nucleus down all possible sequences of proton and neutron emission. To avoid multiple integrations over intermediate emission energies for each sequence, each nuclide on a sequence is assigned an excitation energy based on the excitation and mean emission energy of its parent. Likewise, it is assigned a probability equal to the parent's assigned probability times the probability of the parent emitting the variety of nucleon (proton or neutron) needed to reach its daughter. The assigned probability of a nucleus before it begins to evaporate is 1. To find the proton emission spectrum, the spectrum of a single nuclide, normalized to unit probability of emission, is evaluated for each member of each sequence, based on the member's excitation. Next, the spectrum is weighted by the member's assigned probability and summed over all members and all sequences. The sum is then boosted from the rest frame of the final nucleus being considered to the laboratory frame. Finally, the contributions of both target and projectile are combined. The single-nuclide evaporation spectrum, as well as the mean energies and proton-neutron branching ratios, are found by the standard, elementary technique for evaporation in the absence of angular momentum [54]. The only sophistication is to retain

$$\rho(E^*) \propto \exp(2\sqrt{aE^*}) \tag{3.62}$$

for the density of states, rather than to use a Maxwell-Boltzmann formula.

What are the errors in this approach? First, pre-exponential factors in equation (3.62) are left out. Presumably, the exponentials are much more important. Secondly, the orbital and spin angular momenta of the nucleons are ignored. This is reasonable, because nucleons are known to be evaporated predominantly in states of zero angular momentum and because their spin of 1/2 is negligible compared to L = 70 or 80. On the other hand, the nuclei do end up with considerable spins, of the order of 10, which ties up energy in rotational motion, making it unavailable for evaporation. In this respect, the calculation overestimates evaporation of high energy nucleons. Working in the opposite direction is the use of probability assignments and of mean energies in calculating residual excitations. This amounts to an approximation of the evaporation multiple integrals that favors emission at mean energies at the expense of high and low energy emission. In ^{20}Ne + ^{64}Cu at 252 MeV, however, evaporation at the high end of the jetting energy range is dominated by the first evaporation step of the projectile and is unaffected by this approximation. Finally, changes in Z and A before evaporation begins are ignored, with unknown consequences. In all the

calculations to be presented here, $\mathcal{R}$ was set equal to 1, as suggested by experimental results in the deep-inelastic region.

Each jetting calculation requires the initial L of the nuclei. To compare it with an evaporation calculation or with experiment, one needs, say, the final angle of the projectile fragment. The nuclear dynamics code provides this only inaccurately, as another user of the code has confirmed from the code's predictions of fusion at unrealistically large initial angular momenta [52]. One must therefore presume that the code over-estimates the angular deflection produced by nuclear attraction and dissipation.

Figure 33(a) displays the angular distribution of jetting calculated for L = 82. The nuclear dynamics code associates L = 82 with a final projectile angle, θ_{PF}, of -20°. The true angle is more positive by an unknown amount; the angle, -14°, used in the evaporation calculations presented in Fig. 33(b), is just one possibility. Comparison between Figs. 33(a) and 33(b) in Fig. 33(c) proves that evaporation may sometimes swamp jetting. This is by no means inevitable. At a somewhat lower angular momentum, L = 70, the jetting may be detectable above an evaporative background. To see this, compare the jetting angular distributions in Fig. 31(b) with the evaporative distributions in Figs. 33(b), 34(a), and 34(b). Since the nuclear dynamics code links L = 70 with a final projectile

host, and fly off to infinity. Together, they compose two beams that turn as the nuclei turn. At best, the beams are expected to be feeble, consisting of one nucleon, in order of magnitude.

From this picture follow the minimum bombardment energy for emission and, at a fixed bombardment energy, both the maximum angular momentum that will permit jetting and the maximum energy with which a nucleon can be emitted. With the aid of a model of nuclear dynamics, the number of nucleons emitted in Fermi jets is calculated as a function of nucleon laboratory velocity. Two experimental arrangements in which to measure the emission are available. The colliding nuclei either fuse or not. Measurement of nucleon emission in coincidence with compound nucleus formation is a less discriminating tool than is its measurement in coincidence with the measurement of the final states of nuclei that eventually separate. This is because compound nucleus formation occurs over a large range of initial nuclear angular momenta, whereas each final state of a non-compound event corresponds to a narrow range of initial angular momenta. Exploitation of the non-compound advantage requires that the theoretical nuclear dynamics model accurately describe the entire nuclear trajectory, which the crude model used here cannot do.

An order of magnitude separates estimates of the number of nucleons in Fermi jets from estimates of the total number emitted by

all means. Only the focusing of Fermi jets is calculated to make them stand out from other emission mechanisms by allowing them to be the predominant source of emission in small regions of velocity space. The accuracy demanded of their calculation is no more than the limited accuracy possessed by standard calculations of the contributions made by competing sources, such as evaporation.

For Fermi jets to be produced, the relative nuclear speed must be larger than a threshold speed and much smaller than the Fermi speed. Even if these conditions can be met, errors in the simple model of Fermi jets employed here (called the "basic" model) may be critical.

The magnitude of one possible source of error--disruption of the nuclear media--is unknown. Of the other sources, two-body effects and window diffraction have the potential ability to make Fermi jets impossible to detect, but their actual impact is unknown. Shell effects are likely to be equally large, but should enhance jets as often as they efface them.

There are three approximations in the basic Fermi jet model whose rectification probably alters the jetting pattern substantially, without reducing the total number of particles jetted. First is the neglect of nuclear diffuseness; inclusion may actually improve focusing. The second approximation is a "concentration" of the Coulomb potential at the nuclear surface.

Third is the approximation of an integral over the window by the product of the integrand evaluated at the center of the window and the window area.

Relatively small errors, in the neighborhood of 5-30%, will arise from barrier penetration, quantal nucleon reflection, and nuclear acceleration. Specular reflection, the universality of nuclear densities, and the approximation of nuclear connections by windows are assumptions that should have the same, tolerable impact on jetting as they do on the wall and window formulae. Finally, the Pauli principle, classical reflection, nuclear sphericity, and the universality of nuclear potentials introduce no discernible errors at all.

Among other sources of nucleon emission, evaporation is calculated to mask the Fermi jets in unfavorable situations. The evaporation calculations used here, however, may wrongly favor high energy emission.

The most urgent demand upon the future is to determine theoretically whether there exist circumstances in which Fermi jets are expected to appear despite competition from other emission processes and despite the impact of errors inherent in the basic model of Fermi jets. To accomplish this, a <u>coarse</u> survey of jetting under the influence of all possible combinations of the following variables must be made:

(1) projectile-target combinations, large or small, symmetric or antisymmetric;

(2) bombarding energies;

(3) initial angular momenta, leading to non-compound events with various final states or to compound events.

Unfortunately, the basic model of Fermi jets cannot perform this survey alone. The survey requires simultaneous consideration of the errors in that model and of other emission sources, since both these factors change with the variables listed above.

The basic model already includes the effects of diffuseness at the window in a crude way, which should be straightforward to improve. It is obvious how to put in two-body effects; it is not so obvious what they really are. Integrating over the window should be routine. It need not increase the length of jetting calculations, since it will obviate the trial-and-error process of making sure that nucleon trajectories go through the center of the window. The minor effects of nuclear acceleration can readily be included in an approximate way. To avoid trouble with the Coulomb potentials, consider only neutrons.

Even with these additions, the nucleon trajectories in the Fermi jet model remain straight lines except for surface refraction. Further progress involves major complications. It is necessary to solve differential equations to find the trajectories

striking and useful.

APPENDICES

APPENDIX A

SOME GEOMETRICAL LEMMAS

A.1

Obviously,

$$\oint_S dS\,\hat{n} = \sum_i \hat{e}_i \oint_S dS\, n_i \tag{A1}$$

and

$$n_i = \vec{A}_i \cdot \hat{n} \quad , \tag{A2}$$

if

$$(\vec{A}_i)_j = \delta_{ij} \quad . \tag{A3}$$

Therefore,

$$\oint_S dS\,\hat{n} = \sum_i \hat{e}_i \oint_S d\vec{S} \cdot \vec{A}_i = \sum_i \hat{e}_i \oint_S d\vec{r}\; \vec{\nabla} \cdot \vec{A}_i \quad , \tag{A4}$$

where the second equality is justified by Green's theorem. In view of equation (A3),

$$\vec{\nabla} \cdot \vec{A}_i = 0 \tag{A5}$$

for all i. Finally,

$$\oint_S dS\,\hat{n} = 0 \quad . \tag{A6}$$

A.2

Figure 36 almost proclaims that

$$\frac{d\Omega}{dt} = \oint_S dS\ \hat{n}(\vec{r},t) \cdot \vec{V}(\vec{r},t) \quad . \tag{A7}$$

To see this, break up the original surface into infinitesimal surface elements, ΔS_i. As the surface evolves in time, each point on it moves and, during an infinitesimal time interval Δt, an infinitesimal volume, $\Delta\Omega(\Delta S_i,\Delta t)$, is swept out, beginning at ΔS_i and ending at $\Delta S_i'$. This volume is

$$\begin{aligned}\Delta\Omega(\Delta S_i,\Delta t) &= A(\Delta S_i)\ \vec{V}(\vec{r}_{S_i}) \cdot \hat{n}(\vec{r}_{S_i})\ \Delta t \\ &+ O[A(\Delta S_i)(\Delta t)^2] + O\left\{[A(\Delta S_i)]^2\ \Delta t\right\} \quad ,\end{aligned} \tag{A8}$$

where $\vec{r}_{S_i}$ is some point on ΔS_i. In general, $\Delta\Omega$ might be a complicated volume because ΔS_i could be non-planar and $\vec{V}$ could be non-uniform and non-constant, so that ΔS_i would change size, shape, and orientation, leading to the corrections indicated in the preceding equation. Taking the limits of zero time interval and surface element size,

$$\frac{d\Omega}{dt} = \lim_{\Delta t \to 0} \frac{1}{\Delta t} \lim_{\Delta S_i \to 0} \sum_i \Delta\Omega(\Delta S_i, \Delta t)$$

$$= \lim_{\Delta t \to 0} \frac{1}{\Delta t} \left\{ \Delta t \oint_S dS\, \hat{n} \cdot \vec{V} + O[(\Delta t)^2] \right\} \tag{A9}$$

$$= \oint_S dS\, \hat{n} \cdot \vec{V} \quad .$$

A.3

Consider a (non-planar) surface S and its projection R on some plane having a normal $\hat{w}$, as shown in the upper drawing in Fig. 37. The areas, A, of two corresponding elements, dS and dW, will be related by

$$\frac{A(dR)}{A(dS)} = \hat{n} \cdot \hat{w} \quad , \tag{A10}$$

where $\hat{n}$ is the normal to dS, as the lower drawing in Fig. 37 demonstrates.

A.4

This is very like Section A.1. Again,

$$\oint_S dS\ \vec{r} \times \hat{n} = \sum_i \hat{e}_i \oint_S dS\ (\vec{r} \times \hat{n})_i \tag{A11}$$

and

$$(\vec{r} \times \hat{n})_i = (\vec{A}_i) \cdot \hat{n} \quad , \tag{A12}$$

but this time

$$(\vec{A}_i)_j = \sum_k \varepsilon_{ikj}\ r_k \quad . \tag{A13}$$

Therefore,

$$\oint_S dS\ \vec{r} \times \hat{n} = \sum_i \hat{e}_i \oint_S \overrightarrow{dS} \cdot (\vec{A}_i) = \sum_i \hat{e}_i \oint_S d\vec{r}\ \vec{\nabla} \cdot \vec{A}_i \quad . \tag{A14}$$

Since

$$\vec{\nabla} \cdot \vec{A}_i = \sum_j \frac{\partial A_i}{\partial r_j} = \sum_{jk} \varepsilon_{ikj} \frac{\partial r_k}{\partial r_j} = \sum_{jk} \varepsilon_{ijj} = 0 \quad , \tag{A15}$$

$$\oint_S dS\ \vec{r} \times \hat{n} = 0 \quad . \tag{A16}$$

APPENDIX B

AN EXAMPLE OF A NON-ISOTROPIC DISTRIBUTION

Consider

$$F(\vec{v},\vec{r}) = \frac{N}{\Omega} f(|v_x|)\ \delta(v_y)\ \delta(v_z) \quad , \tag{B1}$$

in which

$$\int_{-\infty}^{+\infty} dv_x \quad f(|v_x|) \quad = \quad 1 \quad . \tag{B2}$$

F is drastically anisotropic, but it is homogeneous in space and satisfies

$$\langle \vec{v} \rangle \quad = \quad 0 \quad . \tag{B3}$$

If the box is motionless, the general pressure formula, equation (2.12), implies that

$$P(\vec{r},t) \quad = \quad \rho \langle \vec{v}^2 \rangle \, [n_x(\vec{r},t)]^2 \quad . \tag{B4}$$

This differs from the corresponding isotropic expression (2.21) only in the replacement of 1/3 by $(n_x)^2$. The force on the gas follows now from (2.33):

$$\vec{F}_{gas} \quad = \quad -\rho \langle \vec{v}^2 \rangle \oint_S dS \quad (n_x)^2 \, \hat{n} \quad . \tag{B5}$$

For any reflection-symmetric box, such as a rectangular solid, the integral obviously vanishes. Distribution anisotropy is insufficient to make $\vec{F}_{gas}$ be non-zero: the box must be somewhat asymmetric as well. For example, let the cone shown in Fig. 38 be chosen, its axis made parallel to the x-axis, and its apex pointed in the -x direction. The integral in equation (B5) is simple:

$$\oint_{cone} dS \quad = \quad \oint_{base} dS \; + \oint_{hat} dS \quad . \tag{B6}$$

On the base, $\hat{n} = \hat{x}$, so

$$\oint_{\text{base}} dS \; (n_x)^2 \; \hat{n} \;=\; \pi r^2 \hat{x} \quad . \tag{B7}$$

On the hat, the y- and z-components of the integral vanish by symmetry and

$$n_x \;=\; -r \; (r^2 + L^2)^{-\frac{1}{2}} \quad . \tag{B8}$$

The area of a surface element on the hat, dS_{hat}, and the area of that element's projection on the base, dS_{base}, are related by the geometrical result (A10), so

$$dS_{base} \,/\, dS_{hat} \;=\; |n_x| \quad , \tag{B9}$$

and the total areas of the base and the hat are in the same ratio. Therefore,

$$\oint_{\text{hat}} dS \; (n_x)^2 \; \hat{n} \;=\; -\pi r^4 (r^2 + L^2)^{-1} \; \hat{x} \quad . \tag{B10}$$

Combining equations (B5)-(B7) and (B10), one finally arrives at

$$\vec{F}_{gas} \;=\; -\rho \, \langle \vec{v}^2 \rangle \, \pi r^2 L^2 (r^2 + L^2)^{-1} \; \hat{x} \quad . \tag{B11}$$

The sign may be understood as follows. A gas particle colliding with the base strikes the wall head on and is reflected directly back, so that its momentum change is twice its original

momentum and is directed in the -x direction. Gas particles strike the hat only a glancing blow, however, so the momentum change is smaller; moreover, the y and z components cancel. Of course, the areas and fluxes are different in each case, but it has already been noted that the hat area is larger by a factor $1/|n_x^{hat}|$ than the base area, whereas equation (2.7) and the symmetry of F imply that the flux for v_x on the hat is $|n_x^{hat}|$ times that for $-v_x$ on the base, so these effects cancel out. This discussion highlights the transience of the distribution function, (B1). Collisions with the hat wall immediately give y and z velocity components to some of the gas particles. This process hints at the relationship between randomization, gas anisotropy, and box asymmetry. At least, it softens the stark anisotropy of the initial distribution.

APPENDIX C

INTEGRAL EVALUATION AND APPROXIMATION

1. Evaluation

Suppose that an integral

$$I = \int d\vec{v}\ F_r(v)\ g(\vec{v}) \tag{C1}$$

is to be evaluated and that it has the property

$$I = \int d\vec{v}\ F_r(v)\ h(\vec{v}\cdot\hat{n}) \qquad , \tag{C2}$$

whether because $g(\vec{v})$ simply equals $h(\vec{v}\cdot\hat{n})$ (for the wall formula) or because the integrals over the components of $\vec{v}$ perpendicular to $\hat{n}$ lead to this result (for the window formula). Suppose further that h has the special form

$$h(\vec{v}\cdot\hat{n}) = \theta(\pm\vec{v}\cdot\hat{n} - U)\ j(\vec{v}\cdot\hat{n}) \qquad . \tag{C3}$$

With these premises,

$$I = 2\pi\int_0^\infty dv\ v^2\ F_r(v)\int_{-1}^{+1} d\mu\ \theta(\pm v\mu - U)\ j(v\mu) \qquad , \tag{C4}$$

if

$$\mu = \vec{v}\cdot\hat{n} \tag{C5}$$

The first thing to tackle is the μ-integral. Let $J(x)$ be an indefinite integral of $j(x)$. An indefinite μ-integral of $j(v\mu)$ is then

$$\frac{1}{v}\ J(v\mu) \qquad . \tag{C6}$$

Integrating by parts,

$$M \equiv \int_{-1}^{+1} d\mu\ \theta(\pm v\mu - U)\ j(v\mu)$$

$$= \left[\theta(\pm v - U)\ \frac{1}{v}\ J(v\mu)\right]_{-1}^{+1} \mp \int_{-1}^{+1} d\mu\ \delta(\pm v\mu - U)\ J(v\mu) \qquad \text{(C7)}$$

$$= \theta(\pm v - U)\ \frac{1}{v}\ J(v) - \theta(\pm v - U)\ \frac{1}{v}\ J(-v) \mp \theta(v - |U|)\ \frac{1}{v}\ J(\pm U) \quad .$$

It will prove easier to do the v-integral if equation (C7) is first rewritten. Let a be positive and suppose $|\varepsilon| = |\eta| = 1$. It is straightforward to verify that

$$\theta(\varepsilon a + \eta b) = \theta(\varepsilon) - \varepsilon\ \theta(-\varepsilon\eta b)\ \theta(|b| - a) \quad . \qquad \text{(C8)}$$

M then becomes

$$M = \pm \frac{1}{v}\ J(\pm v) \mp \frac{1}{v}\ J(\pm U)$$
$$+ \theta(|U| - v) \left\{ \mp \frac{1}{v}\ J[\pm\varepsilon(U)v] \pm \frac{1}{v}\ J(\pm U) \right\} \quad . \qquad \text{(C9)}$$

Equations (C4), (C7), and (2.20) lead to

$$I = \frac{1}{2}\ \frac{N}{\Omega} \langle M \rangle_r \quad . \qquad \text{(C10)}$$

In light of (C9),

$$I = \frac{1}{2}\frac{N}{\Omega}\left\{\pm\langle \frac{1}{v} J(\pm v)\rangle_r \mp \langle\frac{1}{v}\rangle_r J(\pm U)\right.$$

$$\left.\mp \langle\theta(|U|-v)\frac{1}{v} J[\pm\varepsilon(U)v]\rangle_r \mp \langle\theta(|U|-v)\frac{1}{v}\rangle_r J(\pm U)\right\} \quad . \tag{C11}$$

This is true of any integral satisfying (C1)-(C3).

2. Approximation

Suppose $j(x)$ is a polynomial:

$$j(x) = \sum_n^M j_n x^n \tag{C12}$$

(the lower limit of the sum is deliberately not specified). As far as velocity dimension is concerned, $j(v\mu)$ must be a single power of velocity:

$$[j(v\mu)] = [\text{velocity}]^m \quad , \tag{C13}$$

where m is an integer. In the cases of interest, the only velocity dependence of j_n is

$$j_n = j_n(U) \quad . \tag{C14}$$

Dimensional consistency then requires

$$j_n = k_n U^{m-n} \quad , \tag{C15}$$

where k_n is velocity-independent. Using equations (C12) and (C15)

in (C11), one finds

$$I = \frac{1}{2}\frac{N}{\Omega}\left\{\sum_n^M (\pm 1)^n \frac{k_n}{n+1} U^{m-n} \langle v^n \rangle_r - \left[\sum_n^M (\pm 1)^n \frac{k_n}{n+1}\right] U^{m+1} \langle v^{-1} \rangle_r \right.$$

$$\mp \sum_n^M [\pm\varepsilon(U)]^{n+1} \frac{k_n}{n+1} U^{m-n} \langle \theta(|U| - v) v^n \rangle_r \qquad \text{(C16)}$$

$$\left. + \left[\sum_n^M (\pm 1)^n \frac{k_n}{n+1}\right] U^{m+1} \langle \theta(|U| - v) v^{-1} \rangle_r \right\} \quad .$$

In equation (C16), U can be identified with

$$U = (\vec{V} - \vec{V}_o) \cdot \hat{n} \quad . \qquad \text{(C17)}$$

For sufficiently slow deformations,

$$|U| << \langle v \rangle_r \quad ; \qquad \text{(C18)}$$

the approximation of I in this limit is desired. Recall the assumptions about F introduced in connection with equation (2.37). If $g(v)$ is a smooth function of v,

$$\langle \theta(|U| - v) g(v) \rangle_r = 4\pi \frac{\Omega}{N} \int_0^{|U|} dv \; v^2 F_r(v) \; g(v) \quad , \qquad \text{(C19)}$$

where v' is somewhere betwen 0 and $|U|$. The second assumption means that

$$F_r(v') \leqslant \bar{F}_r \equiv (\langle v \rangle_r)^{-1} \int_0^{\langle v \rangle_r} dv \; F_r(v) \quad . \tag{C20}$$

Both assumptions together imply that

$$\langle v \rangle_r = 4\pi \frac{\Omega}{N} \int_0^{\infty} dv \; F_r(v) \; v^3 = O\left[4\pi \frac{\Omega}{N} \int_0^{\langle v \rangle_r} dv \; F_r(v) \; v^3 \right] \quad , \tag{C21}$$

so

$$\bar{F}_r = O\left[\frac{N}{\Omega} (\langle v \rangle_r)^{-3} \right] \quad . \tag{C22}$$

Equations (C19)-(C20) and (C22) then lead to

$$\langle \theta(|U| - v) g(v) \rangle_r \leqslant O\left[(\langle v \rangle_r)^{-3} \int_0^{|U|} dv \; v^2 \; g(v) \right] \quad . \tag{C23}$$

Equations (2.37) and (C23) can now be applied to the expressions for I.

Accordingly, equation (C16) becomes

$$I = \frac{1}{2}\,\frac{N}{\Omega}\,\langle v^M\rangle\, U^{m-M} \left\{ \sum_n^M (\pm 1)^n \frac{k_n}{n+1}\; O\left[(|U|/\langle v\rangle_r)^{M-n}\right] \right.$$

$$- \left[\sum_n^M (\pm 1)^n \frac{k_n}{n+1}\right] O\left[(|U|/\langle v\rangle_r)^{M+1}\right] \mp \sum_n^M \left[\pm\varepsilon(U)\right] \frac{k_n}{n+1} \tag{C24}$$

$$\left. \times\; O\left[(|U|/\langle v\rangle_r)^{M+3}\right] + \sum_n^M (\pm 1)^n \frac{k_n}{n+1}\; O\left[(|U|/\langle v\rangle_r)^{M+3}\right] \right\} .$$

The second term in I in equation (C11) is thus of order

$$(|U|/\langle v\rangle_r)^{M+1} \tag{C25}$$

and the last two terms are smaller, both being of order

$$(|U|/\langle v\rangle_r)^{M+3} \quad . \tag{C26}$$

In the first term, the larger n is, the larger the n-subterm is. Since n is always at least 0 for cases of interest, every subterm dominates terms two through four. Hence, equation (C16) can be written

$$I = \frac{1}{2}\,\frac{N}{\Omega}\left[(\pm 1)^M \frac{k_M}{M+1}\, U^{m-M}\langle v^M\rangle_r + (\pm 1)^{M-1} \frac{k_{M-1}}{M}\, U^{m-M+1}\langle v^{M-1}\rangle_r\right] + O\left[(|U|/\langle v\rangle_r)^2\, U^{m-M}\langle v^M\rangle_r\right] . \tag{C27}$$

APPENDIX D

TEMPERATURES AND NEUTRON EXCESSES

1. Fermi gases at positive temperatures

This subsection follows the suggestions of [56]. The Fermi-Dirac distribution for arbitrary temperatures is

$$F(v) = \frac{N}{\Omega} \frac{1}{\frac{4}{3}\pi v_F^{\,3}} \frac{1}{\exp\left[\beta(\frac{1}{2} mv^2 - \mu) + 1\right]} \quad . \tag{D1}$$

In this expression, μ is the chemical potential, κ is the Boltzmann constant, T is the temperature, and

$$\beta = 1/\kappa T \quad . \tag{D2}$$

Given a function of v, $\Gamma(v)$, such as v^n, the task is to evaluate

$$\begin{aligned} \langle \Gamma(v) \rangle &\equiv \frac{\Omega}{N} \int d\vec{v}\; F(v)\; \Gamma(v) \\ &= \frac{2^{\frac{1}{2}}\, 3}{m^{3/2}\; v_f^{\,3}} \int_0^\infty d\varepsilon \; \frac{\varepsilon^{\frac{1}{2}}\; \Gamma\left[(2/m)^{\frac{1}{2}}\; \varepsilon^{\frac{1}{2}}\right]}{\exp\left[\beta(\varepsilon-\mu)\right] + 1} \quad . \end{aligned} \tag{D3}$$

If

$$f(\varepsilon) = \frac{1}{e^{\beta(e-\mu)} + 1} \tag{D4}$$

and if the integral

$$\psi(\varepsilon) \equiv \int_0^{\varepsilon} d\varepsilon' \, \phi(\varepsilon') \tag{D5}$$

exists, then integration by parts and power series expansion of ψ eventually leads to

$$\int_0^{\infty} d\varepsilon \, f(\varepsilon)\phi(\varepsilon) \cong \sum_{m=0}^{\infty} I_{2m} \frac{\beta^{-2m}}{(2m)!} \psi^{(2m)}(\mu) \quad , \tag{D6}$$

where

$$I_m \equiv \int_{-\infty}^{+\infty} dx \frac{e^x}{(e^x+1)^2} x^m \quad . \tag{D7}$$

The quality of the approximation in equation (D6) depends on two assumptions. First,

$$\beta\mu \gg 1 \tag{D8}$$

must hold in order that $e^{-\beta\mu}$ can be neglected in comparison to $(\beta\mu)^{-m}$, at least for small m. Secondly,

$$\psi(\varepsilon) \underset{\varepsilon \to \infty}{\sim} o(e^{\beta\varepsilon}) \quad , \tag{D9}$$

which is true for most applications.

The integral I_m is evaluated by observing that another integral,

$$J = \int_{-\infty}^{+\infty} dx \; \frac{e^{ikx}}{(e^{x}+1)(e^{-x}+1)} \quad , \tag{D10}$$

can be written in two ways. Expanding the integrand numerator in a power series and integrating term by term,

$$J = \sum_{m=0}^{\infty} \frac{(ik)^m}{m!} I_m \quad . \tag{D11}$$

On the other hand, the integrand of J has poles at odd multiples of $i\pi$. Comparing J with the corresponding contour integral along $\mathrm{Im}\, z = 2\pi$, one finds

$$J = \frac{\pi k}{\sinh \pi k} \quad . \tag{D12}$$

The denominator and then J itself can be expanded in a power series, which, when compared with equation (D11), yields $I_0 = 1$ and

$m > 0$,

$$I_{2m} = (-1)^m (2m)!\, \pi^{2m} \sum_{p=1}^{m} (-1)^p \sum_{\substack{n_1,\ldots,n_p \geqslant 1 \\ n_1+\ldots+n_p = m}} \frac{1}{(2n+1)!\ldots(2n_p+1)!} \quad . \tag{D13}$$

The chemical potential is set by requiring

$$\langle 1 \rangle = 1 \quad , \tag{D14}$$

whence the usual result

$$\mu = \mu_F \left\{ 1 - \frac{\pi^2}{12} (\beta\mu_F)^{-2} + O[(\beta\mu_F)^{-4}] \right\} , \tag{D15}$$

where

$$\mu_F = \tfrac{1}{2} m v_F^{\,2} . \tag{D16}$$

Once this is done,

$$\langle v^2 \rangle_r = \frac{3}{5} v_F^{\,2} \left\{ 1 + \frac{5}{12} \pi^2 (\beta\mu_F)^{-2} + \ldots \right\} \tag{D17a}$$

$$\langle v \rangle_r = \frac{3}{4} v_F \left\{ 1 + \frac{1}{6} \pi^2 (\beta\mu_F)^{-2} + \ldots \right\} . \tag{D17b}$$

At positive temperatures, the ideal gas contribution to the pressure equals the product of the zero-temperature contribution and the curly bracket in equation (D17a). The zero-temperature contribution to the specialized wall formula is multiplied, at positive temperatures, by the bracket in (D17b), which also determines the effect of positive temperatures on the specialized window formula. The impact of positive temperatures on higher order terms in the two formulae can be calculated similarly.

2. Temperature magnitudes

Nuclear collsions can easily dissipate 200 MeV of relative, nuclear motion into internal, nucleonic motion. The temperature can be related to the total internal excitation energy of the fragments,

E^*, by inverting equation (D17a):

$$(\beta\mu_F)^2 \simeq \frac{\pi^2}{4} \frac{A\mu_F}{E^*} \quad . \tag{D18}$$

If E^* is no more than 200 MeV for a collision of two nuclei that together contain, say, 238 nucleons, then $(\beta\mu_F)^2$ is at least 100, so the series in (D15) and (D17) converge very rapidly, (D8) and (D18) are retroactively validated, and temperature effects on the wall and window formulae are small.

3. Neutron excesses

The discussion so far has distinguished neutrons from protons only by allowing four spin-isospin states for each energy eigenvalue. This is equivalent to assuming equal numbers of protons and neutrons. The neutron-proton mass difference has also been ignored, but it is only 7×10^{-4} nucleon masses--entirely negligible at this level of approximation.

For the general case in which $Z \neq N$, the distribution function is a sum of two functions of the form (D1), one for protons and one for neutrons. The symbol A is replaced by Z,N for protons, neutrons and each distribution has its own Fermi speed, chemical potential, and temperature, distinguished by subscripts $q = p,n$. The Fermi speed is

$$v_{Fq} = \frac{2\pi\hbar}{m}\left(\frac{3}{8\pi}\ \frac{N_q}{\Omega}\right)^{1/3} \quad . \tag{D19}$$

For N = Z, this reduces to equation (2.41), which will be denoted v_{Fs} here. For thermal equilibrium,

$$\beta_p = \beta_n = \beta \quad . \tag{D20}$$

The chemical potentials are determined by

$$\langle 1 \rangle_q = 1 \quad , \tag{D21}$$

where the mean value is defined by the first part of equation (D3) with N_i replacing A. When N = Z, this implies

$$\mu_p = \mu_n \equiv \mu_s \quad , \tag{D22}$$

so the two distributions are identical and add up to one distribution of the form (D1) that incorporates v_{Fs}, μ_s, and β, recovering the four-state prescription.

When $Z \neq N$,

$$\langle \Gamma(\vec{v}) \rangle = \frac{Z}{A} \langle \Gamma(\vec{v}) \rangle_p + \frac{N}{A} \langle \Gamma(\vec{v}) \rangle_n \quad . \tag{D23}$$

Wherever v_{Fs} appeared before, the expression

$$(v_{Fs})^k \ \tfrac{1}{2}\left[\left(\frac{2Z}{A}\right)^{1+k/3} + \left(\frac{2N}{A}\right)^{1+k/3}\right] \tag{D24}$$

now replaces it. The factor multiplying $(v_{Fs})^k$ is small. Even for ^{238}U, it equals 1.012 for k = 1 and 1.029 for k = 2, which can be

neglected here.

APPENDIX E

DISSIPATIVE AND COLLECTIVE ENERGY TRANSFERS IN A ONE-DIMENSIONAL EXAMPLE

Consider a box in the form of a rectangular solid that is initially at rest and is filled with a gas of non-interacting particles of mass m moving with velocities parallel to one of the box axes. The particles have but one speed, v_o, and two velocities, $+v_o$ and $-v_o$. For definiteness,

$$F(\vec{v},\vec{r}) = \frac{N}{\Omega}\,\frac{1}{2}\,[\delta(v_x - v_o) + \delta(v_x + v_o)]\,\delta(v_y)\delta(v_z) \quad . \qquad \text{(E1)}$$

The example is essentially one-dimensional. Now, let the box suddenly begin to move with velocity +V along the axis. Assume

$$(0 <)\ V < v_o \quad . \qquad \text{(E2)}$$

What happens? Initially, the energy per particle is $1/2\ m(v_o)^2$. If the gas were just a blob of matter without internal motion, it would acquire an additional energy per particle of 1/2 mV , once it adjusted to the new motion of the box. The same expectation arises from increasing both particle velocities by V, to v_o+V and $-v_o$+V:

$$\tfrac{1}{2}\left[\tfrac{1}{2}m(v_o + V)^2 + \tfrac{1}{2}m(-v_o + V)^2\right] = \tfrac{1}{2}m(v_o)^2 + \tfrac{1}{2}mV^2 \quad . \tag{E3}$$

The actual sequence of events is different. The particles initially having velocity $+v_o$ eventually strike the wall for which they were heading and rebound with velocity $-v_o+2V$. When they reach the opposite wall, they collide again, returning to $+v_o$. Each particle switches back and forth forever, spending half its time at each velocity. The particles that had an initial velocity $+v_o$ periodically all have velocity $-v_o+2V$; later, all return to $+v_o$; mostly, they are divided. Likewise, those particles that originally had velocity $-v_o$ switch back and forth between $-v_o$ and v_o+2V. If L is the length of the box, then, by going to the rest frame of the box, it is easy to see that the period of particles initially having velocity $+v_o$ is $2L/(v_o-V)$ and that of particles initially having velocity $-v_o$ is $2L/(v_o+V)$. These two periods may be close, but they are almost always incommensurable. Eventually, the distributions of the two sets of particles will be practically uncorrelated, so the time-averaged distribution of all the particles gives equal weight to each of the four final velocities. The average energy per particle is then

$$\tfrac{1}{2}m(v_o)^2 + mV^2 \quad . \tag{E4}$$

Half the additional energy has gone into internal motion and half into collective motion. This is confirmed by going to the moving box frame. There, the four equally weighted velocities are $+(v_o-V)$, $-(v_o-V)$, $+(v_o+V)$, and (v_o+V), respectively. The average energy per particle is

$$\tfrac{1}{2}m(v_o)^2 + \tfrac{1}{2}mV^2 \quad , \tag{E5}$$

and the additional $\tfrac{1}{2}mV^2$ obviously is internal excitation.

REFERENCES

[1] D. H. E. Gross and J. Wilczynski, Phys. Lett. 67B, 1 (1977).

[2] J. P. Blocki, J. Randrup, W. J. Swiatecki, C. F. Tsang, Ann. Phys. 105, 427 (1977).

[3] J. S. Sventek, Lawrence Berkeley Laboratory Report, LBL-8407.

[4] G. J. Mathews and J. Randrup, private communication (1979).

[5] Earlier accounts of some of the material in this chapter can be found in [6] and the references therein.

[6] J. Blocki, Y. Boneh, J. R. Nix, J. Randrup, M. Robel, A. J. Sierk, and W. J. Swiatecki, Ann. Phys. 113, 330 (1978).

[7] Equation (2.40) in the absence of drifts was first derived by J. Blocki. The present author subsequently derived (36) independently.

[8] The last equation in (2.61), apart from the contribution of the normal to the dyadic, was first derived in

W. J. Swiatecki, Journal de Physique Supplement 33, C5-45 (1972).

The present author subsequently derived (2.53) independently.

[9] A. Bohr and B. R. Mottelson, Nuclear Structure. Benjamin, New York, 1969, Vol. I, pp. 214 and 237.

[10] H. Hofmann, A. S. Jensen, C. Ngo, K. Reese, P. J. Siemens, to to be published in Phys. Lett. C.

[11] P. Bonche, S. E. Koonin, J. W. Negele, Phys. Rev. C13, 1226

(1976).

[12] S. E. Koonin, Phys. Lett. 61B, 227 (1976).

[13] R. Y. Cusson, R. K. Smith, J. A. Maruhn, Phys. Rev. Lett. 36, 1166 (1976).

[14] S. E. Koonin, K. T. R. Davies, V. Maruhn-Rezwani, H. Feldmeier, S. J. Krieger and J. W. Negele, Phys. Rev. C15, 1359, (1977).

[15] C. Y. Wong and H. H. K. Tang, "The Extended Time-Dependent Hartree-Fock Approximation with Particle Collisions," to be published.

[16] H. Hofmann and P. J. Siemens, Nucl. Phys. A283, 87 (1977).

[17] S. E. Koonin, R. L. Hatch, and J. Randrup, Nucl. Phys. A283, 87 (1977).

[18] S. E. Koonin and J. Randrup, Nucl. Phys. A289, 475 (1977).

[19] J. Randrup and W. J. Swiatecki, NORDITA-78/38 (1978).

[20] For example,

D. K. Scott, Lawrence Berkeley Laboratory Report, LBL-7727, Ch. 1 (1978).

[21] W. J. Swiatecki, private communication.

[22] J. Randrup, Ann. Phys. 112, 356 (1978).

[23] Bohr and Mottelson, op. cit., Vol. II, pp. 75-82.

[24] This work was done in collaboration with J. Randrup.

[25] The development through equation (2.149) was first performed by J. Blocki. The present author subsequently performed it

independently.

[26] Bohr and Mottelson, op. cit., Vol. II, pp. 654-661.

[27] H. Goldstein, Classical Mechanics. Addison-Wesley, Reading, 1950, pp. 21-22.

[28] R. A. Broglia, Bull. Am. Phys. Soc. 23, 550 (1978).

[29] C. F. Tsang, Proc. 27th Nobel Symposium, Ronneby, June 11-14, 1974, Physica Scripta 10A, 90 (1974).

[30] P. Russo, et. al., Nucl. Phys. A281, 509 (1977).

[31] W. D. Myers, W. J. Swiatecki, T. Kodama, L. J. El-Jaick, and E. R. Hilf, Phys. Rev. C15, 2032 (1977).

[32] M. Goldhaber and E. Teller, Phys. Rev. 74, 1046 (1948).

[33] H. Steinwedel and J. H. Jensen, Z. Naturforsch. 52, 413 (1950).

[34] J. Keats, "Ode on a Grecian Urn," Annals of the Fine Arts, No. XV (1820).

[35] J. P. Bondorf, Jour. de Physique C5, 195 (1976).

[36] M. C. Robel, Bull. Am. Phys. Soc. 23, 522 (1978).

[37] J. P. Bondorf, Niels Bohr Institute Preprint NBI-78-15 (1978).

[38] Bohr and Mottelson, op. cit., Vol. I, pp. 165-168.

[39] M. Blann, Nucl. Phys. A213, 570 (1973).

[40] Bohr and Mottelson, op. cit ., Vol. I, pp. 215-216 and 233-238.

[41] S. E. Koonin, private communication (1977).

[42] R. H. Dicke and J. P. Wittke, Introduction to Quantum

Mechanics. Addison-Wesley, Reading, 1960, p. 48.

[43] N. Metropolis, et. al., Phys. Rev. 110, 185 and 204 (1958).

[44] H. W. Bertini, Phys. Rev. 131, 1801 (1963).

[45] K. Chen, et. al., Phys. Rev. 166, 949 (1968).

[46] K. Chen, G. Friedlander, and J. M. Miller, Phys. Rev. 176, 1208 (1968).

[47] K. Chen, G. Friedlander, G. D. Harp, and J. M. Miller, Phys. Rev. C4, 2234 (1971).

[48] J. Hudis and J. M. Miller, Ann. Rev. Nucl. Sci. 9, 159 (1959).

[49] Reviewed in

M. Blann, Ann. Rev. Nucl. Sci. 25, 123 (1975).

[50] Bohr and Mottelson, op. cit., Vol. I, pp. 140-141.

[51] Goldstein, op. cit., Ch. 3.

[52] J. S. Sventek, private communication (1977).

[53] J. P. Bondorf, private communication (1978).

[54] G. Friedlander, J. W. Kennedy, and J. M. Miller, Nuclear and Radiochemistry. Wiley, New York, 2nd ed., 1964, pp. 343-348.

[55] D. K. Scott, private communication (1977).

[56] F. Reif, Fundamentals of statistical and thermal physics. McGraw-Hill, New York, 1965, pp. 393-397 and 402-403.

Table 1. A gas of independent, classical particles is rotated inside a spheroidal box with frequency $\omega = 0.5\times10^{+22}$ sec^{-1}. The effect of starting the gas at rest is compared with that of starting it with a frequency of rotation equal to that of a box (but with a uniform density).

Initial distribution	Asymptotic excitation average (MeV per nucleon)	Asymptotic excitation slope (MeV per nucleon per period)	Standard deviation of the slope (MeV per nucleon per period)
Non-rotating	13.(7)	7×10^{-4}	1.80×10^{-2}
Co-rotating	2.(4)	-0.06	0.09

Table 2.

$\gamma_\lambda/\omega_\lambda$

	$\lambda = 2$	$\lambda = 8$
$^{11}_{5}B$	1.(5)	0.7(1)
$^{120}_{50}Sn$	3.(1)	1.(1)
$^{238}_{92}U$	5.(9)	1.(2)

TABLE 3. The maximum changes in Coulomb potential, $\Delta V_{Coulomb}$, experienced by a nucleon starting at the window, crossing either nucleus and continuing to infinity, are compared with the (maximum) relative proton energy inside and outside either nucleus. $^{20}Ne + {}^{64}Cu$ at 252 MeV.

	$V_{Coulomb}$ (MeV)	E_{proton} (MeV)
Inside nuclei	$\leqslant 4$	$\leqslant 90$
Outside nuclei	$\leqslant 8$	$\leqslant 40$

TABLE 4. Some basic quantities calculated for $^{86}Kr + ^{nat}Se$.

$Z_p = 36$, $A_p = 86$, $A_\mu = 39.78$, $Z_T = 34$, $A_T = 74$.

E_F (MeV)	Protons	Neutrons
projectile	32.9	40.9
target	35.0	39.0

$R_p = 6.30$ Fm $\quad R_T = 6.04$ Fm $\quad \bar{R} = R_p + R_T = 12.33$ Fm

Coulomb barrier = 142.89 MeV

Proton Coulomb barrier for head-on target emission = 10.93 MeV

Lab energy needed to overcome Coulomb barrier = 308.96 MeV

Lab energy threshold for proton emission = 431.28 MeV

Lab energy threshold for neutron emission = 338.10 MeV

TABLE 5. Threshold L's and maximum nucleon emission energies as a function of bombarding energy.

Projectile energy (MeV)	Maximum L for contact	Maximum L for emission of		Maximum energy (MeV) of emitted	
		protons	neutrons	protons	neutrons
338.10	62.7	*	0.0	*	0.6
357.75	81.2	*	51.5	*	5.0
377.39	96.1	*	72.8	*	7.6
397.04	109.0	*	89.2	*	9.6
416.68	120.6	*	103.0	*	11.4
436.33	131.1	†	115.2	†	13.0
455.97	140.9	†	126.1	†	14.4
475.62	150.0	77.4	136.3	14.9	15.8
495.26	158.6	92.9	145.7	16.1	17.1
514.91	166.7	106.3	154.5	17.2	18.3
534.55	174.5	118.1	162.9	18.3	19.5
554.20	182.0	128.8	170.8	19.3	20.6
573.84	189.1	138.7	178.4	20.3	21.7
593.49	196.0	148.0	185.7	21.3	22.7
613.13	202.6	156.7	192.7	22.2	23.8
632.78	209.1	164.9	199.5	23.1	24.8
652.42	215.3	172.8	206.0	24.0	25.7
672.07	221.4	180.3	212.3	24.9	26.7
691.71	227.3	187.5	218.5	25.7	27.6
711.36	233.1	194.4	224.5	26.6	28.5
731.00	238.7	201.2	230.3	27.4	29.4

*No emission

†Projectile emission, but no target emission.

TABLE 6. Angular and energy ranges of protons emitted from $^{16}O + ^{58}Ni$ at 315 MeV for extreme values of L.

	Emitting Nucleus			
	Target		Projectile	
L	0	100	0	100
θ (degrees)				
Minimum	-160	-66	-180	40
Maximum	+160	-44	+180	97
Difference	320	22	360	57
E (MeV)				
Minimum	8	10	0	18
Maximum	63	53	12	27
Difference	55	43	12	9

TABLE 7. The order of magnitude of the total number of protons emitted as a function of L for ^{20}Ne + ^{64}Cu at 252 MeV.

L	0	10	20	30	40	50	60	70	80	90	100
$O(N_p^1 + N_p^2)$	3	3	3	3	3	2	2	2	1	0.4	0.02

TABLE 8. The time intervals during which particles jet at various energies.

^{20}Ne + ^{64}Cu at 252 MeV L = 70 Target emission at 45°			
Proton Energy (MeV)	10	20	30
t_o (10^{-22} sec)	0.32-0.49	0.47-0.76	1.18-1.29

FIGURE CAPTIONS

Fig. 1. Dynamic nuclear systems. Top: a single deforming nucleus, to which the wall formula applies. Middle: a system with a constriction that is not small; no known one-body formula applies to it. Bottom: two nuclei connected by a small region; here, the window formula applies.

Fig. 2. At a point $\vec{r}$ on a nuclear surface S, the surface normal is $\hat{n}(\vec{r})$ and the surface velocity is $\vec{V}(\vec{r})$.

Fig. 3. The volume swept out by particles moving with velocity $\vec{u}$ to strike a surface element of area dS in time dt is a cylinder whose base area is dS and whose normal height is $\vec{u}\cdot\hat{n}\,dt$. A cross section of the cylinder, cut perpendicular to the surface element is shown. The surface element is made small enough to be approximated by a plane surface.

Fig. 4. When a particle strikes the surface, its incident velocity, $\vec{u}$, and reflected velocity, $\vec{u}'$, are assumed to make equal angles with the surface normal, $\hat{n}$.

Fig. 5. Three different distribution functions, F_r, are plotted as functions of v. The vertical scales are identical, all giving F_r. The horizontal scales are also identical, giving v. In the upper drawing, F spreads evenly over |U|

and $\langle v \rangle_r$; in the middle drawing, F_r is concentrated around $\langle v \rangle_r$; In the bottom drawing, it is concentrated around $|U|$.

Fig. 6. Nuclei 1 and 2 are in contact. The dotted line denotes the window surface, W. At a point on it, $\vec{r}$, the window velocity is $\vec{V}$ and the normal to the window (defined to point out from 1) is $\hat{n}_1$.

Fig. 7. Two gases, 1 and 2, with the same drift velocity are separated by an imaginary surface (dashed line) moving at a velocity $\vec{B}$ with respect to them. Drawing (a) is made in an inertial frame where the drift velocities vanish. Drawing (b) is made in a frame moving at velocity $\vec{B}$ with respect to the first frame.

Fig. 8. Particles (open circles) with the same mass and velocity, $\vec{v}$ (arrows), are enclosed in a surface (dashed line). The surface is moved, in the lower drawing, so that it encloses one more particle than it does in the upper drawing.

Fig. 9. The nucleon mean free path, λ, (solid line) and attenuation factors, A, (dashed lines) are plotted as functions of incident nucleon energy (measured outside the nucleus). The attentuation factor is defined as the probability that

a nucleon survives passage through a nucleus without being scattered; it is calculated according to equation (3.8), where s is taken to be the nuclear diameter. The left-hand vertical scale measures λ in Fermis. The right-hand scale measures A. The horizontal scale refers only to neutrons. (For protons, the proton-nucleus barrier energy must be subtracted from the proton energy before the graph is used.)

Fig. 10. (A mirror image of Fig. 2.) The volume swept out by particles recoiling with velocity $\vec{u}'$ from a surface element of area dS in time dt is a cylinder of base area dS and normal height $|\vec{u}' \cdot \hat{n}|dt$. A cross section of the cylinder, cut perpendicular to the surface element, is shown.

Fig. 11. A Fermi gas starts at zero temperature in a cubical box at time t. The box begins to deform and the evolved state of the gas is shown at t + dt. Coordinate and velocity space are both limited to two dimensions in the figure, for simplicity. The shaded regions are those occupied by the gas.

Fig. 12. The contrast between the effect of a sharp and of a diffuse nuclear surface on a nucleon colliding with it. The top drawings show a collision taking place at $\vec{r}$. Both

represent the nucleon trajectory by a directed line to the left of $\vec{r}$ that approaches from the top and recedes toward the bottom. In the upper right drawing, shading denotes the surface region. The lower drawings plot schematically the respective variations of the combined (nuclear plus Coulomb) potential energy along a line parallel to $\hat{n}$ and passing through $\vec{r}$. The origins are at $\vec{r}$ and zero energy. The ordinate is the potential energy of a nucleon (a proton) and the abscissa is the distance from $\vec{r}$ along $\hat{n}$. Both potential drawings are meant to show the same (Coulomb) potential energy far from the surface. (For a neutron, the Coulomb potential is absent.) They differ in that the nuclear potential is a step function for the sharp surface, but changes more gradually in the diffuse surface. Strictly speaking, the existence of a non-uniform Coulomb potential means that a proton trajectory always curves, as it does in the upper right drawing, but the trajectory can be approximated by a straight line outside the nuclear potential, as shown in the upper left drawing.

Fig. 13. A gas of independent, classical particles rotates with angular frequency ω inside a spheroid. The mean excitation energy per particle (MeV) is plotted as a function of time (in units of the rotational period). The gas initially is

a Fermi gas, but two different initial drift velocities are specified. The closed circles reflect a drift that is identically zero everywhere; the open circles, one that is rotating in a rigid body fashion at angular frequency ω. Excitation is plotted at quarter-period intervals. Solid lines are the results of least-squares fits of straight lines to the calculated points. Projection of the lines on the time axis yields the interval over which the fits were made. With each calculated point is associated a statistical error bar derived from the Monte-Carlo process. The bars vary within the narrow range indicated in the key to the figure and are not added onto the circles.

Fig. 14. Comparison of calculated and experimental most probable fission-fragment kinetic energies as a function of $Z^2/A^{1/3}$. The kinetic energies calculated for non-viscous flow are given by the dot-dashed curve. The dashed curve shows the results for infinite two-body viscosity, and the solid curve shows the results for the one-body dissipation considered here. The experimental data are for cases in which the most probable mass division is into two equal fragments; the open symbols represent values for equal mass divisions only and the solid symbols represent values

averaged over all mass divisions. The original sources for the experimental data are given in [6].

Fig. 15. The final orbital angular momentum as a function of the initial angular momentum for an idealized ^{86}Kr nucleus bombarding an idealized ^{197}Au nucleus at laboratory energies of 600, 800, and 1000 MeV. The window formula, in the form of the Proximity Friction, was used to describe the dissipation of energy. The value $l_f = 5/7\ l_i$ corresponds to the rolling condition which, within the limitations of the model, corresponds to total relaxation in the relative angular degree of freedom. A large part of the cross section is seen to correspond to such a relaxed situation.

Fig. 16. Energy vs. angle plots (Wilczynski diagrams) for the idealized collision of ^{86}Kr on ^{197}Au at three (lab) energies. The labels on the circled points give the final orbital angular momentum appropriate to the angle and energy indicated. The interaction barrier E_B (the same, in the model used, for the entrance and exit channels) is indicated.

Fig. 17. Two nuclei in collision are connected by a window (dashed line) through which nucleons (solid arrows) pass. The

dashed arrow indicates the path such a nucleon may then follow.

Fig. 18. In the one-dimensional case, the nuclear centers, the nuclear positions, and the velocities of all nucleons and nuclei are collinear. In the rest frame of 1, a nucleon (wavy line) that crosses 1 will confront at the surface of 1 a potential step, V, equal to the sum of the Fermi energy, E_F, and the separation energy, S. The most rapid such nucleon will arrive with a speed that is the sum of the Fermi speed, v_F, and the speed of nucleus 2, τ_2. (The shaded area represents the Fermi sea in 1.)

Fig. 19. The top drawing shows two nuclei. The middle one plots schematically the sum of the Coulomb and nuclear potentials along the dashed line joining the nuclear centers in the top drawing. The bottom drawing shows the idealized potential to be used in jetting calculations. The peaks have zero thickness. Different mean Coulomb energies produce different square-well depths; both are neglected.

Fig. 20. A nucleon passes through the window at a; crosses the interior, b; penetrates the surface at c; and, d, proceeds to infinity.

Fig. 21. The point on the surface through which the nucleon tries to pass, $\vec{r}_S$, is determined by projecting $\vec{u}_1$ from $\vec{r}_W$ to the surface. The normal to the surface at $\vec{r}_S$ is $\hat{n}_S$.

Fig. 22. The nucleon velocity approaching $\vec{r}_S$ is $\vec{u}_1$; just leaving, $\vec{v}_1$; and at infinity, $\vec{v}_1^{\infty}$. The lower drawing shows how the total potential--nuclear potential for nucleon of type i, $-V_i$ or 0, plus Coulomb potential for that nucleon, $V_{ci}(\vec{r})$--varies ideally along $\hat{n}_S$ in the vicinity of $\vec{r}_S$. (The peak has zero width).

Fig. 23. A nucleon trajectory is designated by solid arrows. The indicated angles are all equal.

Fig. 24. Since the normal to the window pointing out from 2, $\hat{n}_{W2}$, parallels $\vec{r}_1-\vec{r}_W$ and since, at first contact, $|\vec{r}_1-\vec{r}_W| = |\vec{r}_S-\vec{r}_1|$, the indicated angles are all equal.

Fig. 25. $^{86}Kr + {}^{74}Se$. Maximum calculated laboratory energy (MeV) for jetted protons (1) and neutrons (2) as a function of projectile energy.

Fig. 26. Calculated, initial proton jetting from $^{16}O + {}^{58}Ni$ at 315 MeV is depicted. The emission envelope is denoted by the saw-toothed and wavy lines, save where both are overriden by a solid line. Two or more points in the Fermi sphere

project into the same point in the laboratory (shading). (a) Target emission at L = 90; (b) Target emission at L = 0; (c) Projectile emission at L = 80; (d) Projectile emission at L = 20.

Fig. 27. Positive angles are defined by the side of the beam the projectile is on initially. Everything is restricted to the reaction plane. The normal $\hat{n}_{W2}$ is shown for target emission.

Fig. 28. Points are selected in that part of the Fermi sphere of nucleus 2 allowed by equation (3.43) and are restricted to the reaction plane. The z′-axis parallels $\hat{n}_{W2}$. Five values of $q_{z'}$, labeled 1,2,...5, are selected, ranging in equal steps from the threshold in (3.43) to just under v_{Fi}^2, the difference between which is exaggerated in the diagram. Each value of $q_{z'}$ is scanned in equal steps from the least to the greatest possible values $q_{x'}$. In the laboratory diagrams, saw-toothed lines connect the points for which q nearly equals v_{Fi}^2; wavy lines, those for which $q_{z'}$ is the threshold value in (3.43) (the two lines meet in circles); and dashed lines connect points for which $q_{z'}$ is fixed at a value above the threshold.

Fig. 29. Trapping in the nuclear dynamics code occurs when, for

large times, t, the separation of the nuclear centers oscillates transiently about an asymptotic value.

Fig. 30. Calculated Fermi jet protons from ^{20}Ne + ^{64}Cu at 252 MeV. L = 82. Proton laboratory energies and angles are compared. A dot indicates that jetting begins at the first instant of nuclear contact; a cross, later. (a) Target emission; (b) Projectile emission.

Fig. 31. These graphs portray to proton jet calculations in ^{20}Ne + ^{64}Cu at 252 MeV. (a) Jetting for L = 82 is displayed in a polar plot in which the radius is the proton laboratory energy (MeV), the polar angle is the proton laboratory angle, and the contours give the number of protons (10^{-4} per MeV per steradian). (b)-(f) L = 70: (b) Laboratory angular distribution of jetting at fixed proton energies (MeV); (c)-(f) Energy spectra at various fixed proton laboratory angles: (c) -25°, (d) -65°, (e) $+55^{o}$, and (f) $+130^{o}$. At each angle, all the emission comes exclusively from one nucleus or the other. (g) L = 0 and the proton angle is 0°; only the target emission spectrum is shown.

Fig. 32. Schematic energy spectra at a fixed angle. Pure jetting, shown at the top, may be observable even when partly obscured by other emission processes.

Fig. 33. Angular distributions of protons (per MeV per steradian) at fixed energies (MeV) for ^{20}Ne + Cu at 252 MeV. (a) Calculated jetting for L = 82; (b) Calculated evaporation for full relaxation, with projectile fragments (PF) at -14°; (c) Comparison of (a) and (b).

Fig. 34. Calculated angular distributions of proton evaporation (per MeV per steradian) at fixed energies (MeV) for ^{20}Ne + ^{63}Cu at 252 MeV. Full relaxation. The final projectile angle is (a) -30°, (b) -41°.

Fig. 35. Fermi jet and evaporation calculations are compared for ^{20}Ne + ^{64}Cu at 252 MeV by means of contour plots in velocity space. The contours give the number of protons (per Mev per steradian) and the velocity is measured parallel and perpendicular to the beam, in units of c. Postive angles are now defined by the side of the beam on which the projectile fragment ends up. (a) Fermi jets for L = 70 (which the nuclear dynamics code associates with $\theta_{PF} = +41.5^{o}$). (b) Evaporation for $\mathcal{R} = 1$ and $\theta_{PF} = +14$. Dots marked "TF" and "PF" denote the final projectile and target fragment velocities and the line through them represents a mirror symmetry. The innermost irregular closed region about PF experiences no evaporation at all. The dark lines

making up its border consist of several contour lines too close to be distinguished visually. (c) Sum of the emissions shown in (b) and (c). The evidences of jetting are outward bulges in some of the contours in the upper right-hand part of the drawing.

Fig. 36. The upper drawing shows how, during time Δt, a surface element ΔS_i that is initially located at $\vec{r}_{S_i}$ moves to $\vec{r}'_{S_i}$ and deforms into $\Delta S'_i$. The two initial and final surface elements are symbolized by irregular shapes whose boundaries are solid lines. In the process, the surface normal changes from $\hat{n}_{S_i}$ to $\hat{n}'_{S_i}$ and the element sweeps out volume $\Delta\Omega$, whose outline is indicated by dashed lines. The lower drawing illustrates an approximate calculation of the magnitude of $\Delta\Omega$. The calculation neglects changes in $\hat{n}_{S_i}$ and in the size and shape of ΔS_i, which it assumes to be small enough to be approximated as a plane. The volume swept out is then a cylinder of base area ΔS_i and normal height $\vec{V}(\vec{r}_{S_i})\cdot\hat{n}_{S_i}\, t$. The lower drawing is a section of the cylinder that parallels $\hat{n}_{S_i}$.

Fig. 37. The upper drawing presents S, a two-dimensional surface in three-space. The projection of S on a plane, whose normal is $\hat{w}$, is R. A surface element dS with normal $\hat{n}$

then projects into a surface element dR. The lower drawing relates the area of dS to that of dR. It is a section through dS (and dR) made parallel to both $\hat{n}$ and $\hat{w}$. The two indicated angles are both equal.

Fig. 38. A cone of height L and base radius r is oriented so that its axis parallels the x-axis and its apex points in the -x direction.

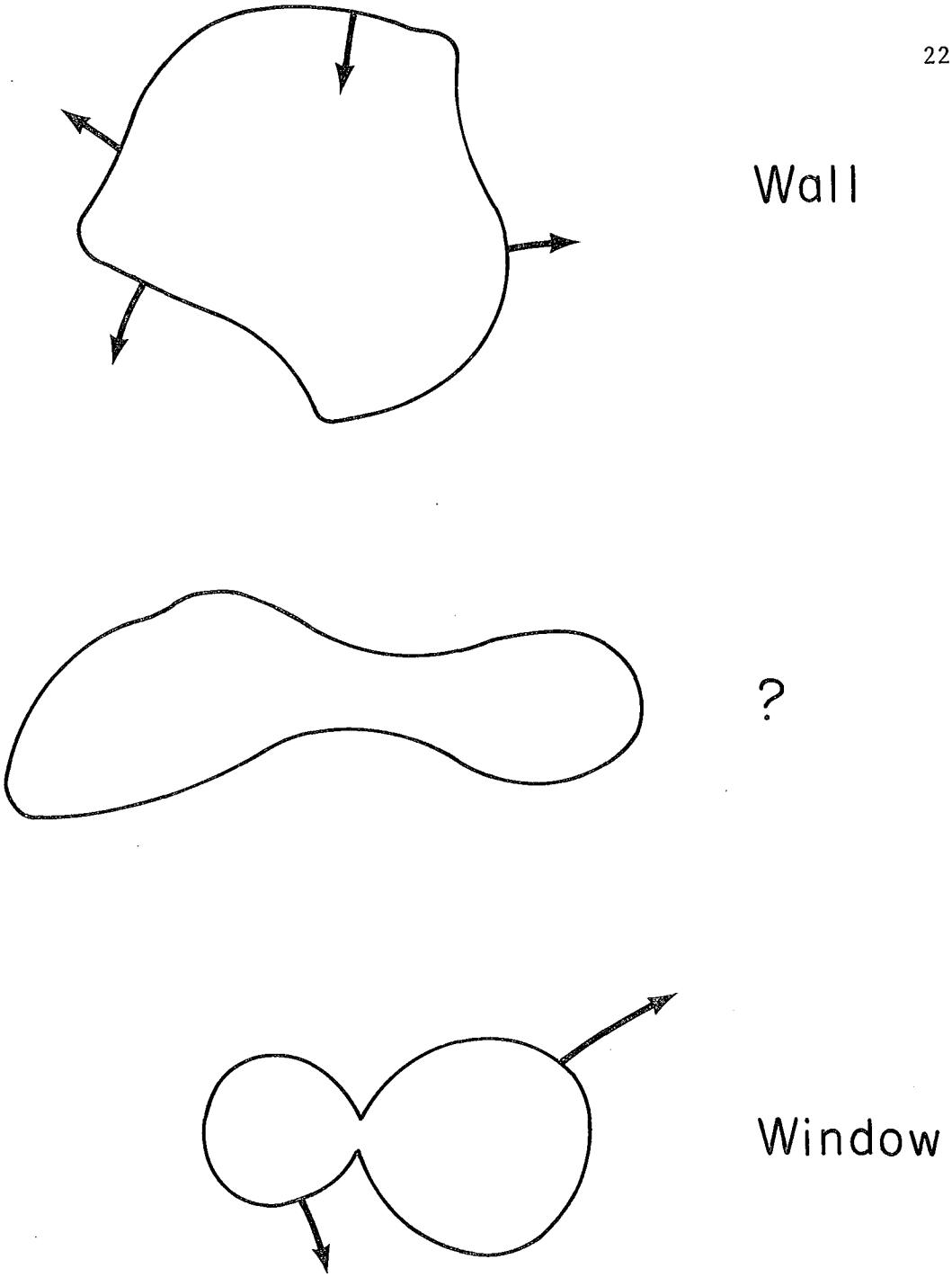

Fig. 1

XBL 7811-12547

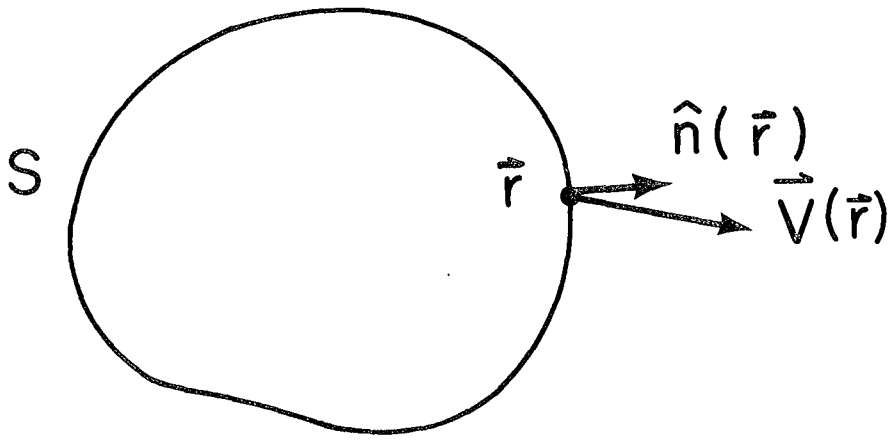

XBL 7811-12549 A

Fig. 2

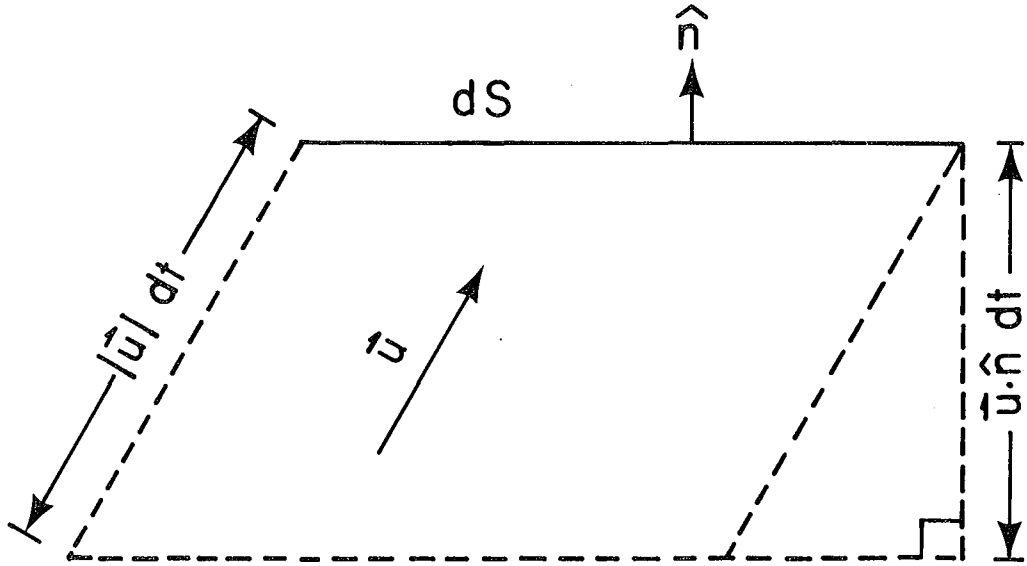

XBL 7811-12724

Fig. 3

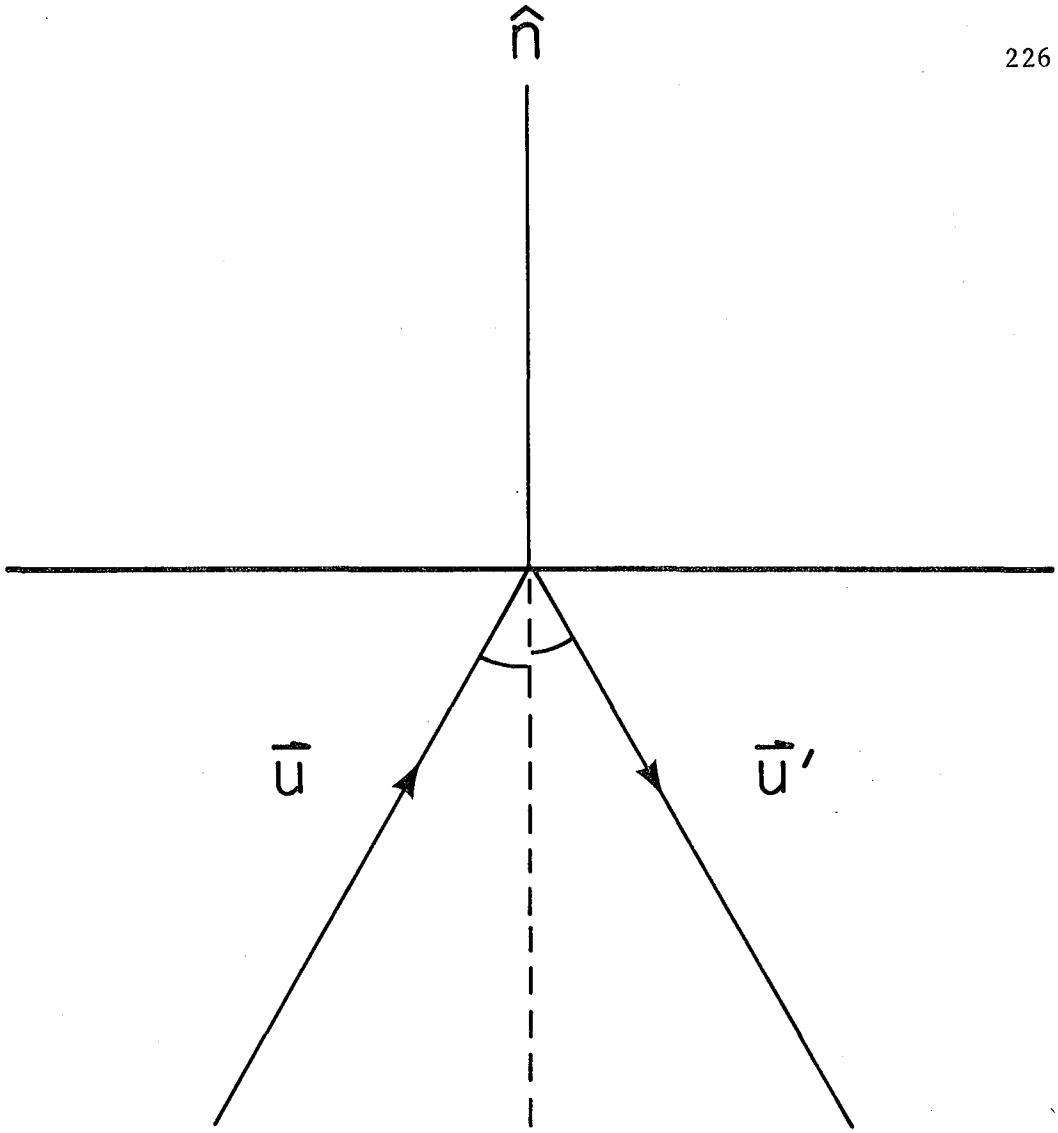

XBL 7811-12722

Fig. 4

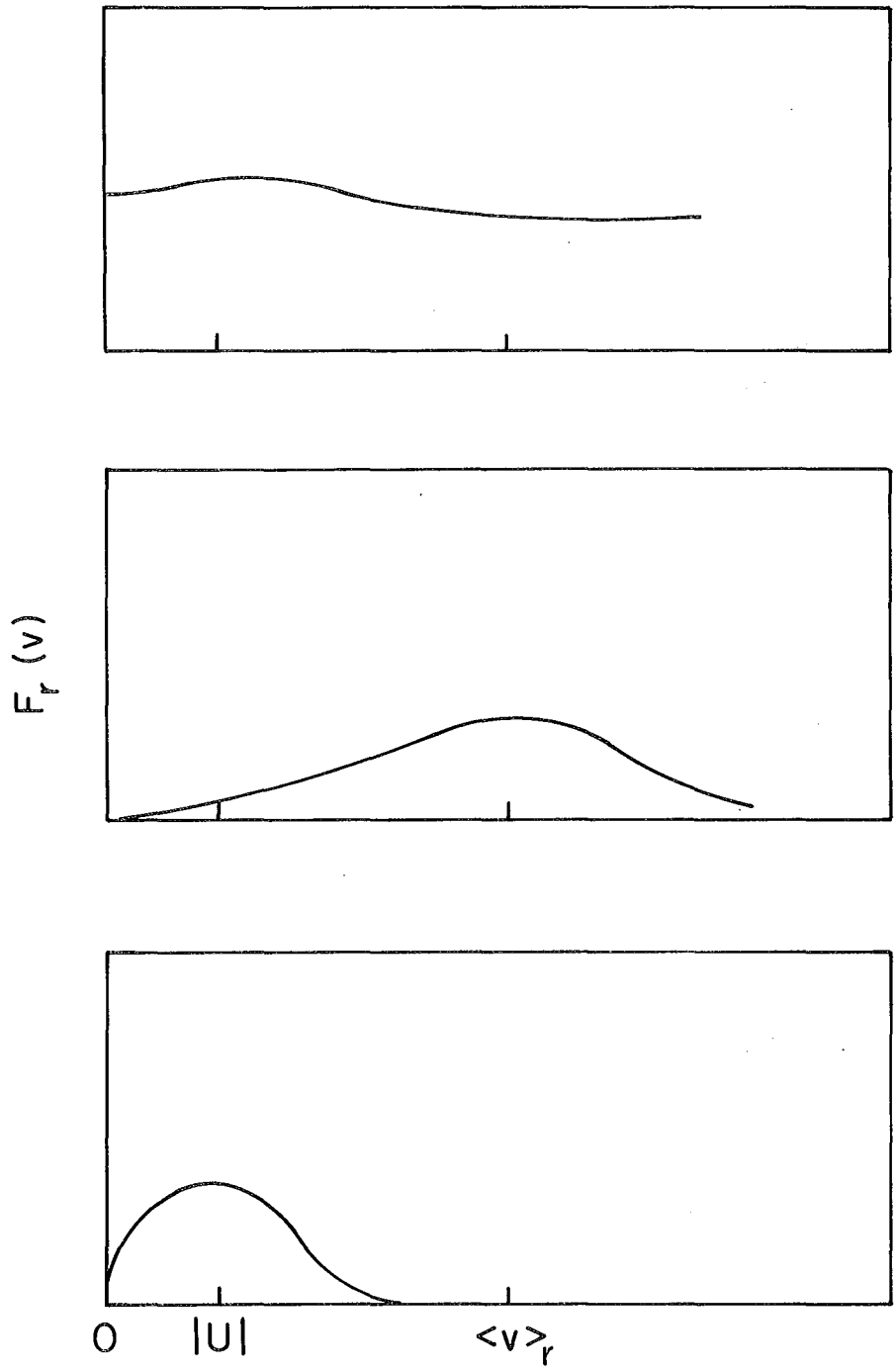

XBL 7811-12723

Fig. 5

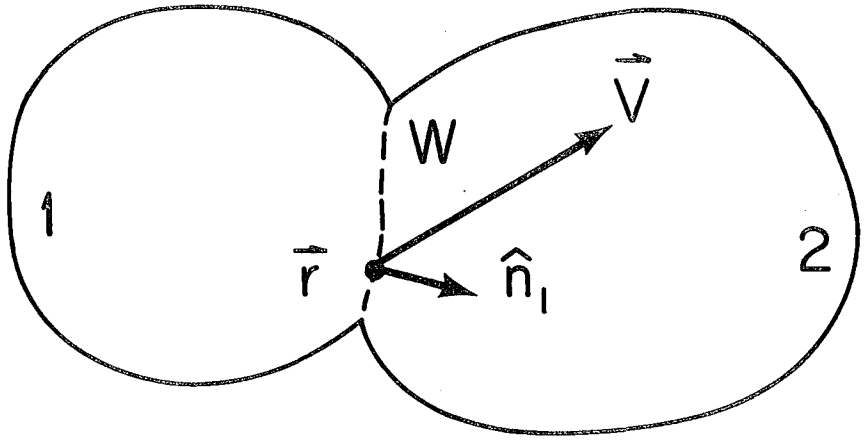

XBL 7811-12546 A

Fig. 6

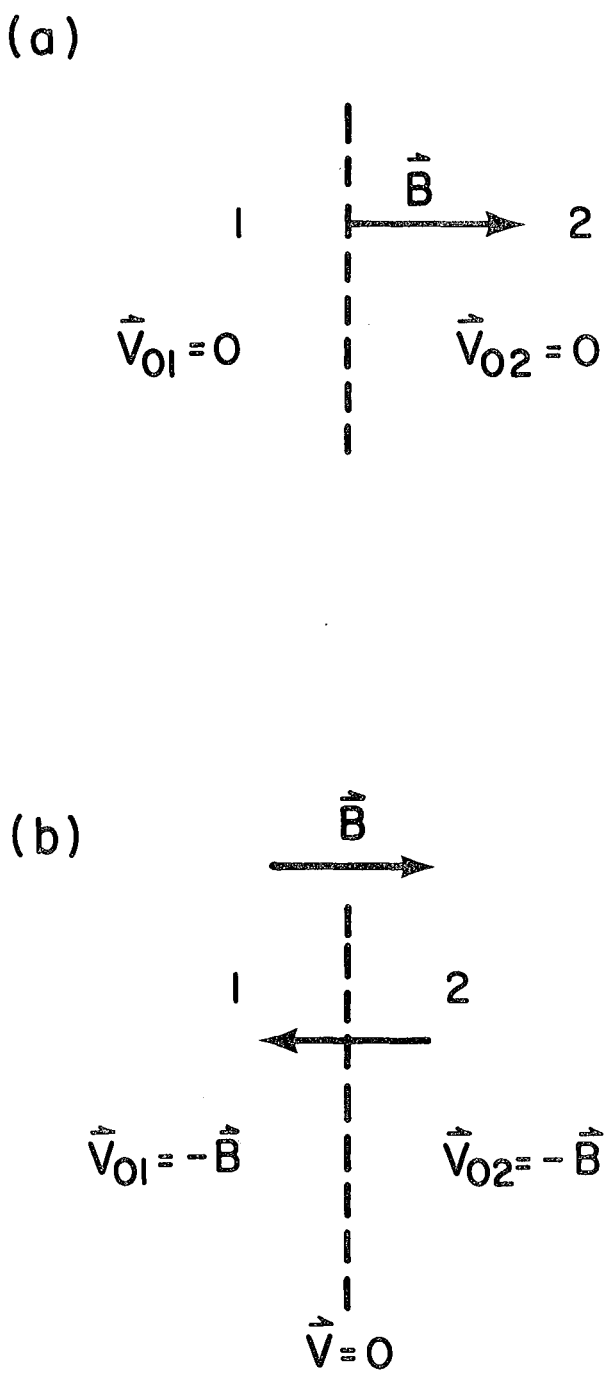

XBL 7812-13413

Fig. 7

XBL 7812-13417

Fig. 8

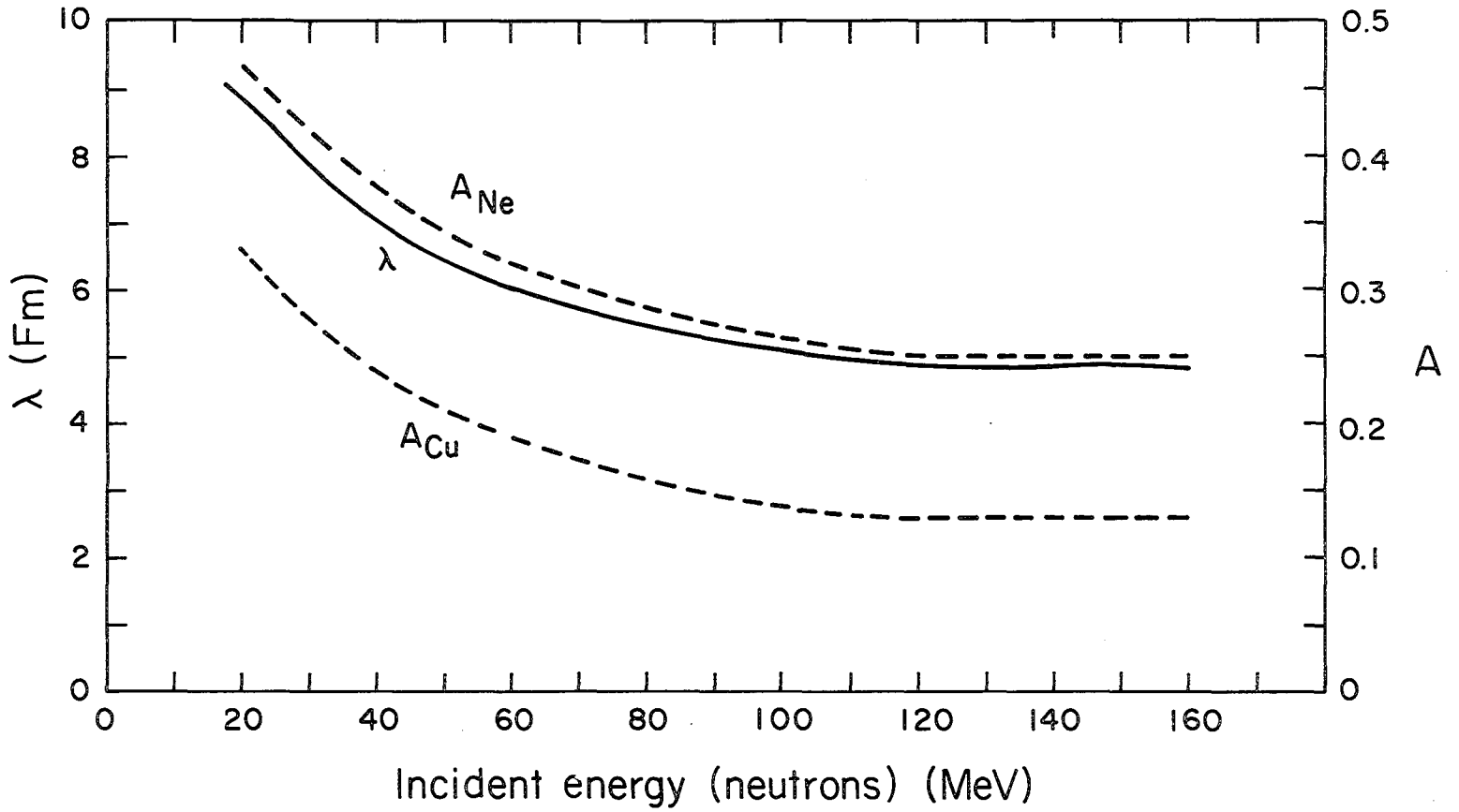

XBL 7811-12533A

Fig. 9

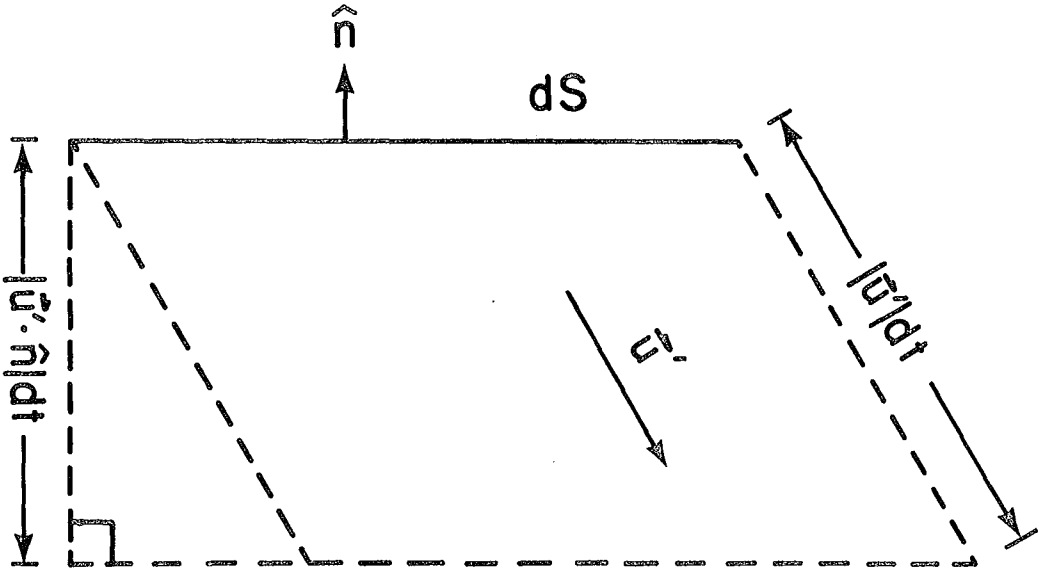

XBL 7812-13414

Fig. 10

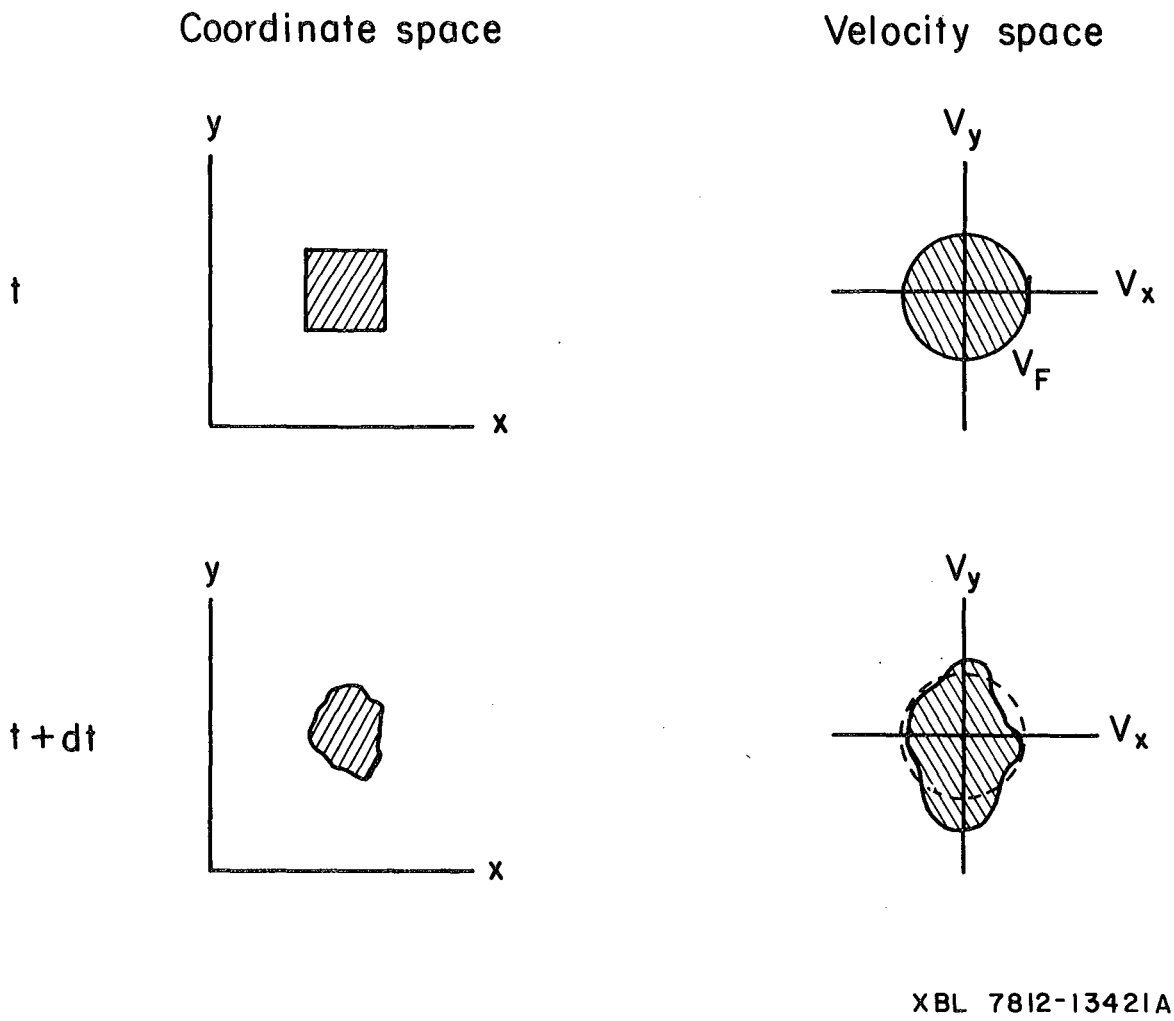
Coordinate space
Velocity space
t
y
x
V_y
V_x
V_F
t+dt
y
x
V_y
V_x
XBL 7812-13421A

Fig. 11

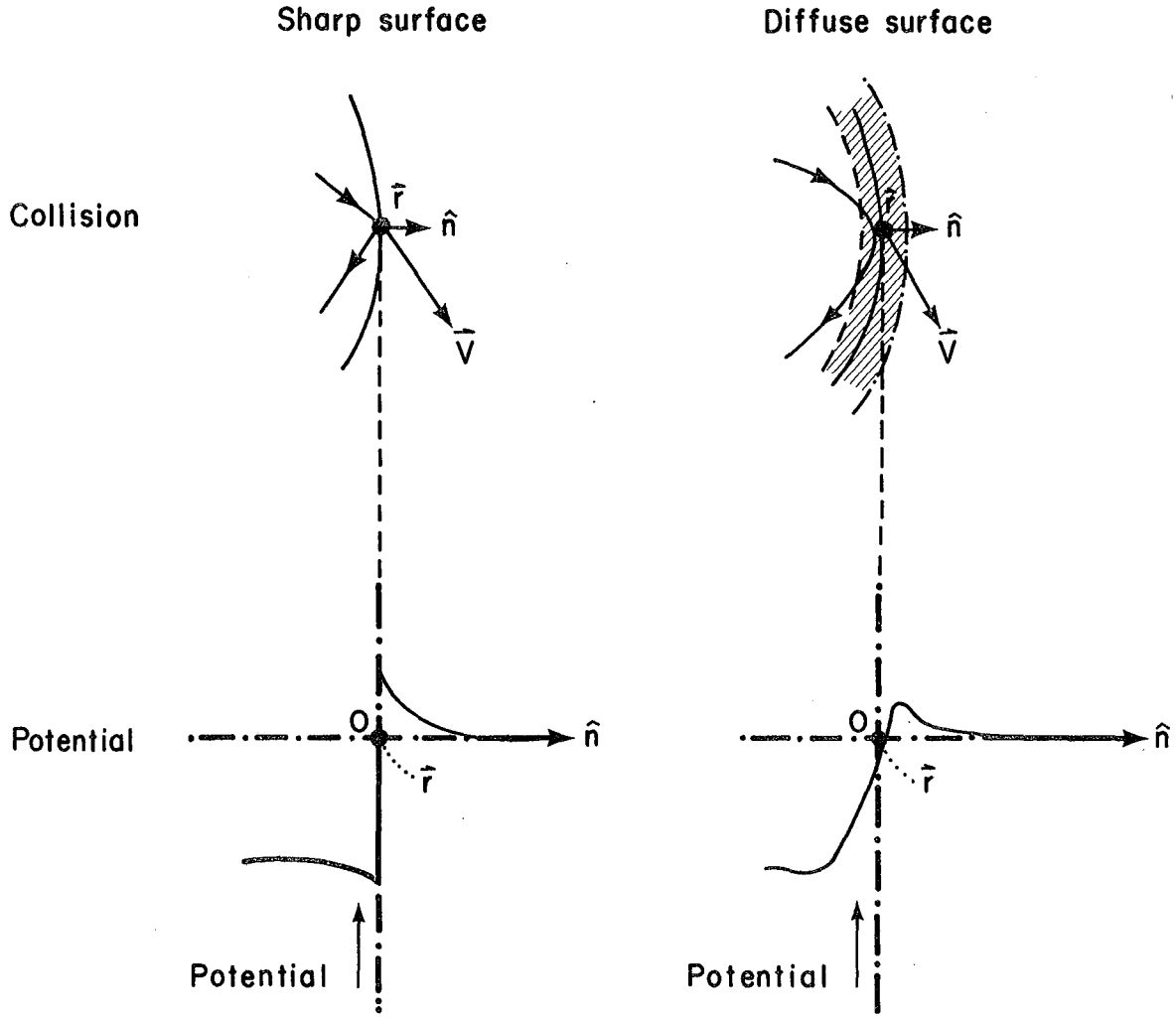

XBL 7812-13412

Fig. 12

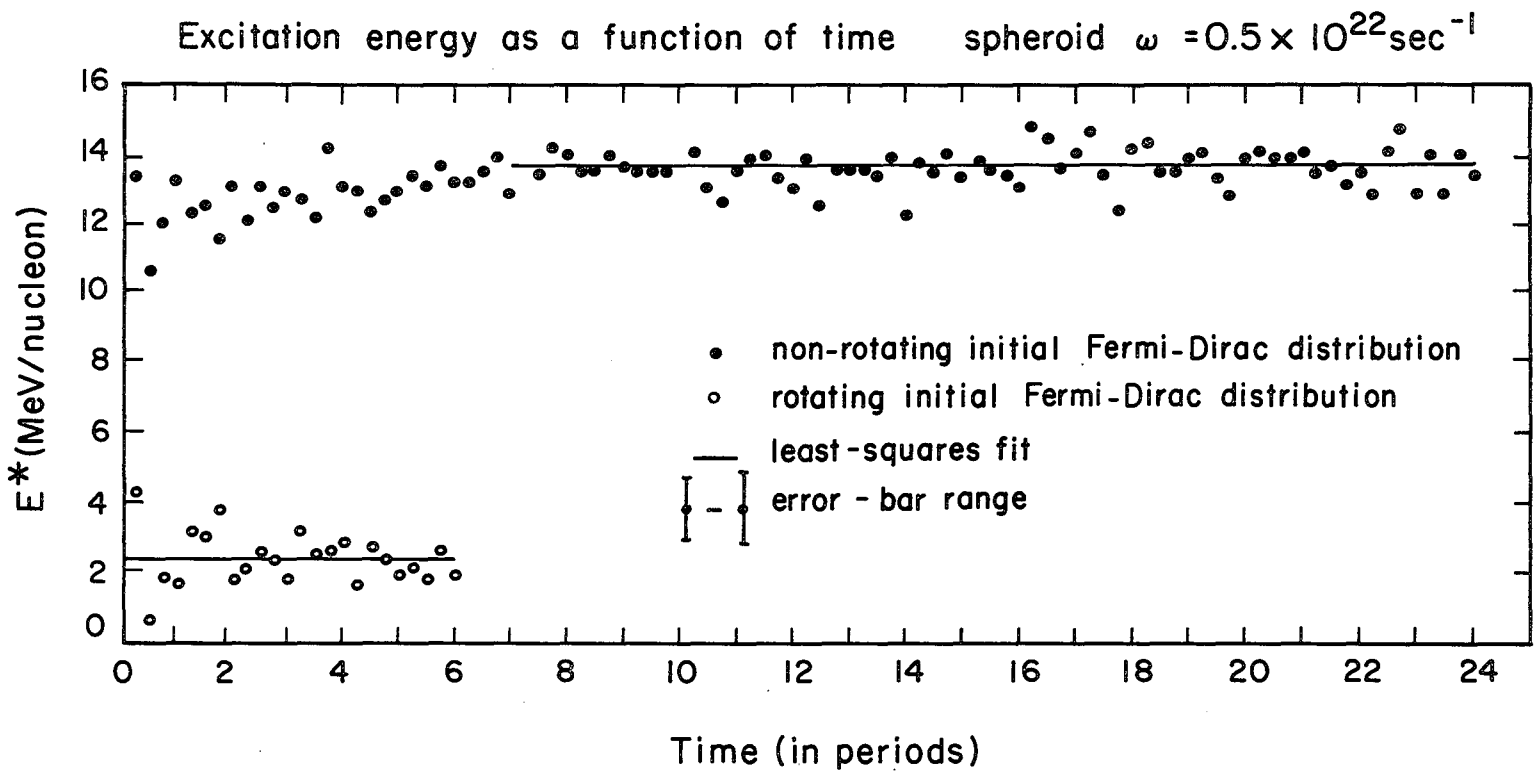

Fig. 13

XBL 7812-13416

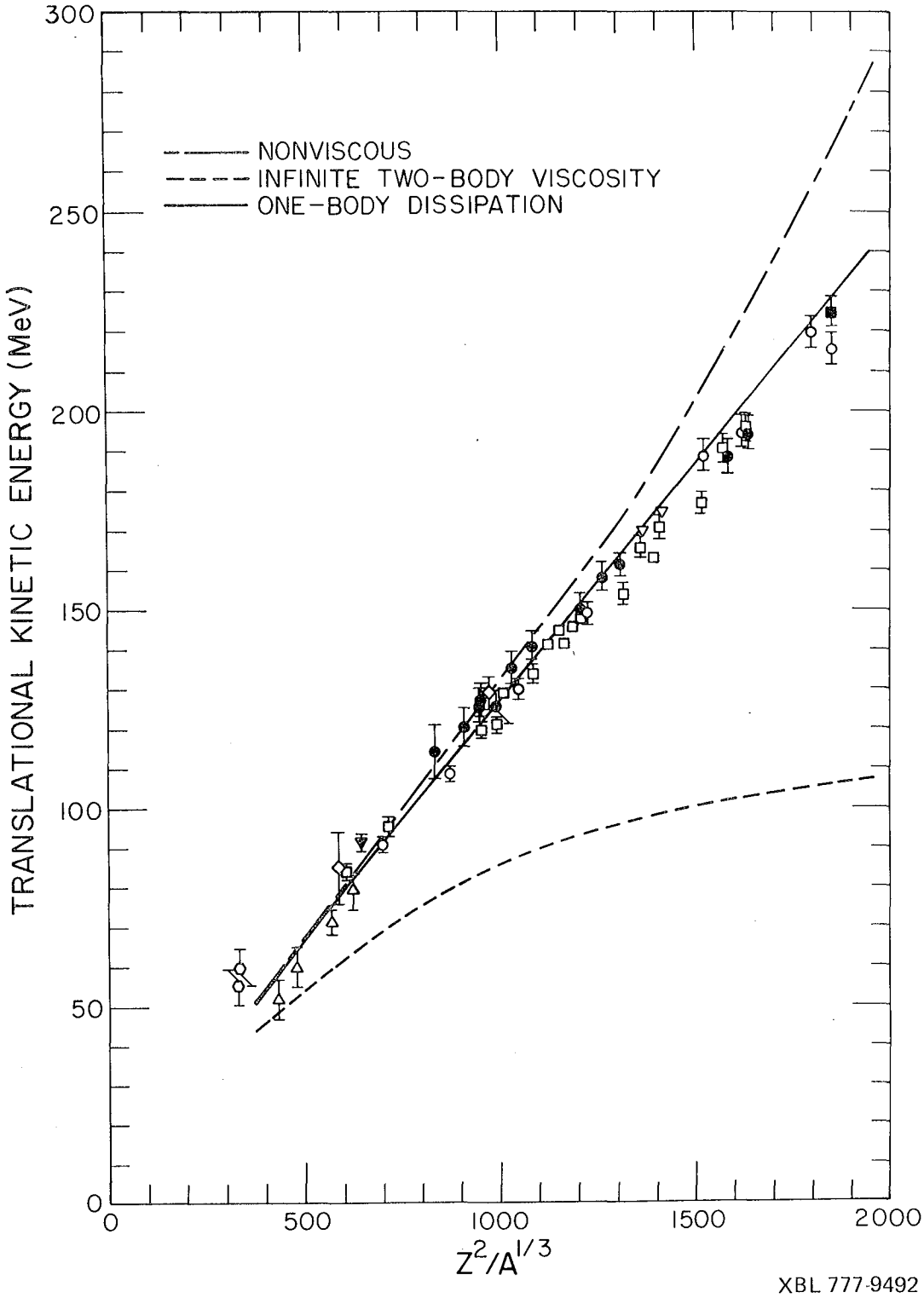
NONVISCOUS
INFINITE TWO-BODY VISCOSITY
ONE-BODY DISSIPATION
TRANSLATIONAL KINETIC ENERGY (MeV)
300
250
200
150
100
50
0
0
500
1000
1500
2000
$Z^2/A^{1/3}$
XBL 777-9492

Fig. 14

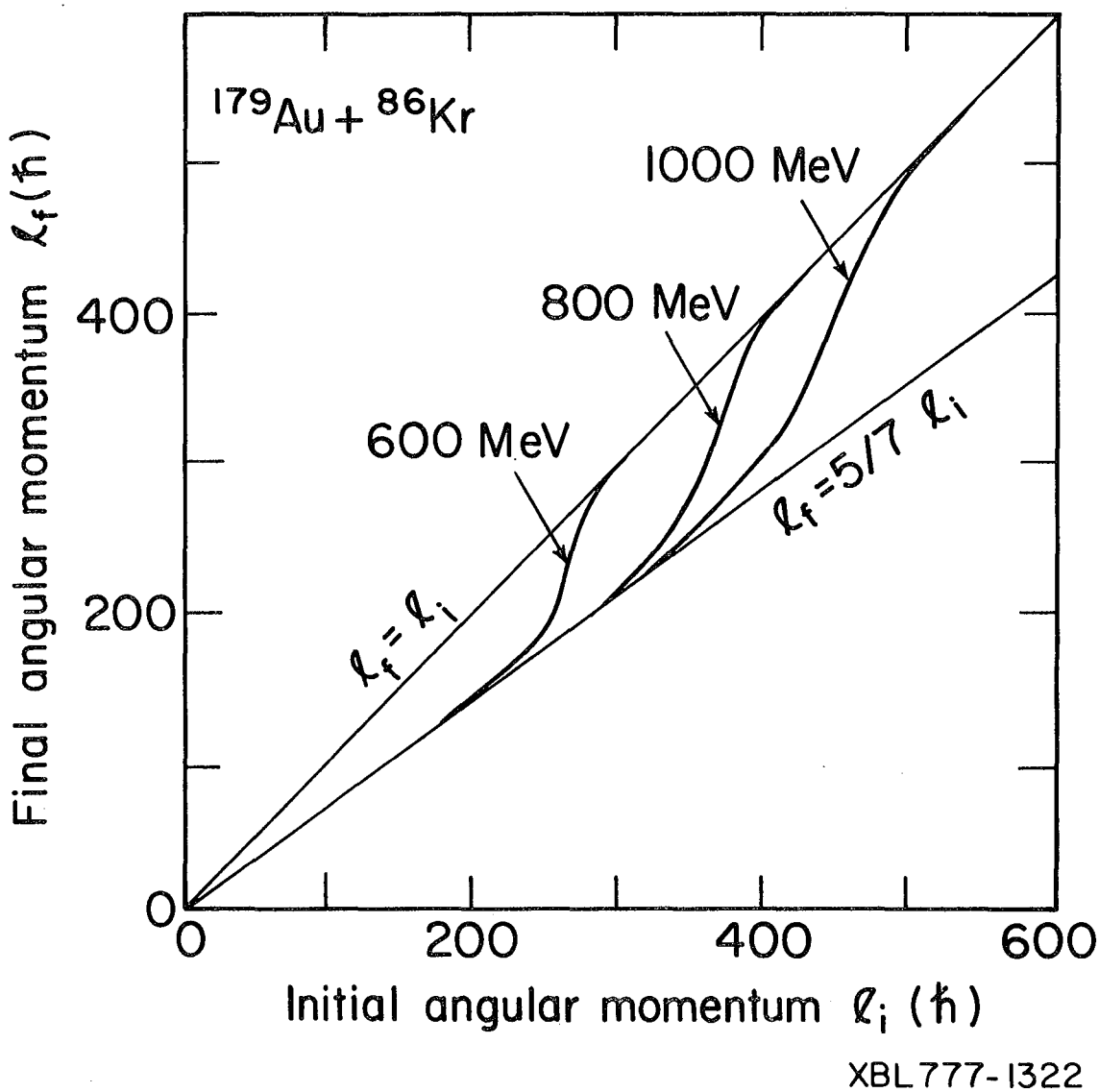
$^{179}Au + ^{86}Kr$
1000 MeV
800 MeV
600 MeV
$\ell_f = \ell_i$
$\ell_f = 5/7\ \ell_i$
Final angular momentum $\ell_f (\hbar)$
Initial angular momentum $\ell_i (\hbar)$
0
200
400
600
XBL 777-1322

Fig. 15

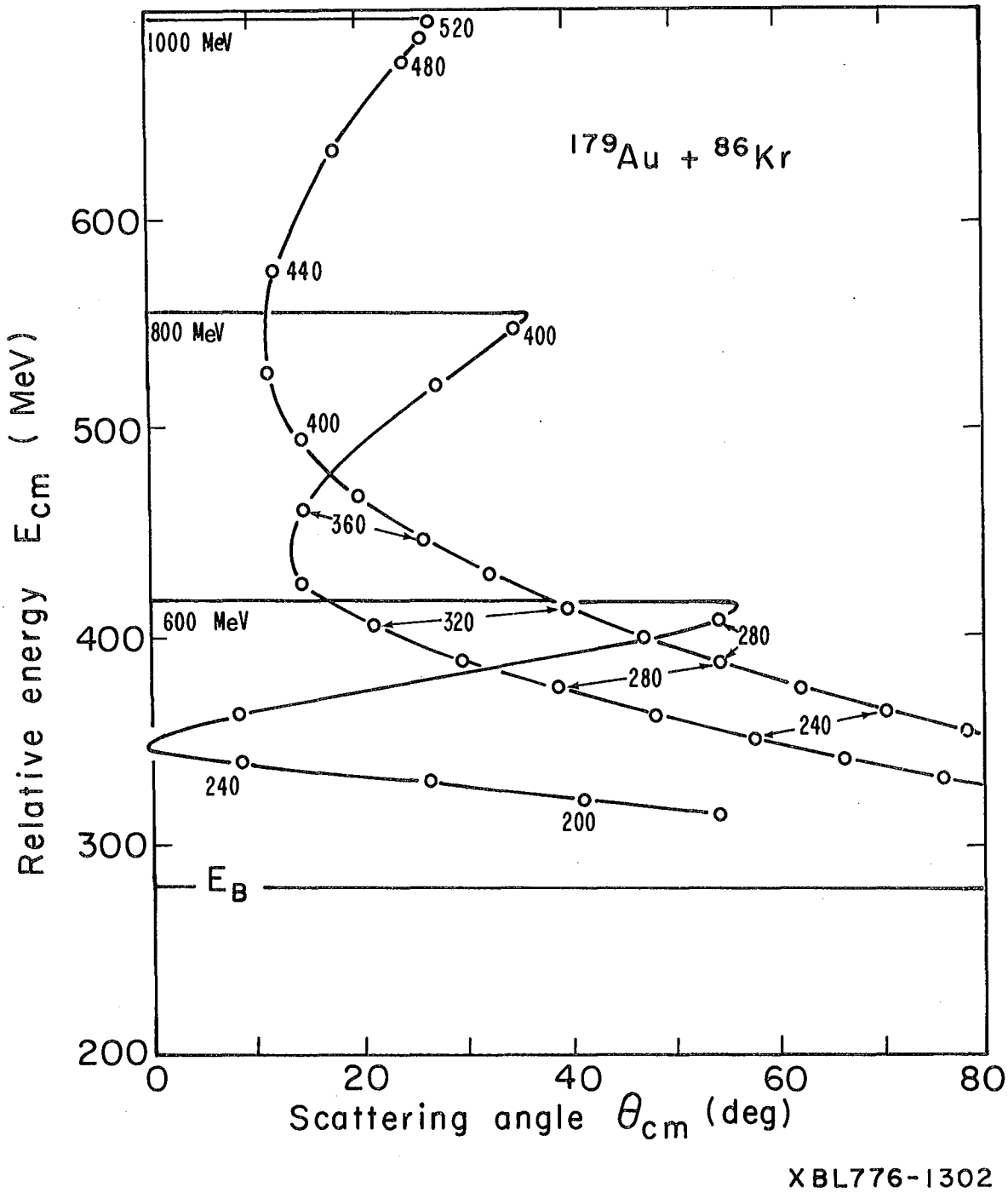

XBL776-1302

Fig. 16

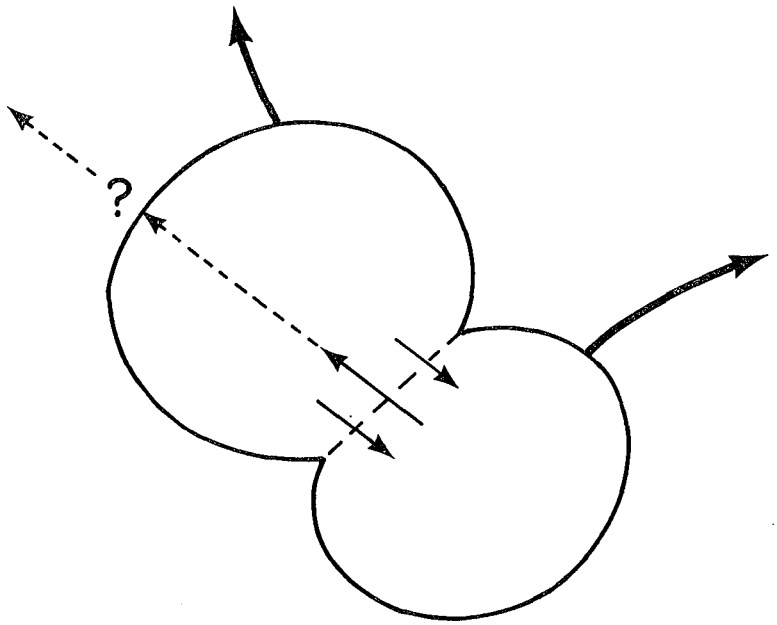

XBL 7811-12540

Fig. 17

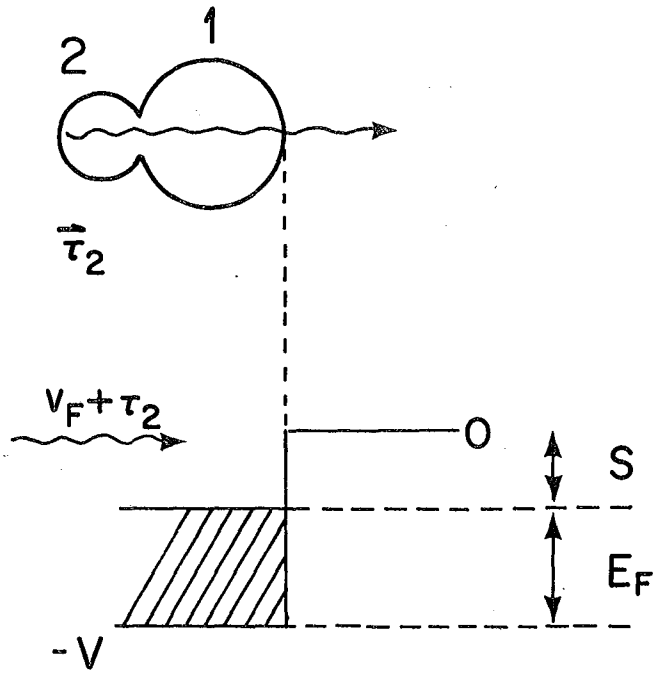

XBL 7811-12538

Fig. 18

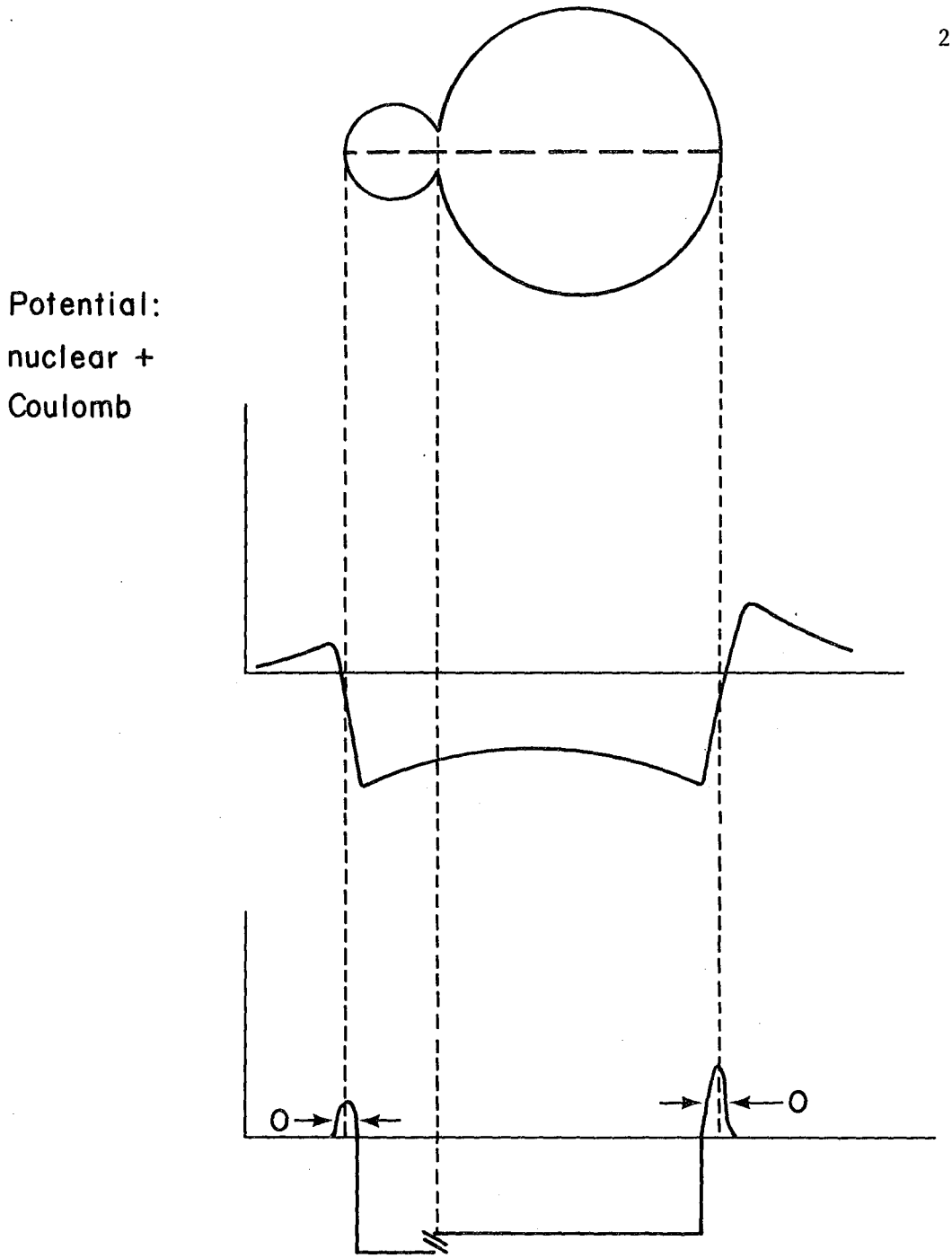

Fig. 19

XBL 7811-12537

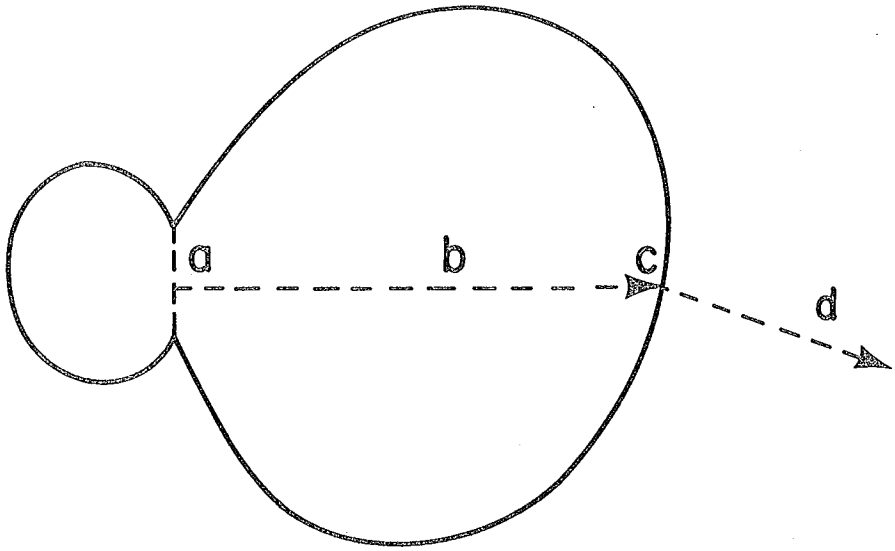

XBL 7811-12539A

Fig. 20

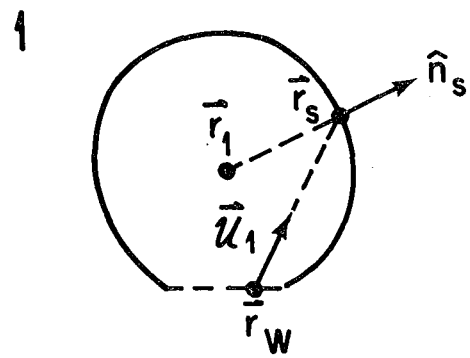

XBL 7811-12536

Fig. 21

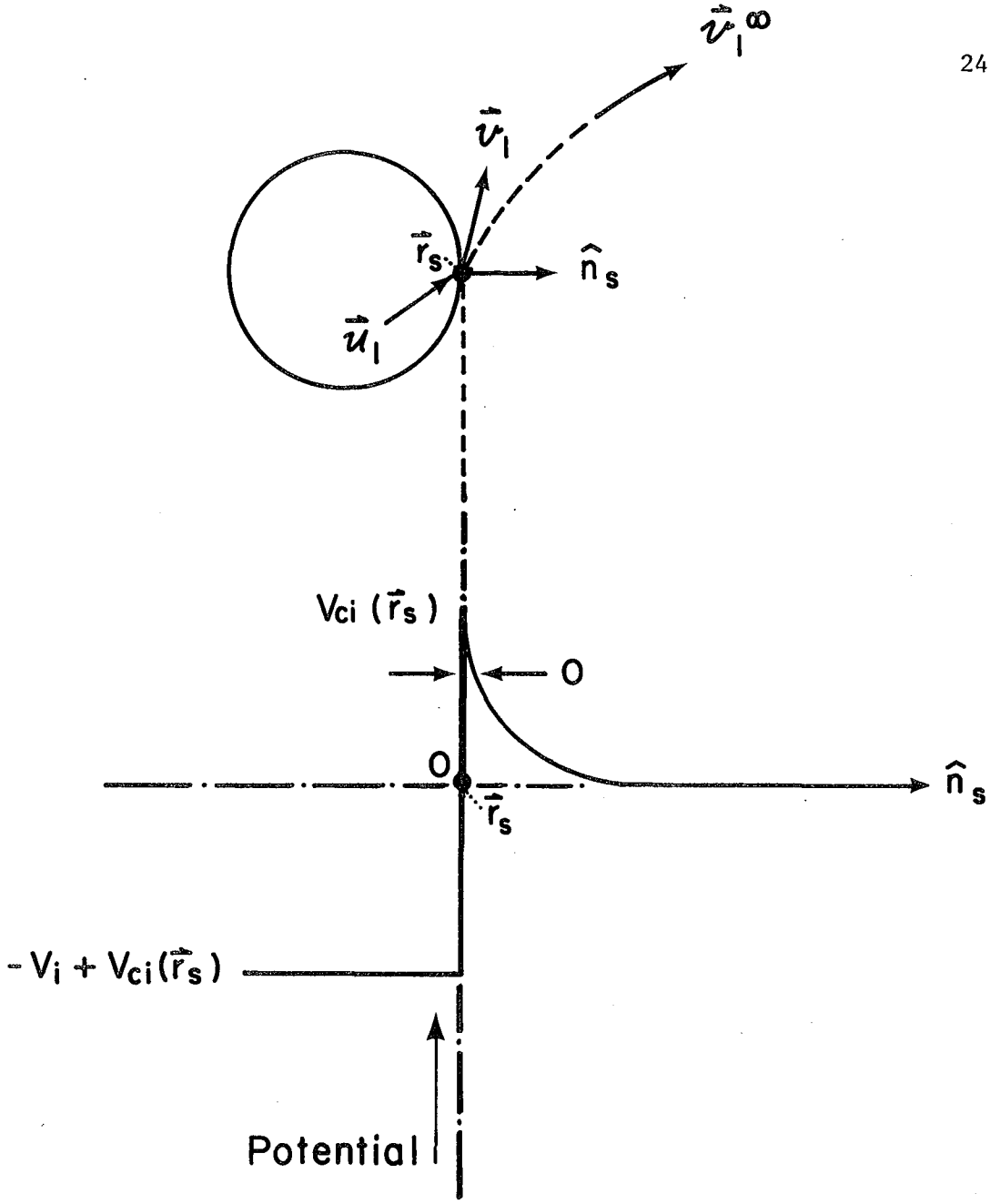

Fig. 22

XBL 7811-12535

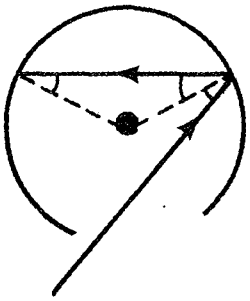

XBL 7811-12534

Fig. 23

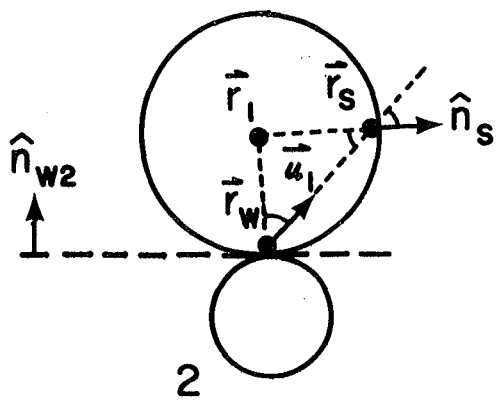

XBL 7811-12532

Fig. 24

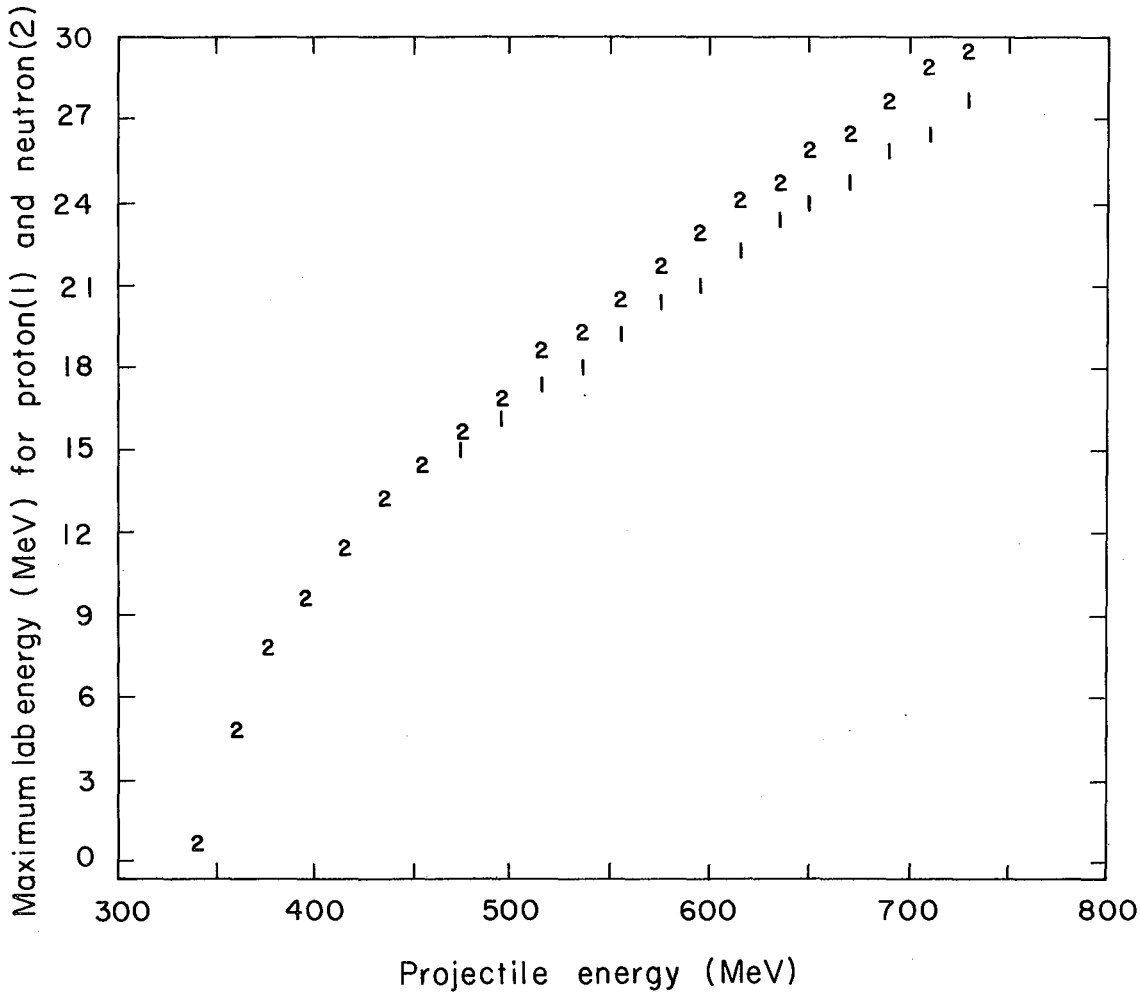

XBL 7811-12541

Fig. 25

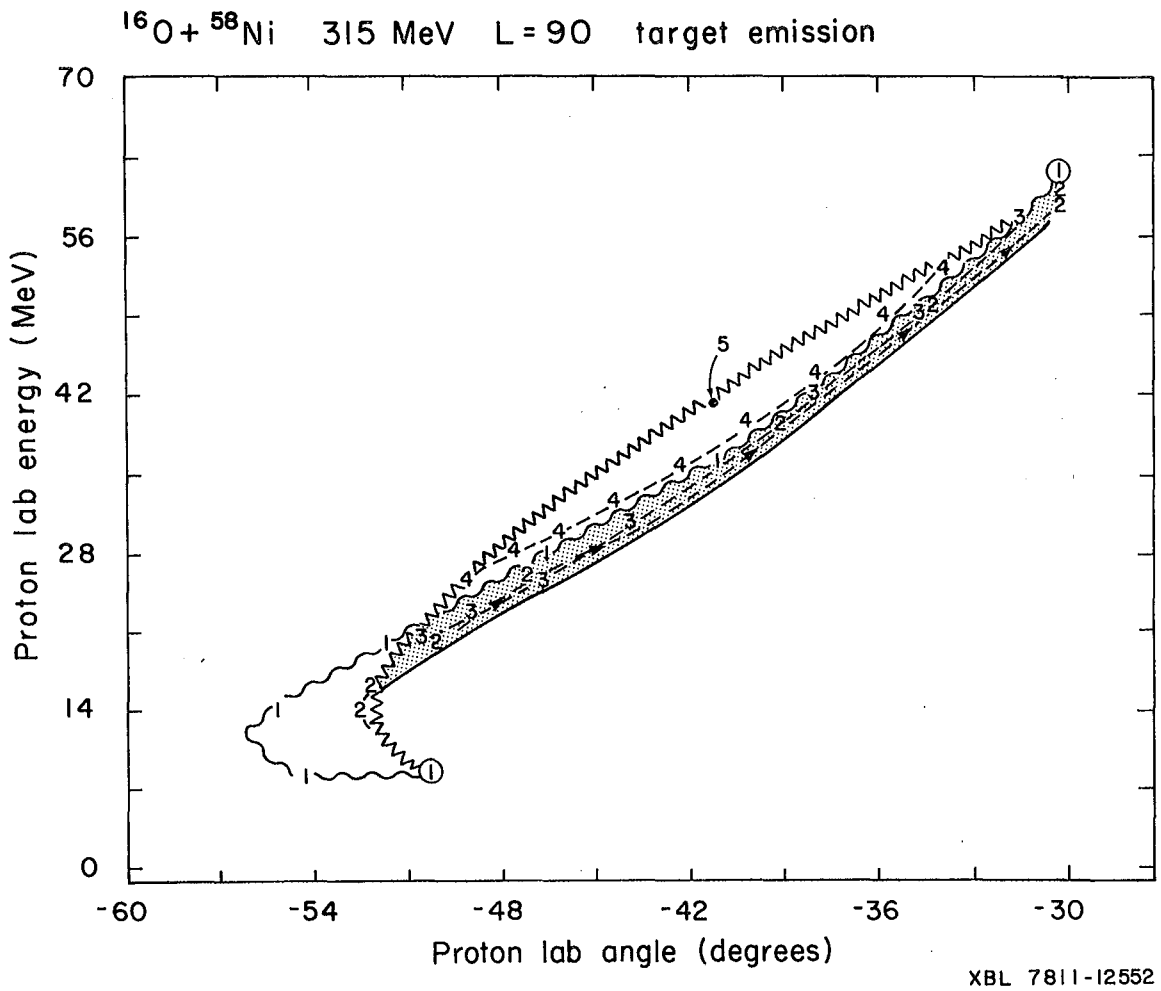
$^{16}O + ^{58}Ni$ 315 MeV L = 90 target emission
Proton lab energy (MeV)
Proton lab angle (degrees)
70
56
42
28
14
0
-60
-54
-48
-42
-36
-30
XBL 7811-12552

Fig. 26(a)

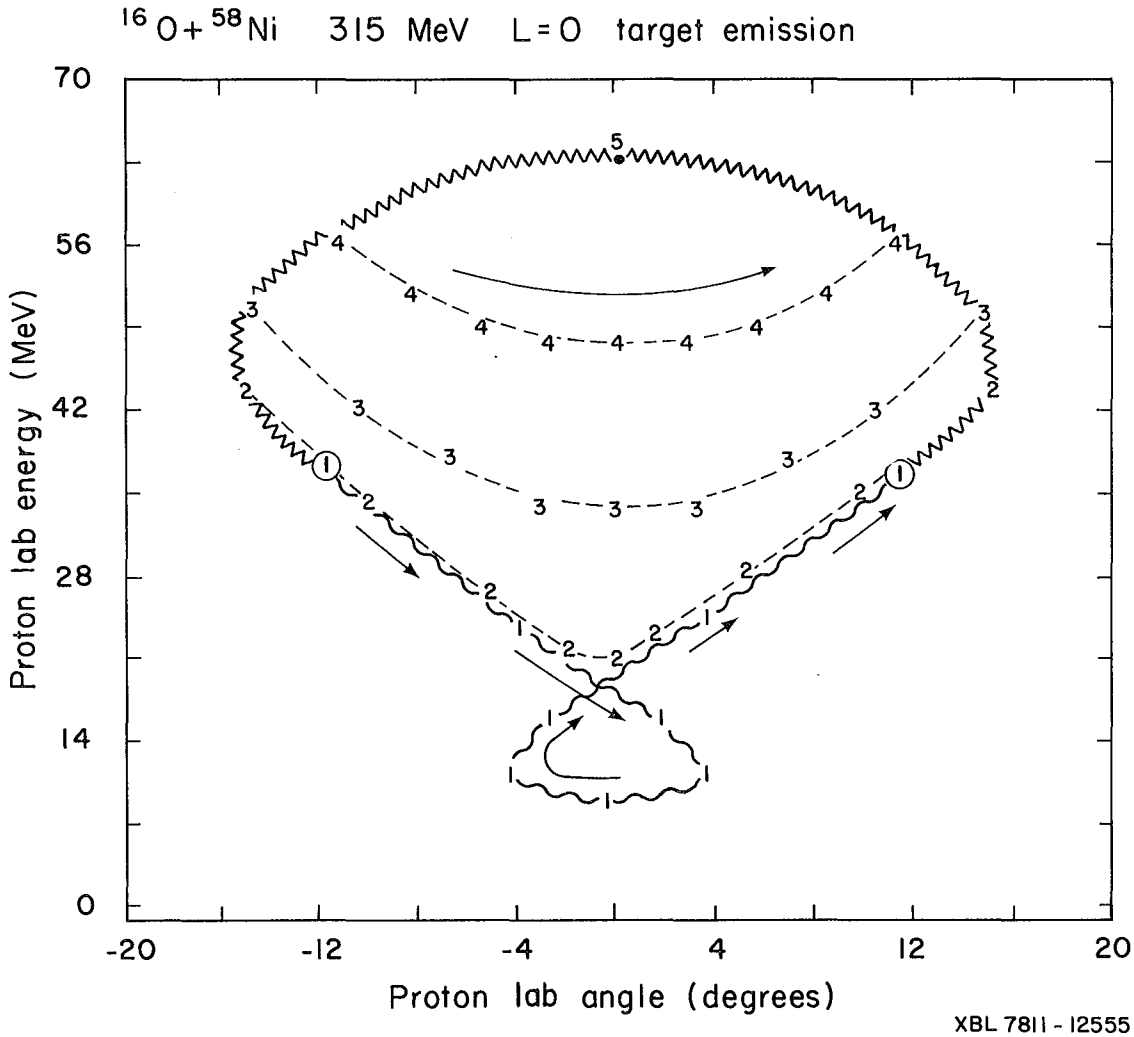
$^{16}O + ^{58}Ni$ 315 MeV L=0 target emission
Proton lab energy (MeV)
Proton lab angle (degrees)
70
56
42
28
14
0
-20
-12
-4
4
12
20
XBL 7811 - 12555

Fig. 26(b)

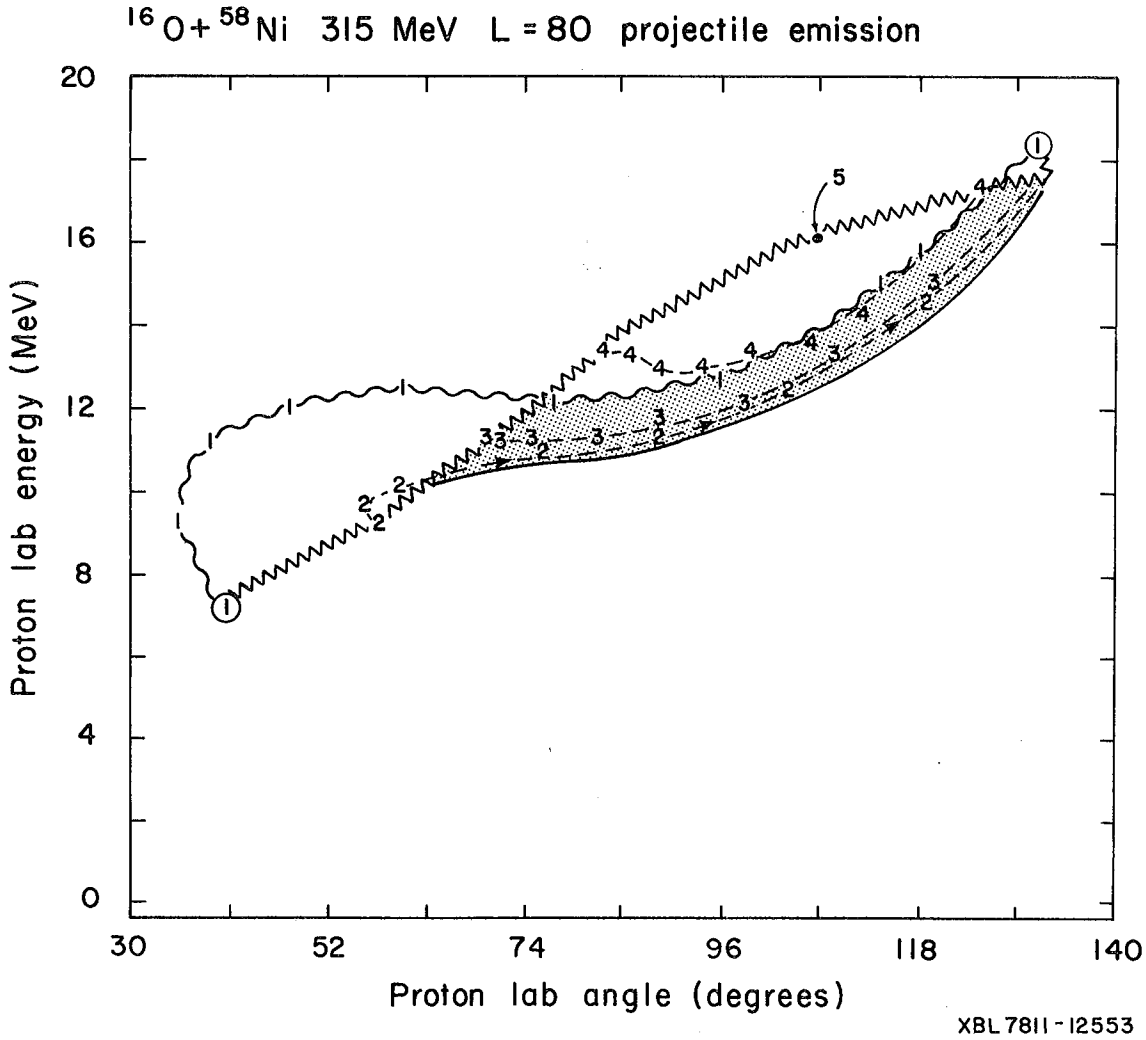
$^{16}O + ^{58}Ni$ 315 MeV L = 80 projectile emission
Proton lab energy (MeV)
Proton lab angle (degrees)
20
16
12
8
4
0
30
52
74
96
118
140
5
XBL 7811-12553

Fig. 26(c)

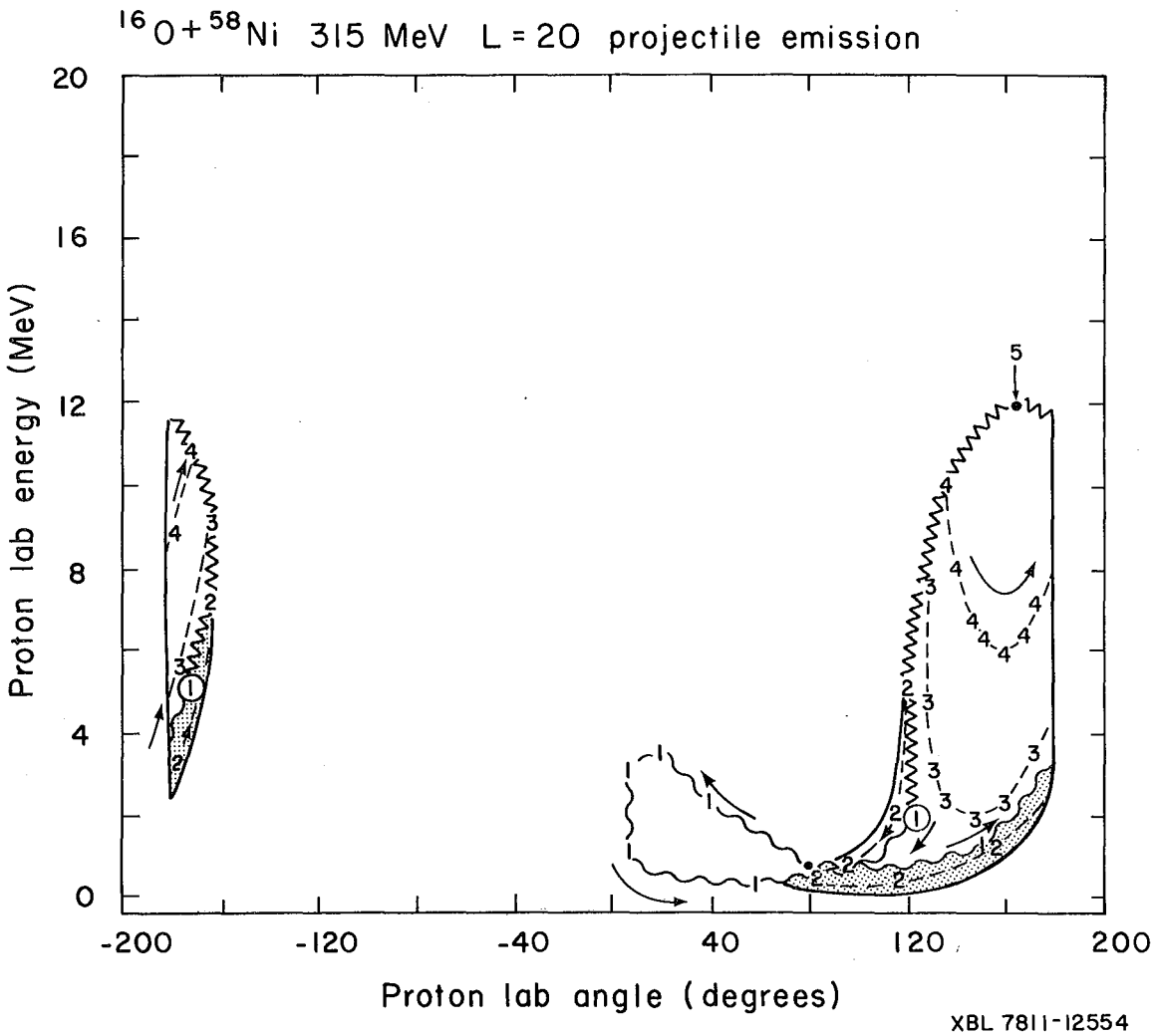
$^{16}O + ^{58}Ni$ 315 MeV L = 20 projectile emission
Proton lab energy (MeV)
Proton lab angle (degrees)
20
16
12
8
4
0
-200
-120
-40
40
120
200
XBL 7811-12554

Fig. 26(d)

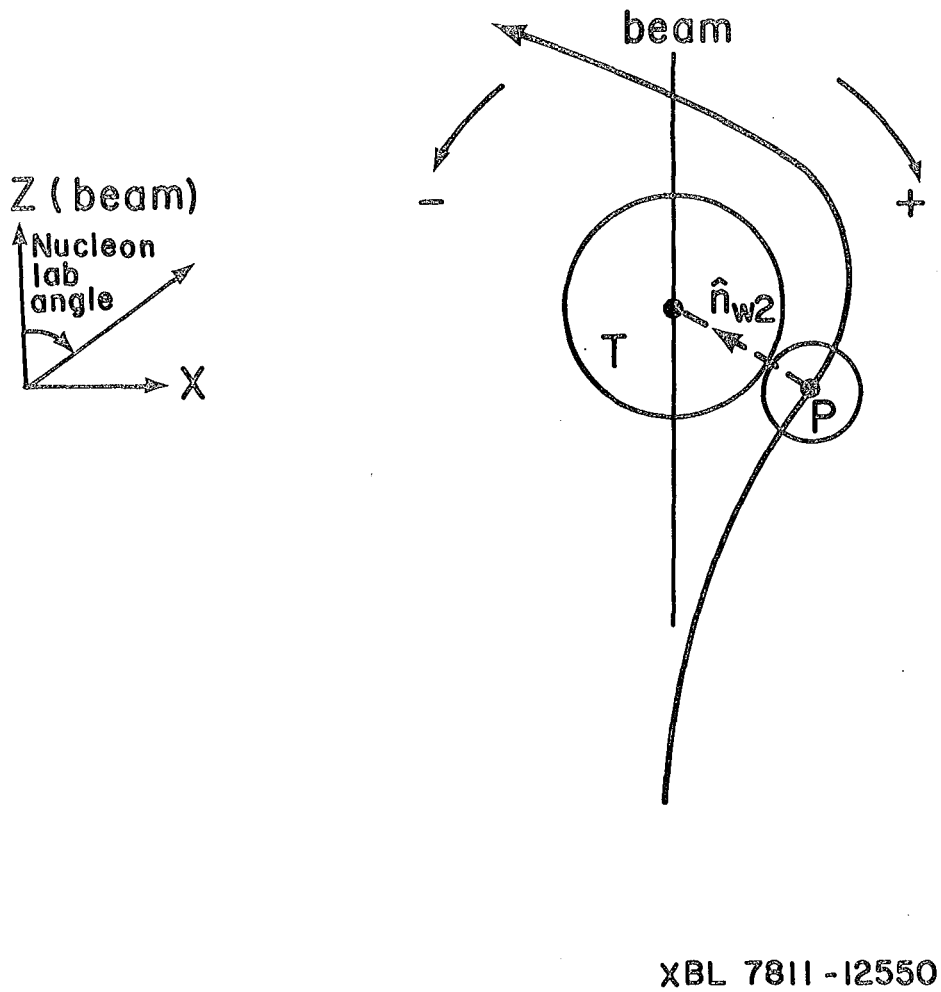

Fig. 27

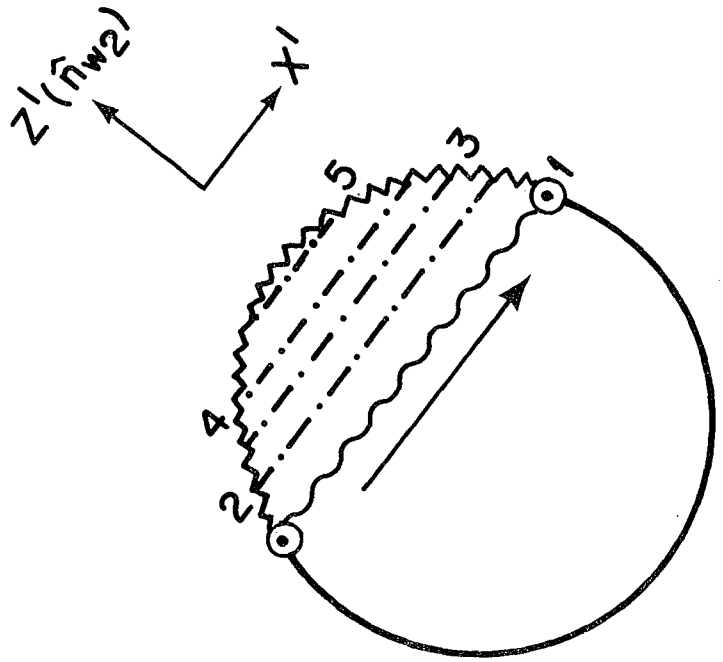

XBL 7811-12551 A

Fig. 28

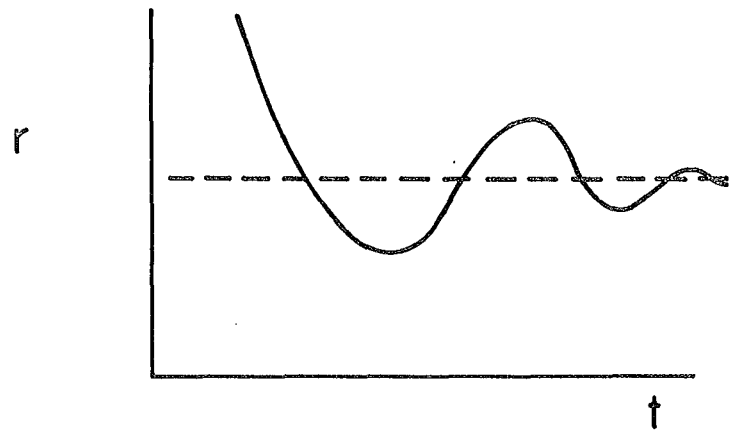

XBL 7811-12531

Fig. 29

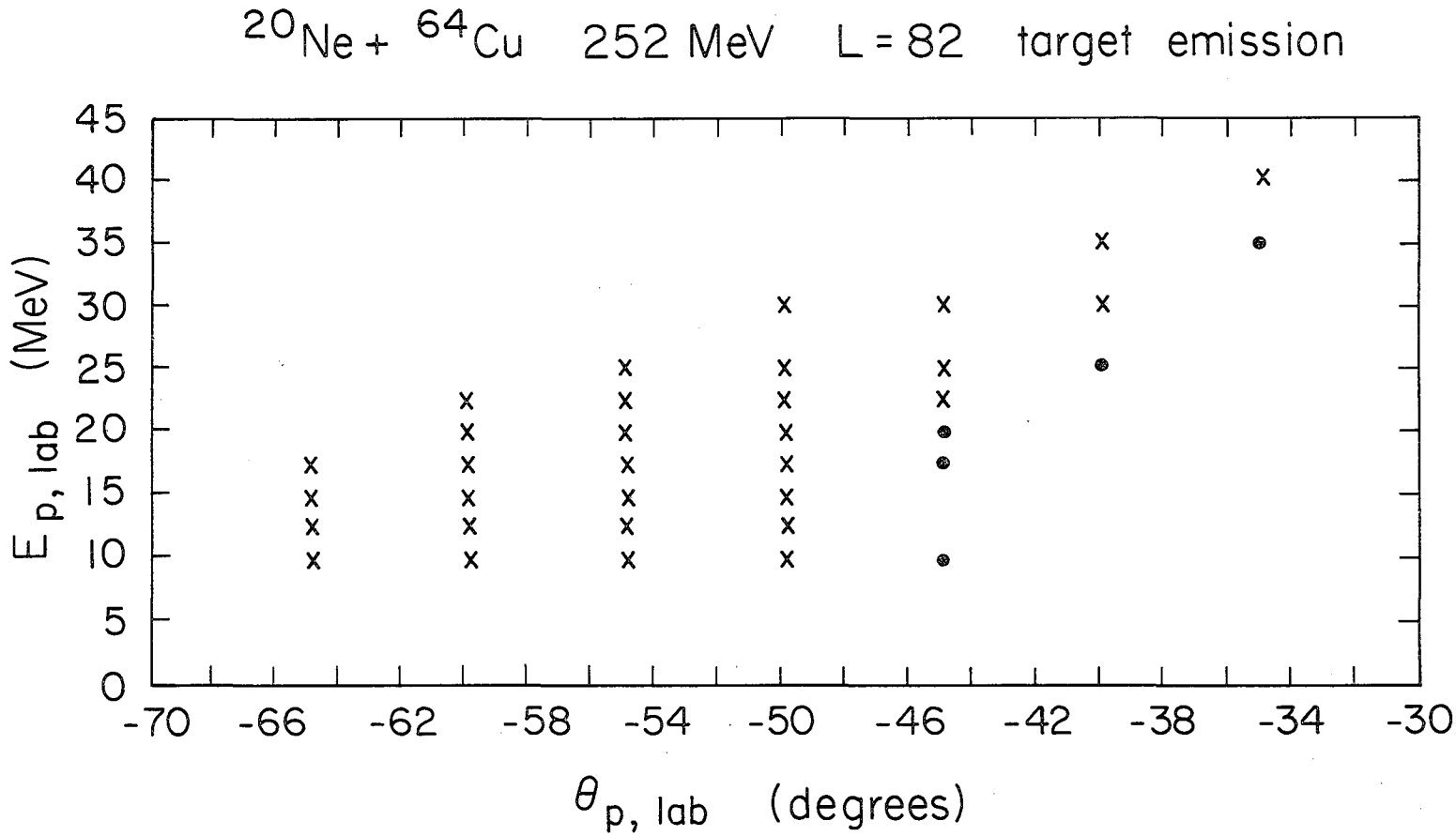

XBL 7811-12557

Fig. 30(a)

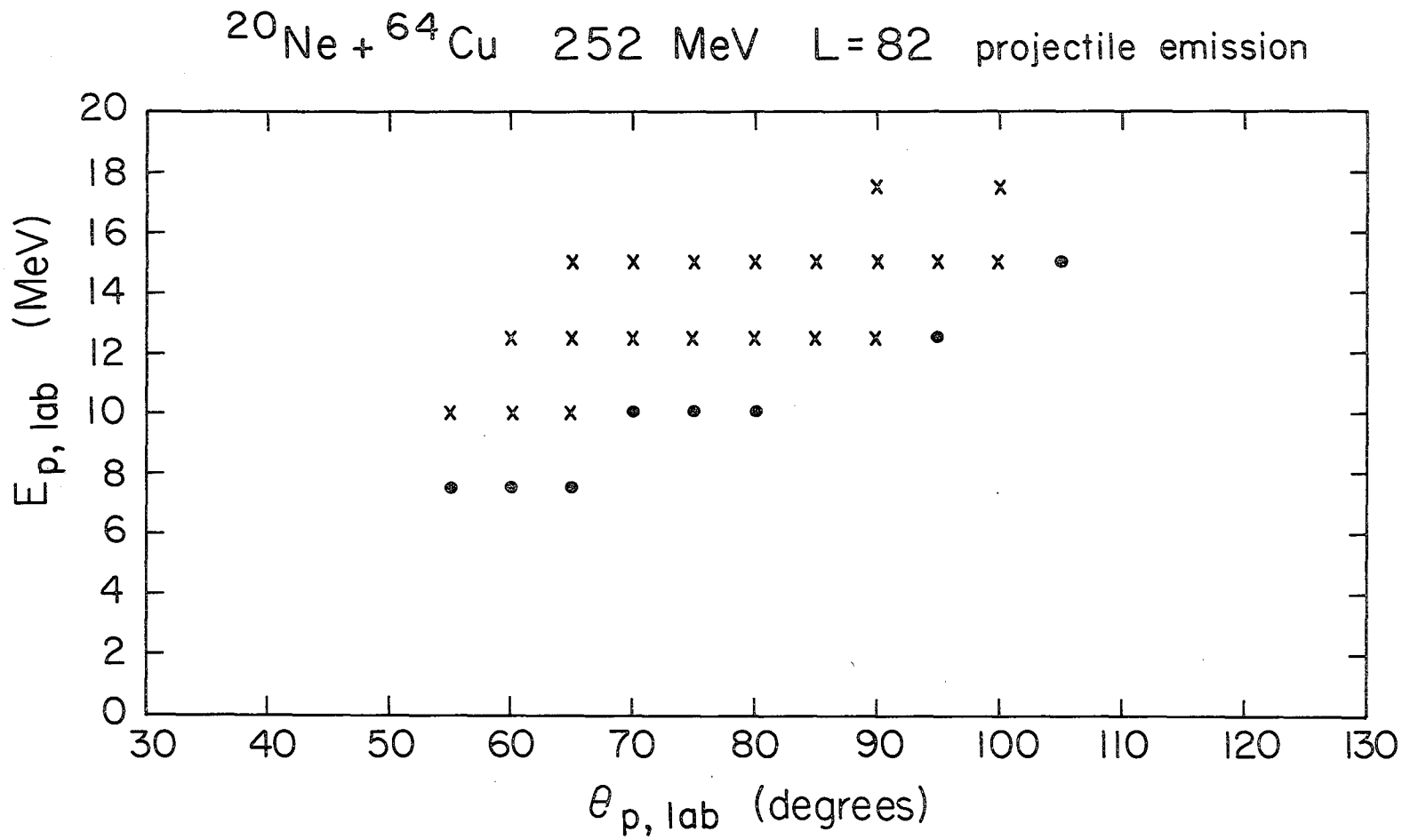

XBL 7811-12556

Fig. 30 (b)

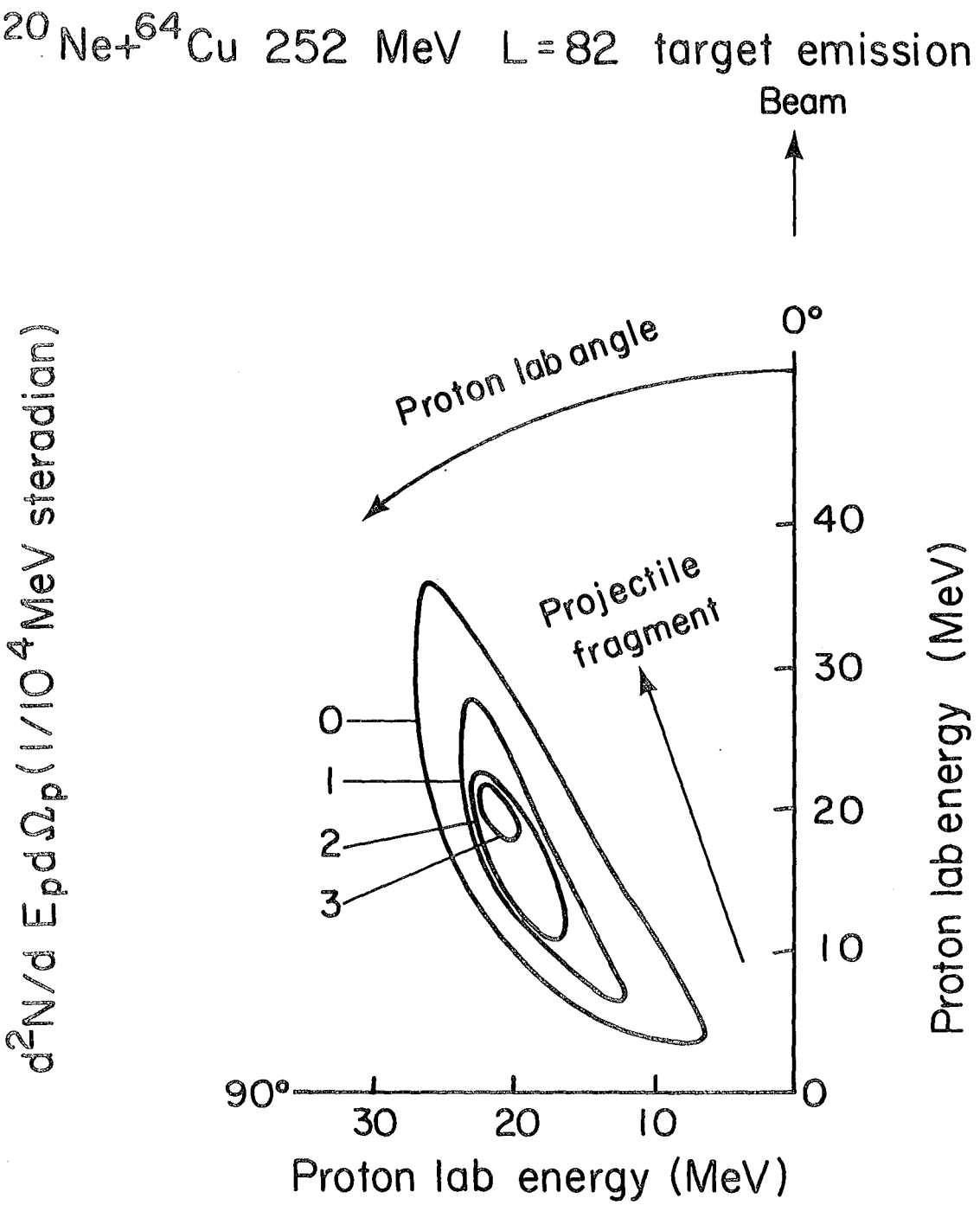

Fig. 31(a)

XBL 7811-12558

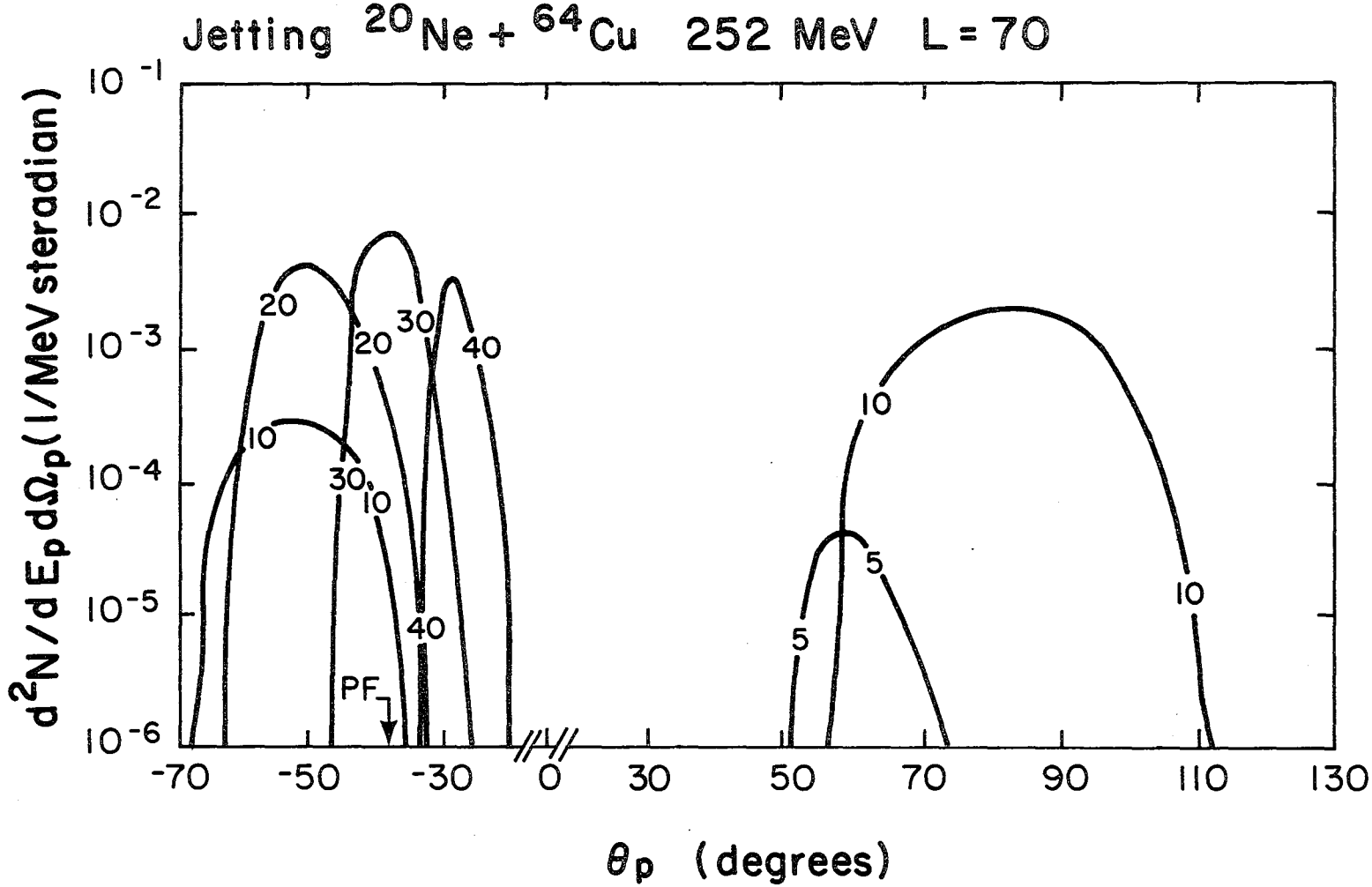

XBL 7811-12562

Fig. 31(b)

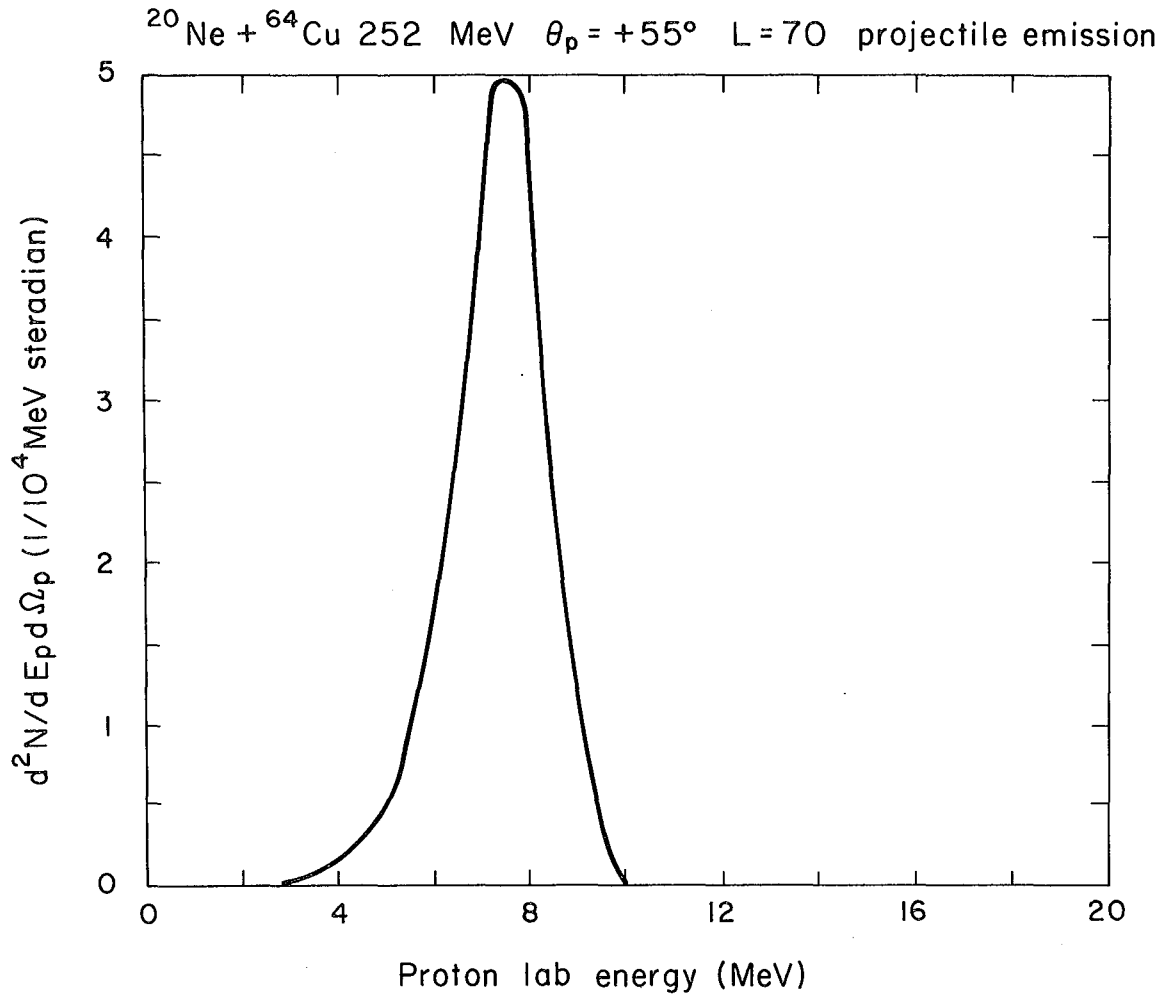

XBL 7811-12544

Fig. 31(e)

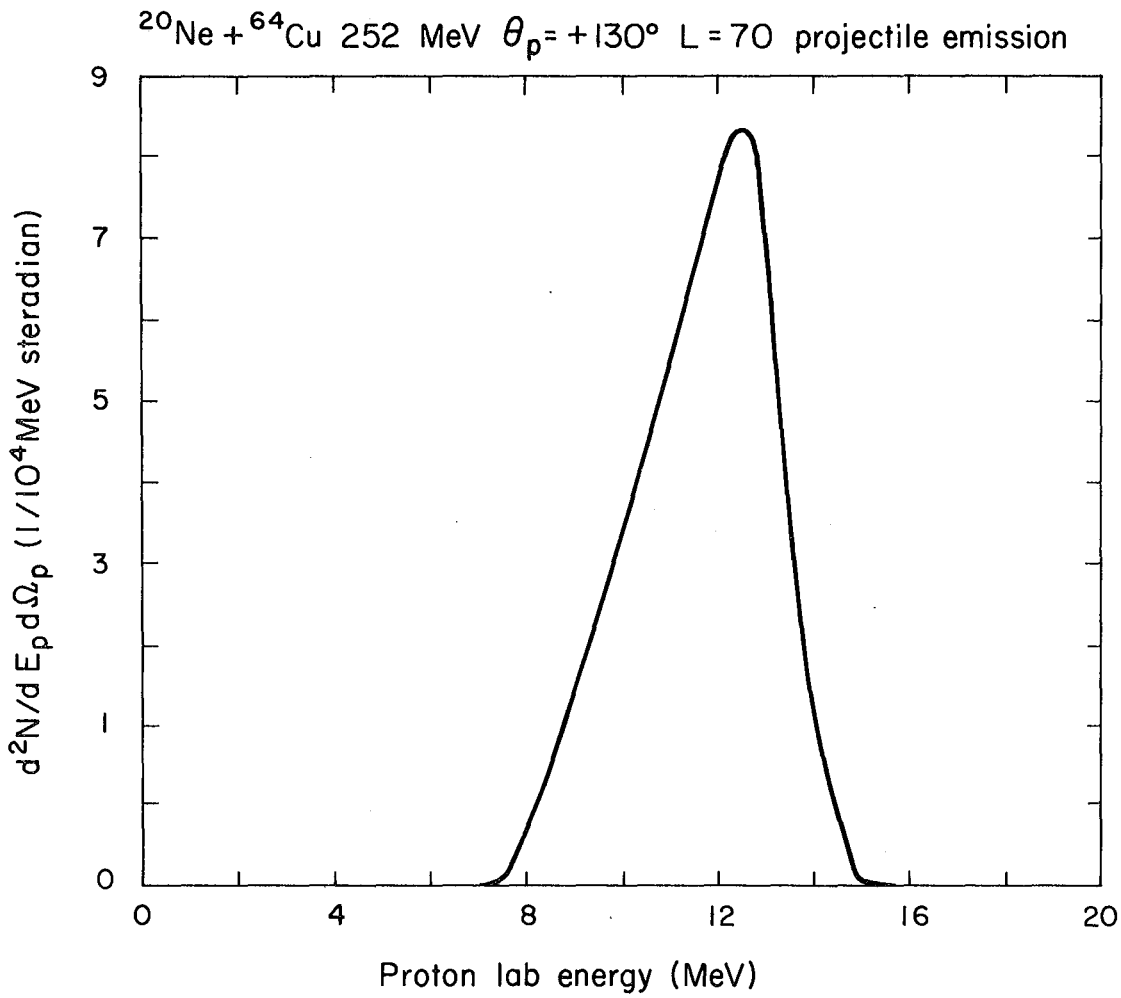

XBL 7811-12545

Fig. 31(f)

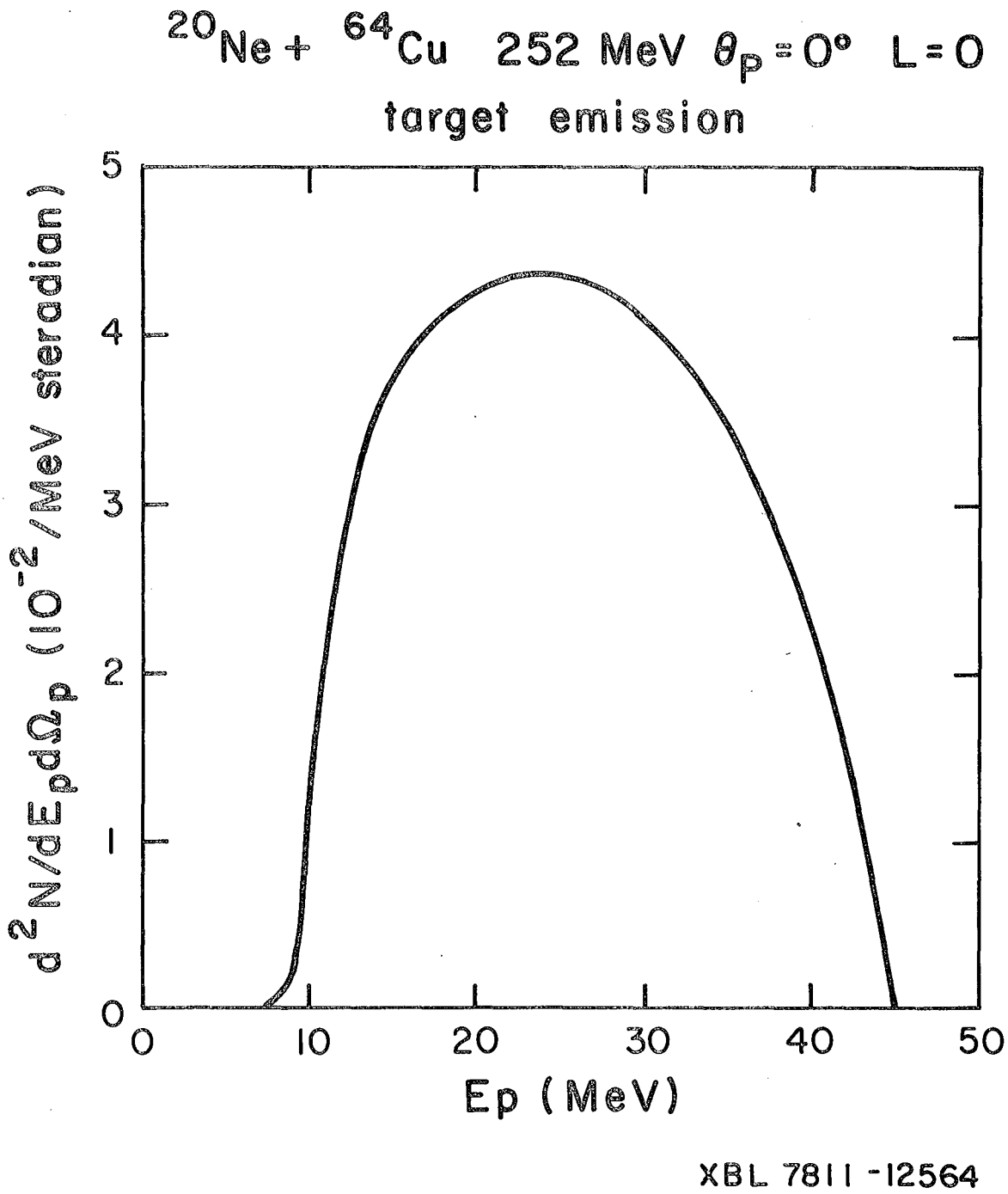
$^{20}Ne + {}^{64}Cu$ 252 MeV $\theta_p = 0°$ L=0
target emission
$d^2N/dE_p d\Omega_p$ (10^{-2}/MeV steradian)
0
1
2
3
4
5
0
10
20
30
40
50
Ep (MeV)
XBL 7811-12564

Fig. 31(g)

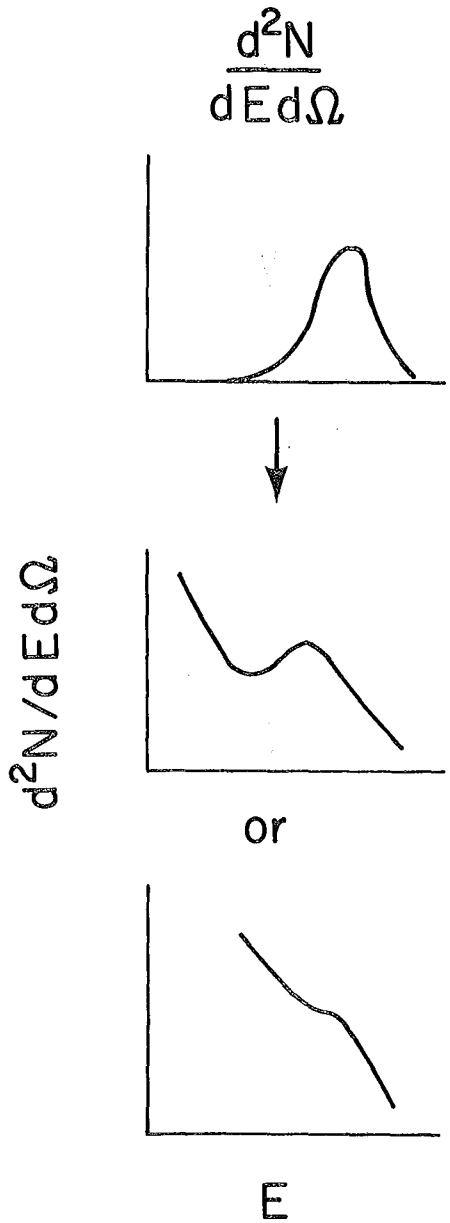

XBL 7811-12548

Fig. 32

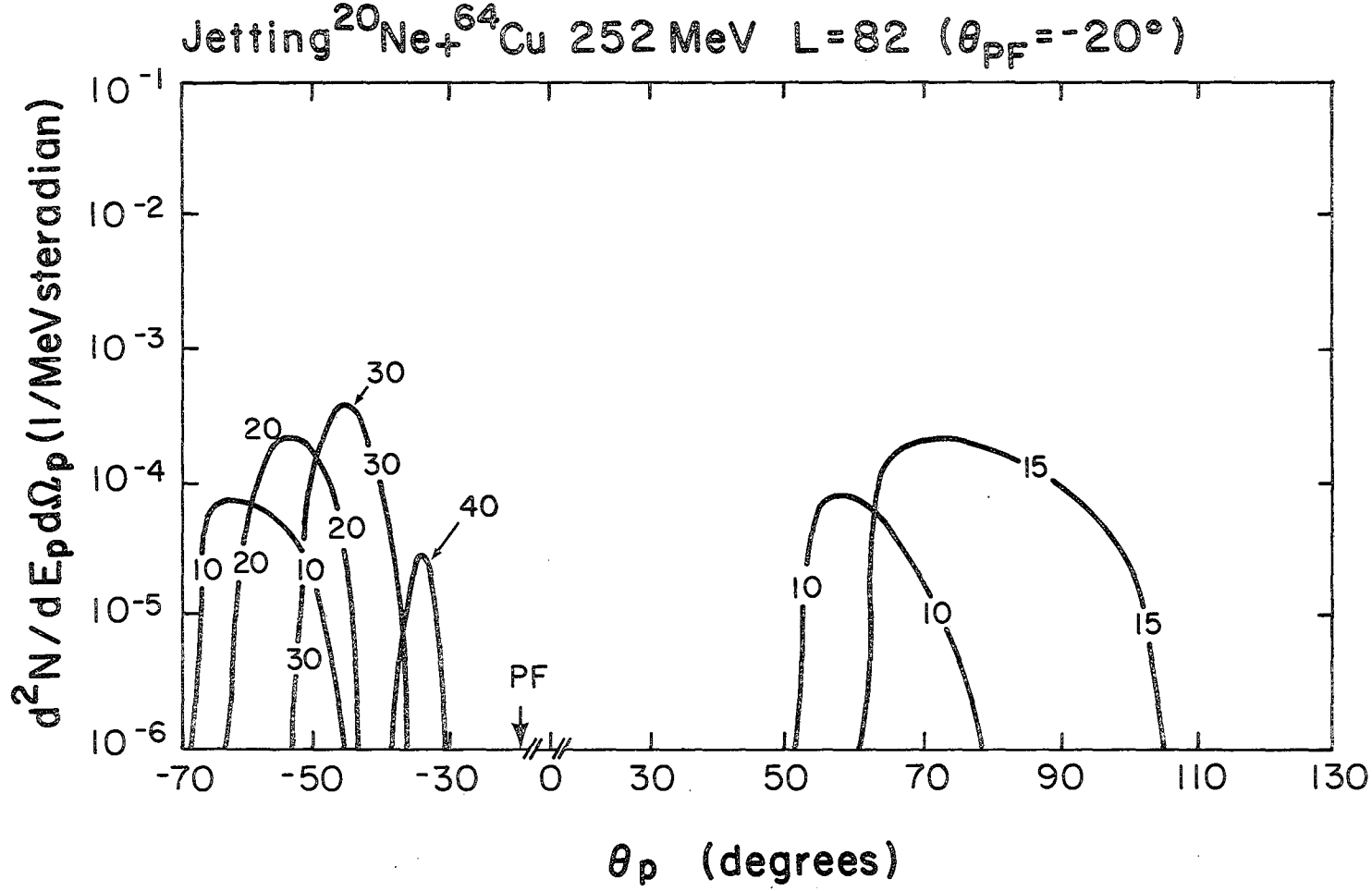

XBL 7811-12559

Fig. 33(a)

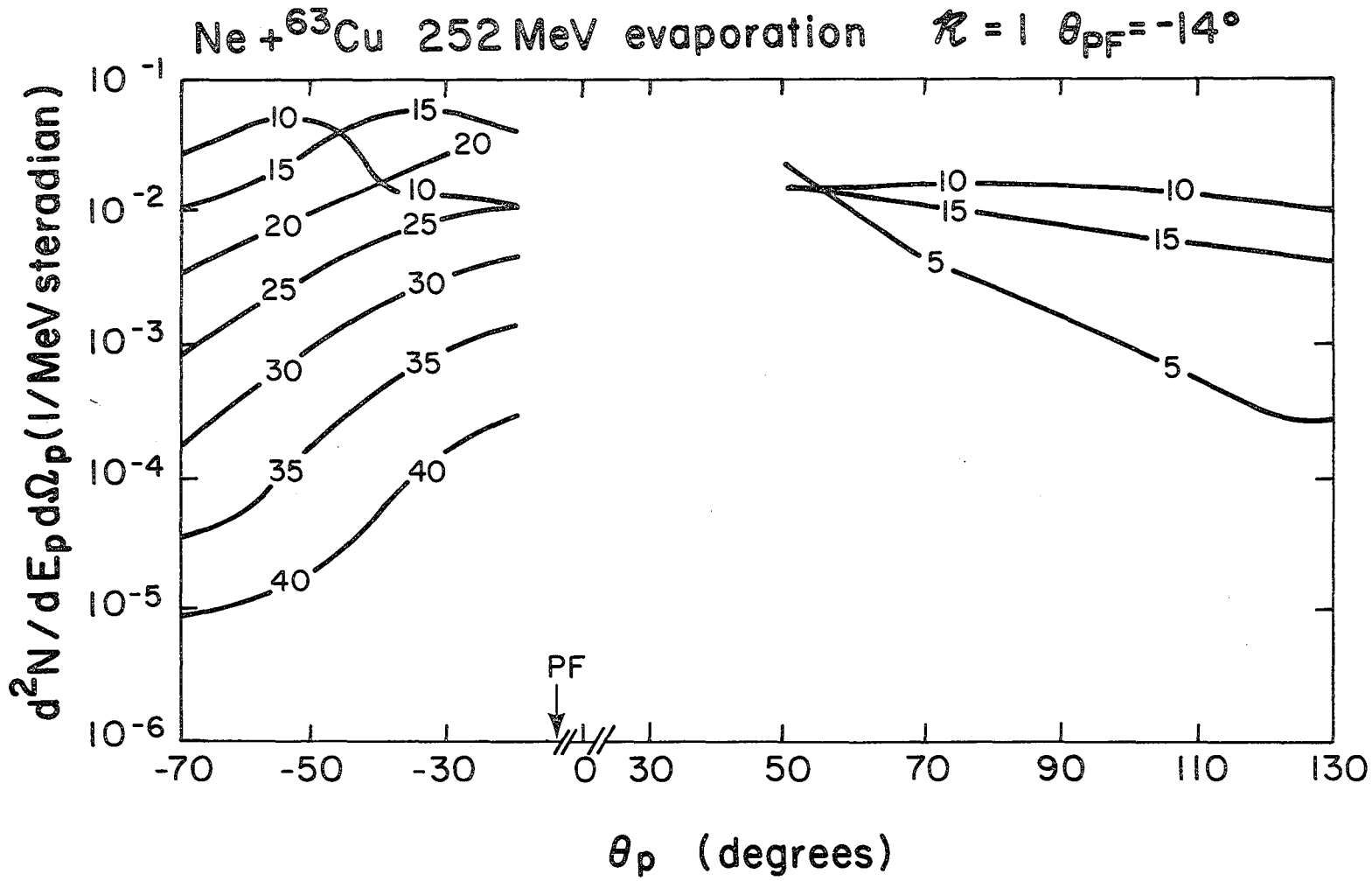

XBL 7811-12563

Fig. 33(b)

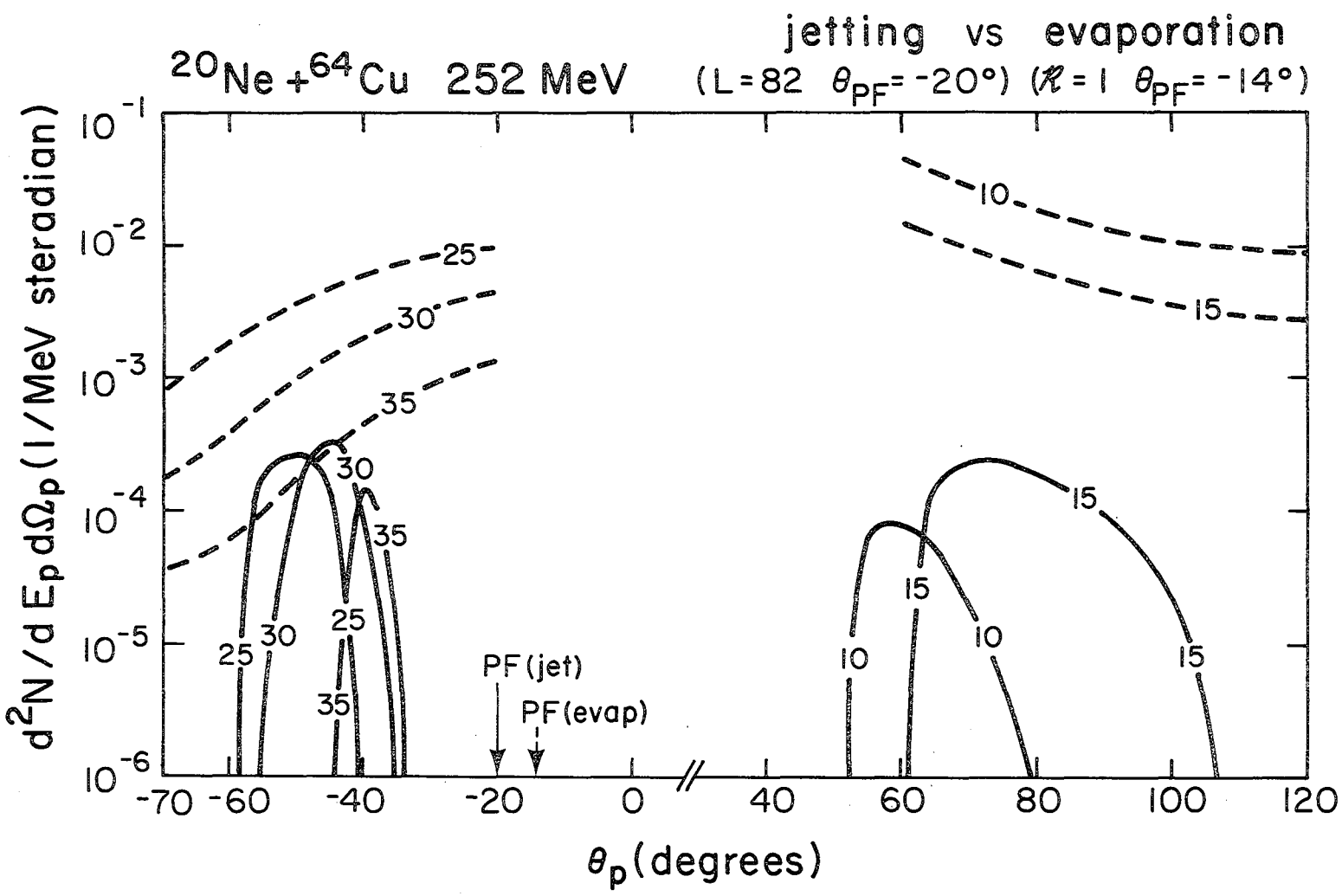

XBL 7811-12565

Fig. 33(c)

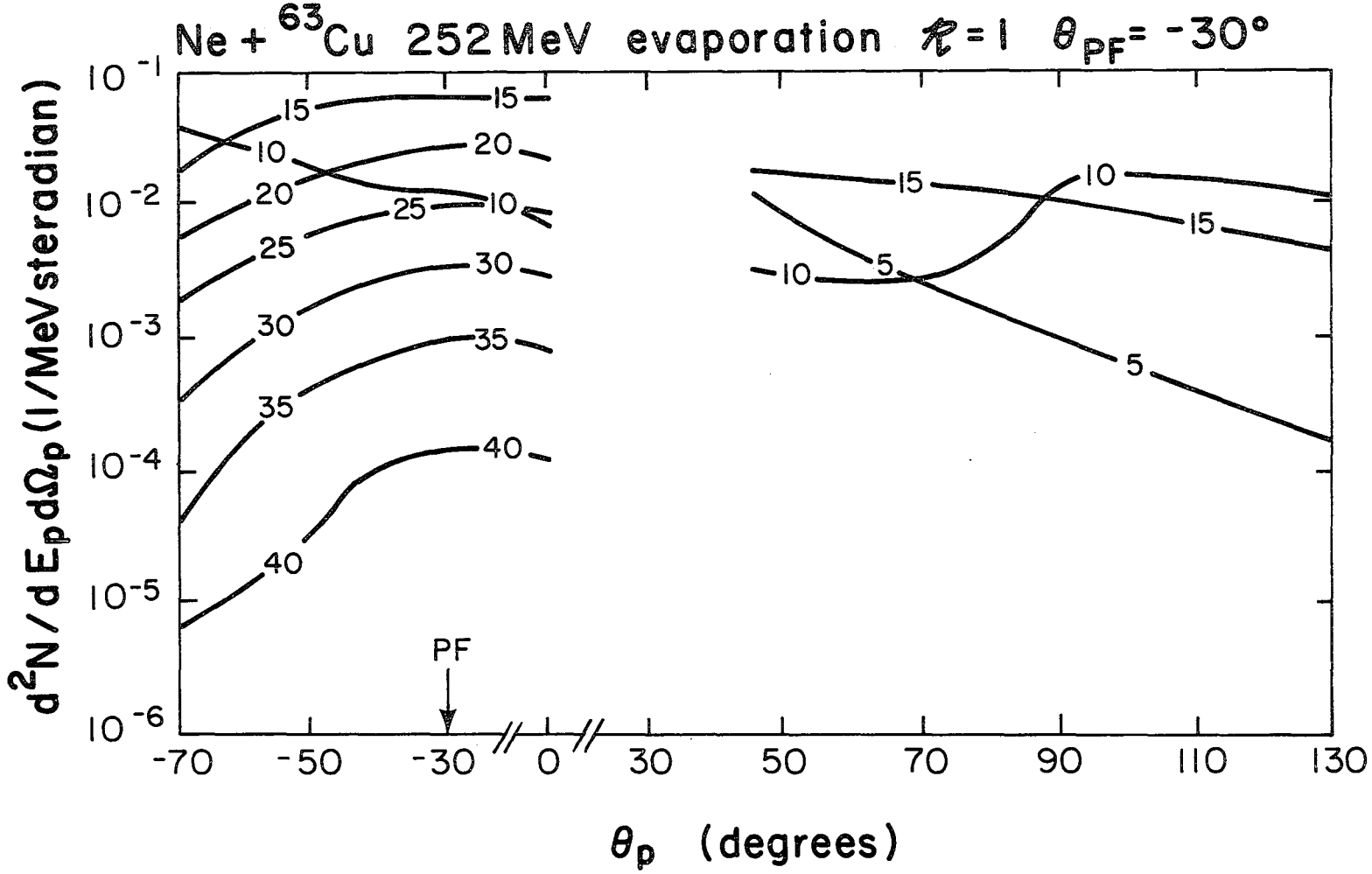

Fig. 34(a)

XBL 7811-12561

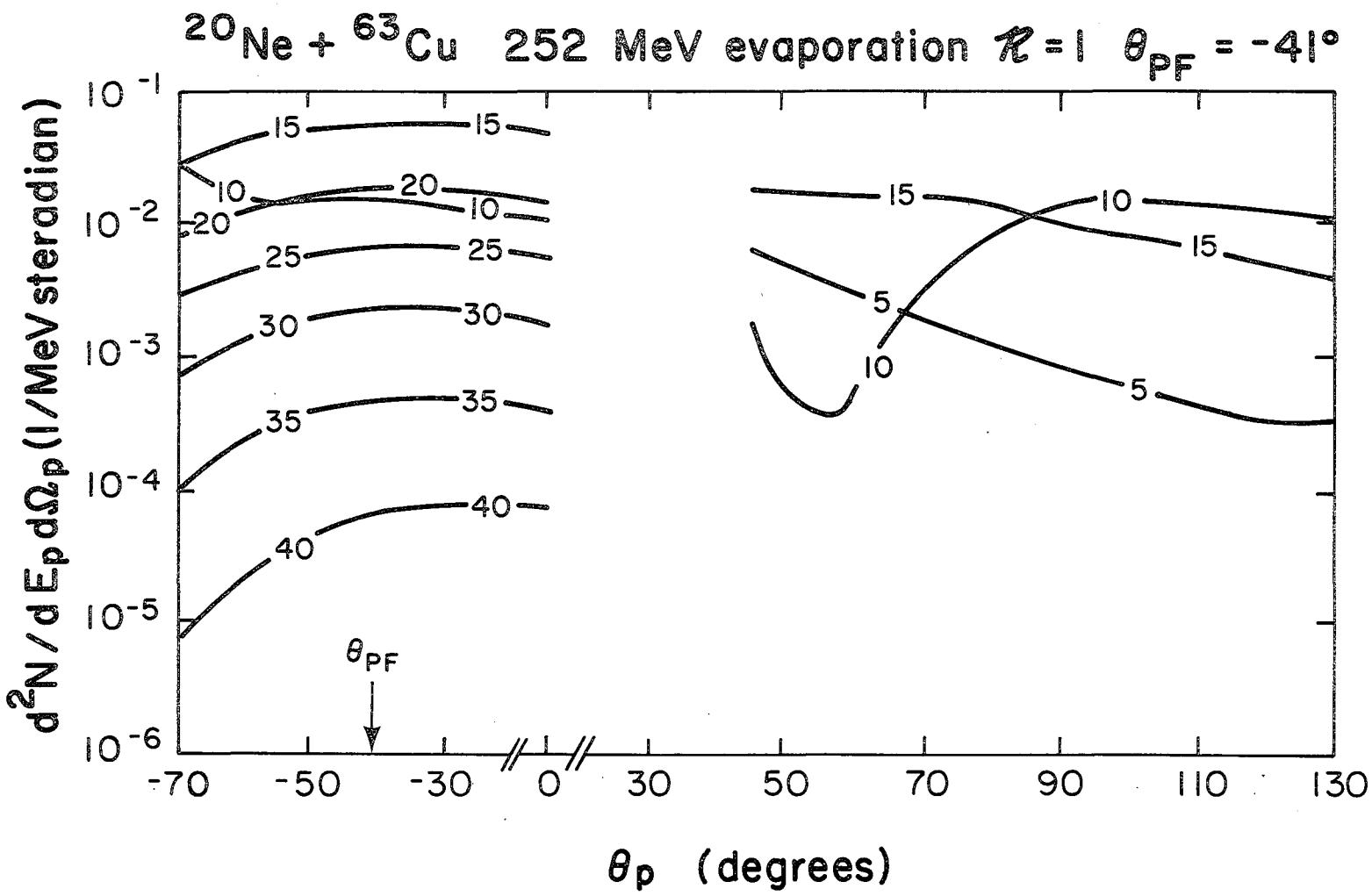

Fig. 34(b)

XBL 7811-12560

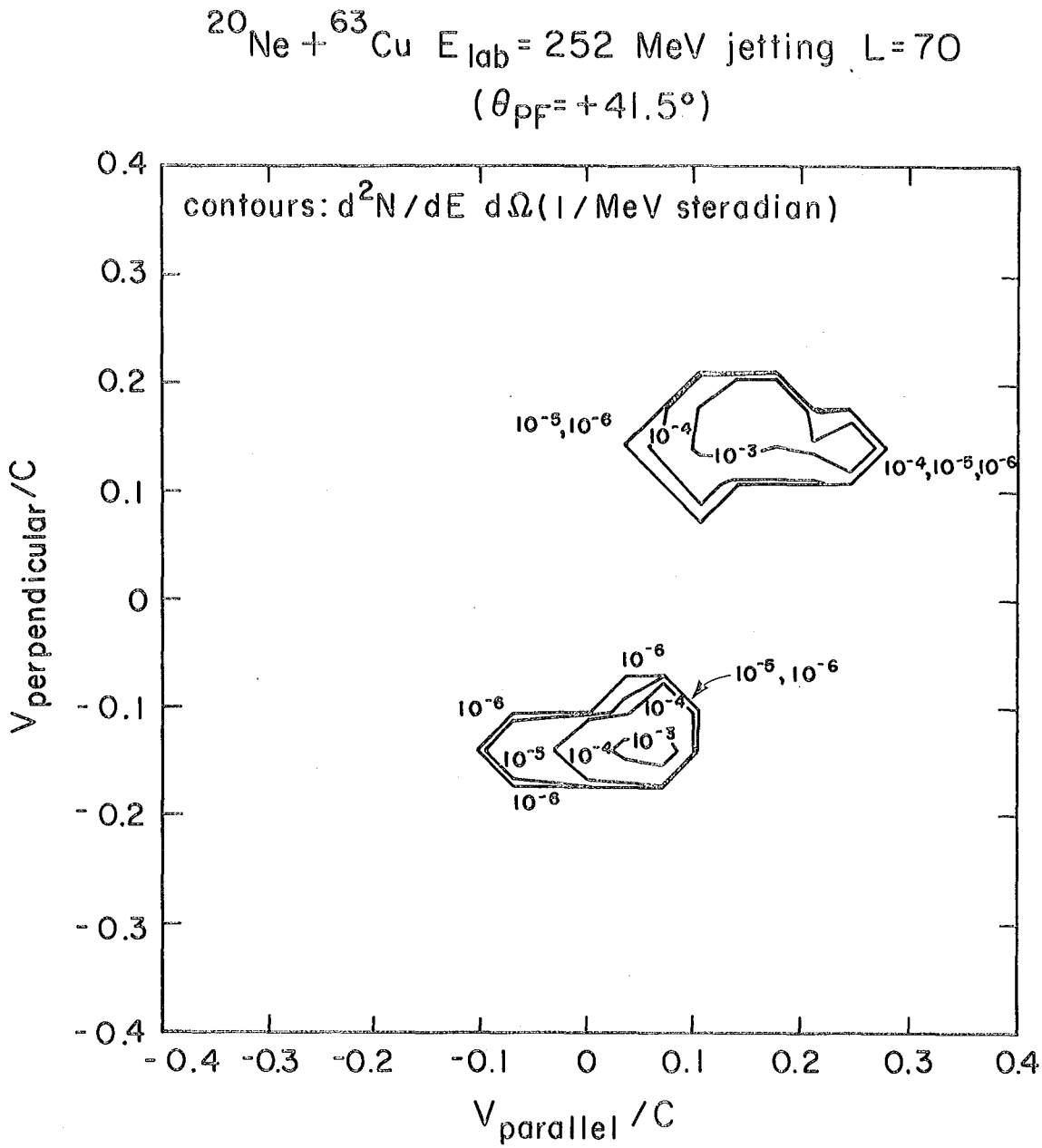

XBL 7812-13418A

Fig. 35 (a)

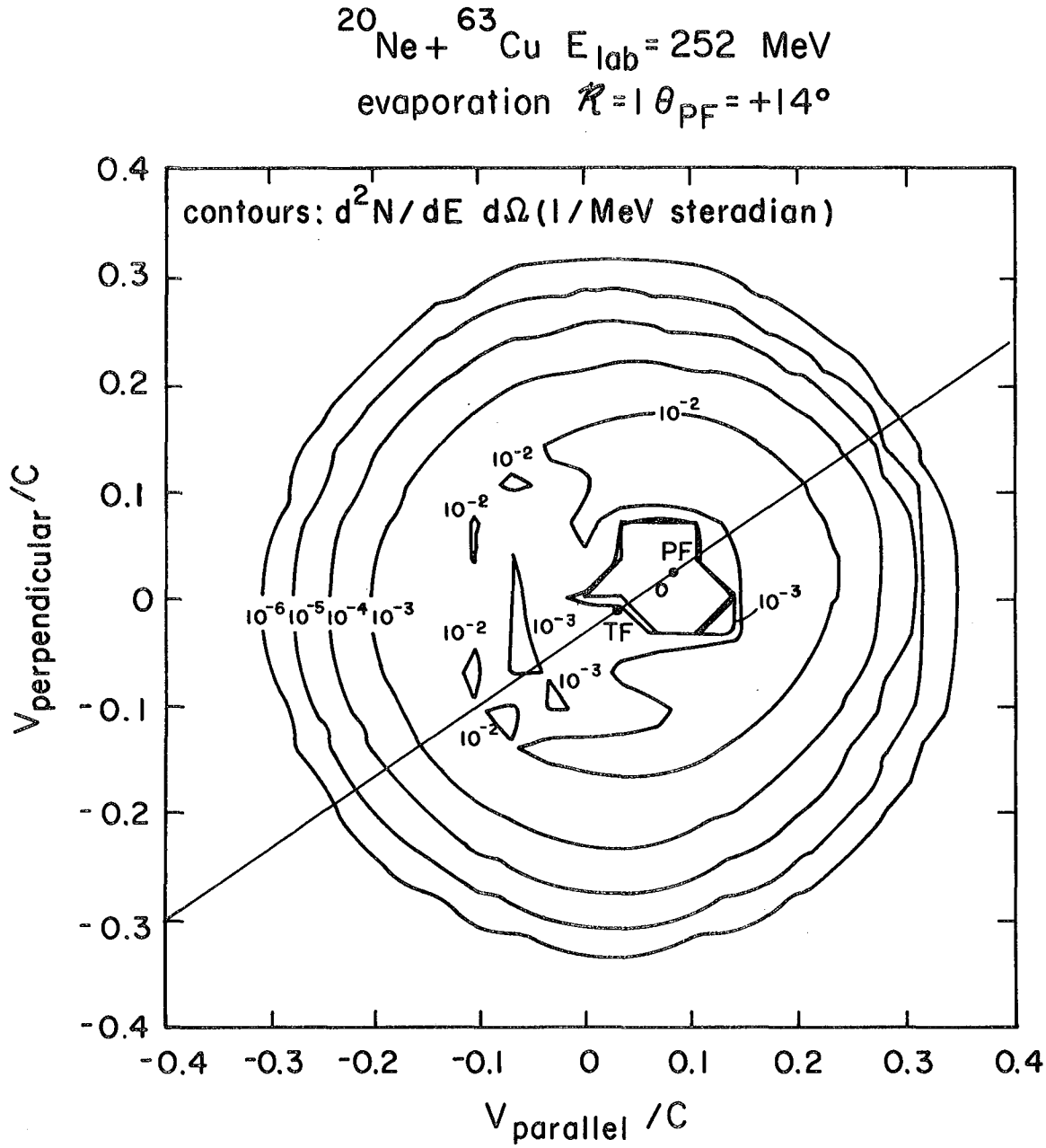

XBL 7812-13420A

Fig. 35(b)

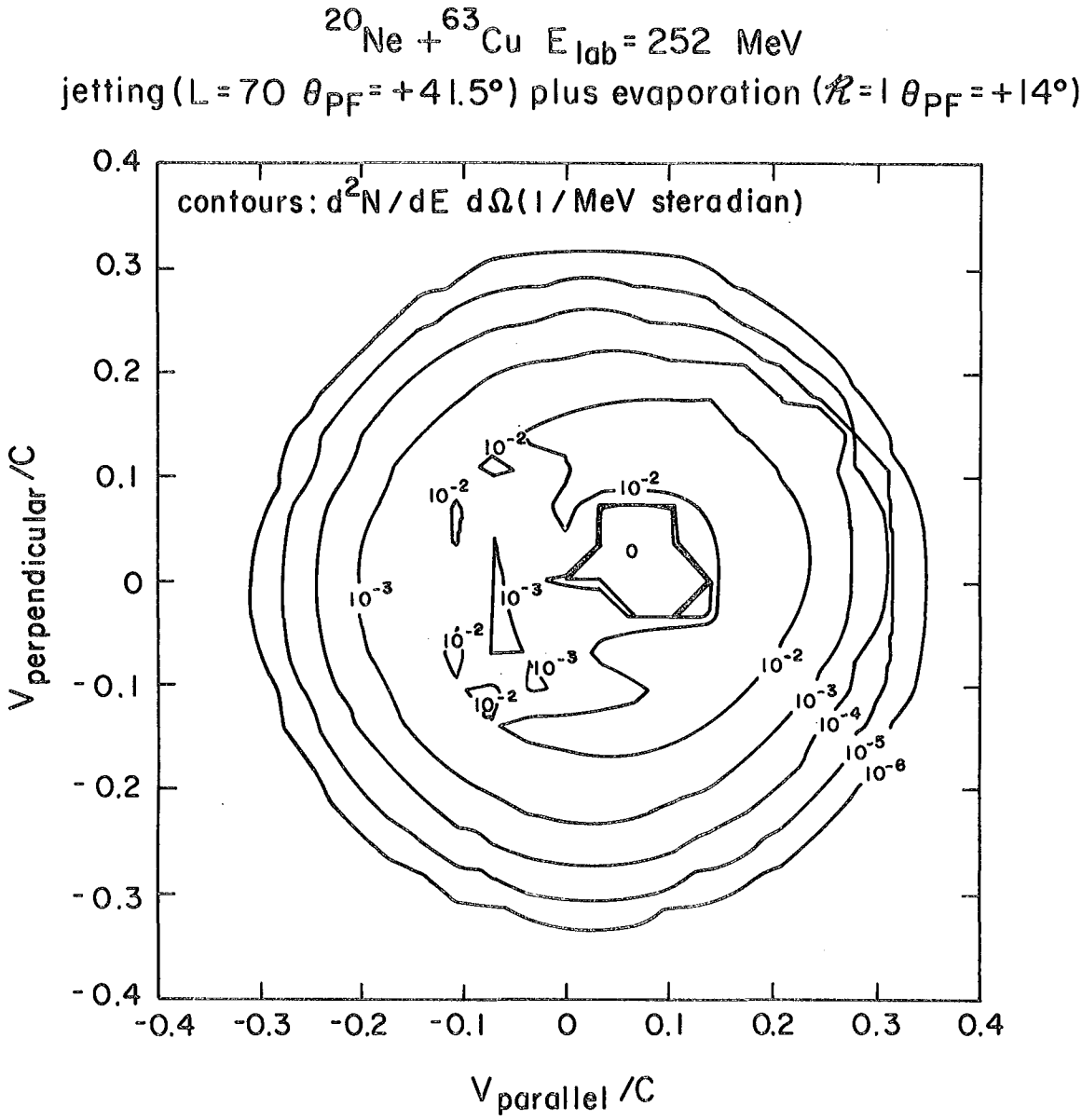

XBL 7812-13419A

Fig. 35(c)

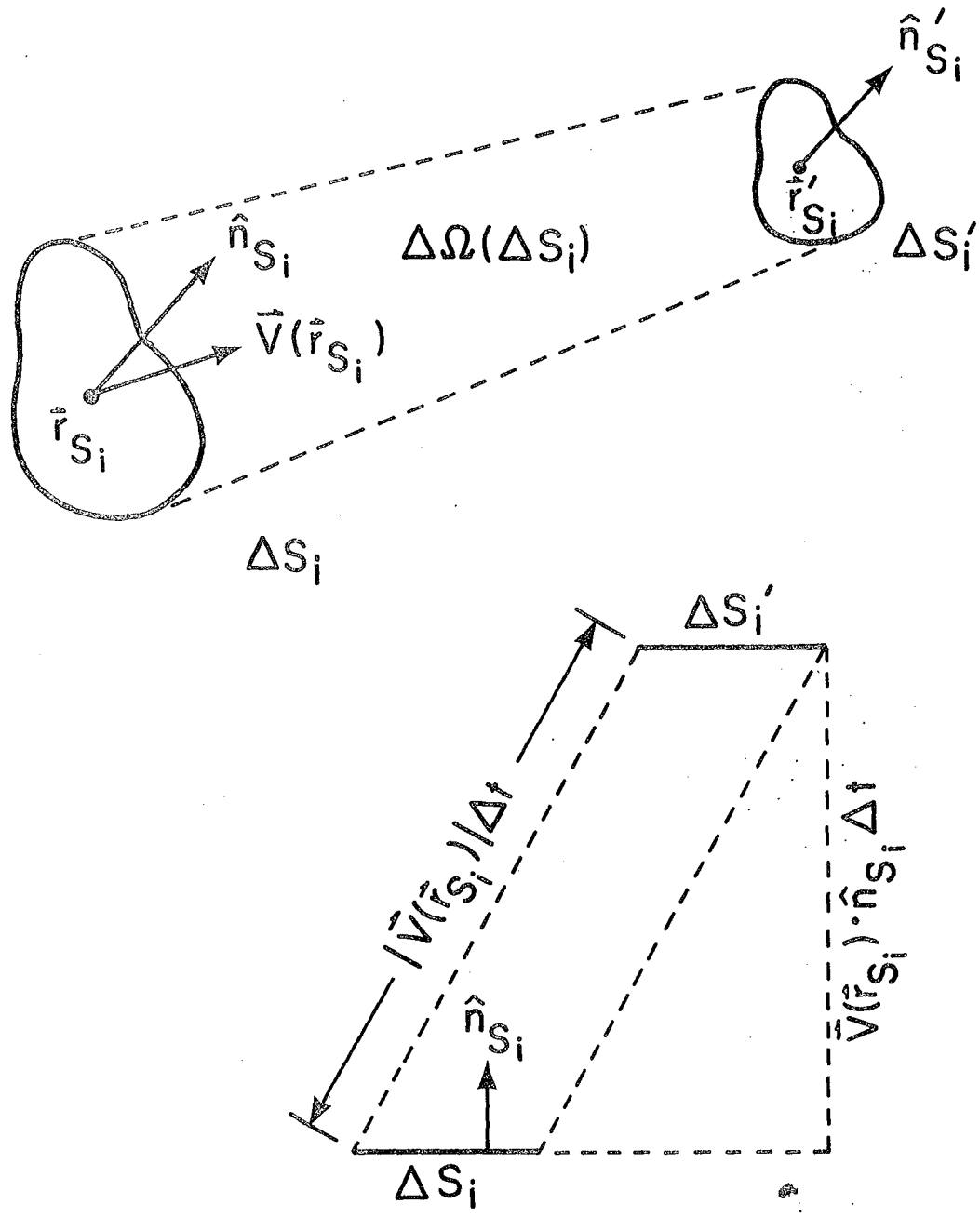

Fig. 36

XBL 7812 - 13423

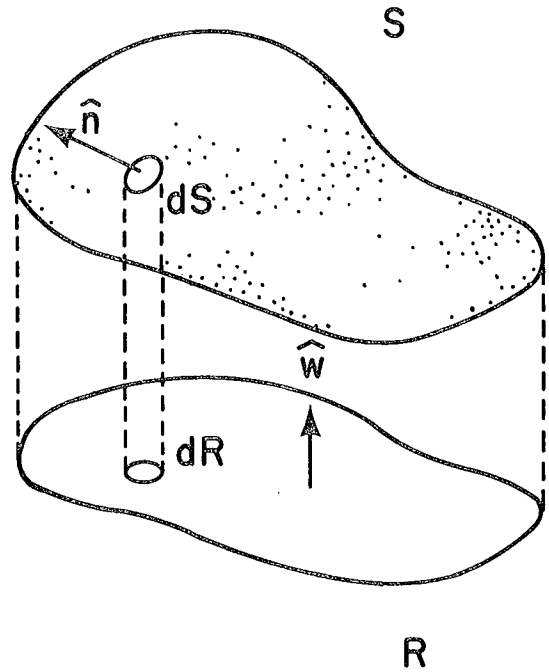

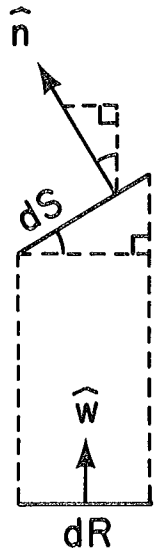

Fig. 37

XBL 7812 - 13422

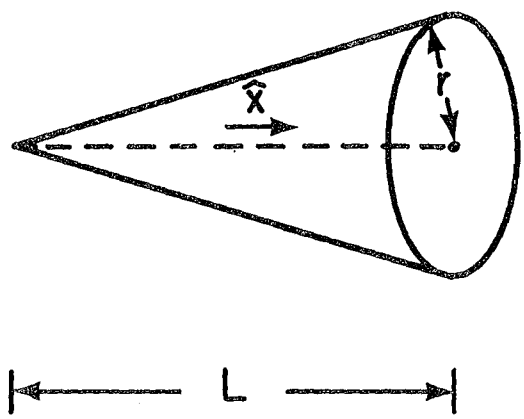

XBL 7812-13415

Fig. 38

This report was done with support from the Department of Energy. Any conclusions or opinions expressed in this report represent solely those of the author(s) and not necessarily those of The Regents of the University of California, the Lawrence Berkeley Laboratory or the Department of Energy.

Reference to a company or product name does not imply approval or recommendation of the product by the University of California or the U.S. Department of Energy to the exclusion of others that may be suitable.

TECHNICAL INFORMATION DEPARTMENT
LAWRENCE BERKELEY LABORATORY
UNIVERSITY OF CALIFORNIA
BERKELEY, CALIFORNIA 94720